

**ATOMISTIC INVESTIGATION OF DEFORMATION  
CHARACTERISTICS OF ENERGETIC MATERIAL TKX-50  
UNDER SHOCK BY DEVELOPING A QUANTUM  
CHEMISTRY-BASED FORCEFIELD**

A Dissertation  
By

**Md. Rifat Hossain**  
0421102127

Under the supervision of  
**Dr. Mohammad Jane Alam Khan**

MASTER OF SCIENCE IN MECHANICAL ENGINEERING



Department of Mechanical Engineering  
Bangladesh University of Engineering and Technology  
Dhaka, Bangladesh

July, 2023

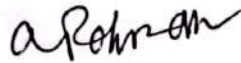
This thesis titled "Atomistic Investigation of Deformation Characteristics of Energetic Material TKX-50 under Shock by Developing a Quantum Chemistry-Based Forcefield," submitted by Md. Rifat Hossain, Roll No: 0421102127 Session: April 2021, has been accepted as satisfactory in partial fulfillment of the requirement for the degree of MASTERS OF SCIENCE in Mechanical Engineering on 26<sup>th</sup> July, 2023.

## BOARD OF EXAMINERS



Dr. Mohammad Jane Alam Khan  
Assistant Professor  
Department of Mechanical Engineering, BUET, Dhaka-1000

Chairman  
(Supervisor)



Dr. Muhammad Ashiqur Rahman  
Professor and Head  
Department of Mechanical Engineering, BUET, Dhaka-1000

Member  
(Ex-Officio)



Dr. Mohammad Abdul Motalab  
Professor  
Department of Mechanical Engineering, BUET, Dhaka-1000

Member  
(Internal)



Dr. Kazi Mohammad Shorowordi  
Professor  
Department of Materials and Metallurgical Engineering, BUET, Dhaka-1000


Member  
(External)

## Candidate's Declaration

This is to certify that the work presented in this thesis entitled, "**Atomistic Investigation of Deformation Characteristics of Energetic Material TKX-50 under Shock by Developing a Quantum Chemistry-Based Forcefield,**" is the outcome of the research carried out by Md. Rifat Hossain under the supervision of Dr. Mohammad Jane Alam Khan, Professor, Department of Mechanical Engineering, Bangladesh University of Engineering and Technology (BUET), Dhaka-1000, Bangladesh.

It is also declared that neither this thesis nor any part thereof has been submitted anywhere else for the award of any degree, diploma or other qualifications.

Signature of the Candidate



06-08-23

---

Md. Rifat Hossain

0421102127

## **Dedication**

First of all, I would want to dedicate my study to the scientific communities all over the world. These communities have assisted me in every facet of this study by sharing their knowledge, and the study would not have been feasible without the advancements in scientific understanding. I would also like to dedicate this to my family, as well as my doctoral advisor Dr. Mohammad Jane Alam Khan, as well as my fellow master's degree classmates Sanjit Sikder and Mehady Hasan, for their unwavering support during this journey. And as a last note, I would want to thank everyone who has supported me with their generosity throughout this research.

# **Table of Contents**

<b>Candidate's Declaration</b>	<b>iii</b>
<b>Dedication</b>	<b>iv</b>
<b>Acknowledgment</b>	<b>xiii</b>
<b>ABSTRACT</b>	<b>xiv</b>
<b>CHAPTER 1</b>	
<b>INTRODUCTION</b>	<b>1</b>
<b>1.1 Energetic Materials</b>	<b>1</b>
<b>1.2 Application of Energetic materials</b>	<b>3</b>
<b>1.3 Motivation for the study</b>	<b>5</b>
<b>1.4 Statement of Objectives</b>	<b>7</b>
<b>1.5 Outline of Thesis</b>	<b>8</b>
<b>CHAPTER 2</b>	
<b>LITERATURE REVIEW</b>	<b>9</b>
<b>2.1 TKX-50 (Dihydroxulammonium-5,5'-bistetrazole-1,1'-diolate)</b>	<b>9</b>
<b>2.2 Classical Molecular Dynamics Forcefield for Energetic Materials</b>	<b>11</b>
<b>2.3 Previous works of TKX-50 and Shock sensitivity study of Energetic Materials</b>	<b>14</b>
<b>CHAPTER 3</b>	
<b>BACKGROUND THEORY AND METHODOLOGY</b>	<b>19</b>
<b>3.1 introduction</b>	<b>19</b>
<b>3.2 Density Functional Theory</b>	<b>22</b>
<b>3.3 AB Initio Calculation</b>	<b>25</b>
<b>3.3.1 Self Consistent Field (SCF) method</b>	<b>28</b>

<b>3.3.2 Post Self Consistent Field Method</b>	<b>31</b>
<b>3.3.4 Basis Functions</b>	<b>33</b>
<b>3.4 Force Field Parameterization</b>	<b>36</b>
<b>3.5 Population Methods for Estimating Partial Atomic Charges</b>	<b>38</b>
<b>3.5.1 Electrostatic Potential (ESP) Method:</b>	<b>40</b>
<b>3.6 ORCA</b>	<b>41</b>
<b>3.7 MultiWfn</b>	<b>42</b>
<b>3.8 Avogadro</b>	<b>44</b>
<b>3.9 Molecular Dynamics Simulations</b>	<b>45</b>
<b>3.9.1 General Procedure of Molecular Dynamics Simulation</b>	<b>46</b>
<b>3.10 Equilibrium Molecular Dynamics and Non-Equilibrium Molecular Dynamics</b>	<b>47</b>
<b>3.11 Buckingham Potential</b>	<b>48</b>
<b>3.12 Cut-off Radius</b>	<b>50</b>
<b>3.13 Integration of Equations of Motion</b>	<b>50</b>
<b>3.13.1 Verlet Algorithm:</b>	<b>51</b>
<b>3.13.2 Leap-Frog Algorithm</b>	<b>51</b>
<b>3.13.3 Velocity-Verlet Algorithm</b>	<b>52</b>
<b>3.14 Periodic Boundary Conditions</b>	<b>53</b>
<b>3.15 LAMMPS</b>	<b>54</b>
<b>3.16 OVITO</b>	<b>55</b>
<b>3.17 VMD</b>	<b>56</b>
<b>3.18 Elastic Constants and Mechanical Properties</b>	<b>57</b>
<b>3.19 Volume Fluctuation Formula for generating Heat Capacity by MD simulation</b>	<b>59</b>
<b>3.20 Hugoniot Shock Simulation</b>	<b>60</b>

**CHAPTER: 4**

<b>RESULTS AND DISCUSSIONS</b> -----	<b>64</b>
<b>4.1 Forcefield Development for TKX-50</b> -----	<b>64</b>
<b>4.1.1 Geometry Optimization</b> -----	<b>64</b>
<b>4.1.2 Data Acquisition</b> -----	<b>64</b>
<b>4.1.3 Format Conversion for the XYZ System</b> -----	<b>65</b>
<b>4.1.4 Calculation of Quantum Chemistry</b> -----	<b>66</b>
<b>4.1.5 Optimization and Acceleration of the Simulation</b> -----	<b>66</b>
<b>4.1.6 Observations and Discussion</b> -----	<b>66</b>
<b>4.1.7 Forcefield Parameterization</b> -----	<b>68</b>
<b>4.1.7.1 Bond Stretch Parameterization</b> -----	<b>69</b>
<b>4.1.7.2 Angle Bending Parameterization</b> -----	<b>72</b>
<b>4.1.7.3 Torsional moment Parameterization</b> -----	<b>74</b>
<b>4.1.8 Forcefield Validation and predicted Mechanical and Thermodynamic Properties</b> -----	<b>80</b>
<b>4.1.8.1 Simulation Protocol</b> -----	<b>81</b>
<b>4.1.8.2 Crystal, Mechanical and Thermodynamic properties</b> -----	<b>82</b>
<b>4.1.8.3 Elastic constant, shear, bulk modulus calculation</b> -----	<b>83</b>
<b>4.1.8.4 Constant volume Heat Capacity (<math>C_v</math>)</b> -----	<b>86</b>
<b>4.2 Uniaxial Hugoniot Shock Simulation Study on TKX-50</b> -----	<b>88</b>
<b>4.2.1 Simulation protocol</b> -----	<b>88</b>
<b>4.2.2 Time evolution</b> -----	<b>91</b>
<b>4.2.3 Pressure-Volume-Temperature dependence</b> -----	<b>100</b>
<b>4.2.4 Study of Shear band formation</b> -----	<b>102</b>

**CHAPTER 5**

**CONCLUSION AND FUTURE RECOMMENDATIONS ----- 110**

**5.1 Conclusion----- 110**

**5.2 Future Recommendations----- 112**

**REFERENCES ----- 114**

**Nomenclature ----- 123**



## List of Figures

Figure 2.1 First cook off test of TKX-50 [11] .....	10
Figure 3.1 Flow chart of solving Kohn Sham Equation with Self Consistent Field (SCF) method [58].....	30
Figure 3.2 Schematic diagram of a basic MD simulation.....	46
Figure 3.3 Particle's interaction according to LJ model .....	49
Figure 3.4 Periodic boundary condition [73].....	54
Figure 4.1: Unit cell of TKX-50 with periodic conformation collected from the CIF file of CCDC [10].....	65
Figure 4.2: Molecular Formula of TKX-50 [71] .....	65
Figure 4.3 Optimized Molecular structure of TKX-50.....	67
Figure 4.4 Comparison of the bond stretch of C1-C1 bond type for FF and QM .....	71
Figure 4.5 Comparison of the angle bending stretch of C1_N4_N3 angle type for FF and QM ..	73
Figure 4.6: The configuration of 0°(Figureure (a)) and 180°(Figureure(b)) are shown here. Here yellow circles show the torsion barrier of N1_C1_C1_N1. ....	75
Figure 4.7: Comparison of N1_C1_C1_N1 torsion barrier (in kcal/mol) between FF and QM. The blue dots are from QM data and the red line is from FF. ....	75
Figure 4.8: The configuration of -120°(Figure (a)) and +60°(Figure (b)) are shown here. Here yellow circles show the torsion barrier of H4_N9_O3_H2.....	76
Figure 4.9: Comparison of H4_N9_O3_H2 torsion barrier (in kcal/mol) between FF and QM. The blue dots are from QM data and the red line is from FF. ....	76
Figure 4.10 Energy fluctuation for the last 50 picoseconds .....	87
Figure 4.11 Time Evolution of Hugoniot energy difference per molecule E-Eh obtained from Hugoniot simulations of shock compression along [100] using $e_0 = -55627.759$ kcal/mol for the case of $P_{xx} = 3$ to 13 GPa for simulation cell of 4800 molecules.....	90
Figure 4.12 Time Evolution of Hugoniot energy difference per molecule E-Eh obtained from Hugoniot simulations of shock compression along [100] using $e_0 = -109060.64$ kcal/mol kcal/mol	

for the case of $P_{xx} = 3$ to 13 GPa for simulation cell of 6480 molecules .....	90
Figure 4.13 Stress along [100] direction against time step for system with 4800 molecules .....	92
Figure 4.14 Stress along [100] direction against time step for system with 6480 molecules .....	92
Figure 4.15 Rise of temperature as a function of time step for shock pressure $P_{xx} = 3$ GPa, 5 GPa, 7 GPa, 9 GPa, 11 GPa, and 13 GPa along [100] direction for system with 4800 molecules .....	93
Figure 4.16 Rise of temperature as a function of time step for shock pressure $P_{xx} = 3$ GPa, 5 GPa, 7 GPa, 9 GPa, 11 GPa, and 13 GPa along [100] direction for system with 6480 molecules .....	94
Figure 4.17 Time evolution of Volume compression ratio ( $V/V_0$ ) for shock pressure $P_{xx} = 3$ GPa, 5 GPa, 7 GPa, 9 GPa, 11 GPa, and 13 GPa along [100] direction for system with 4800 molecules .....	95
Figure 4.18 Time evolution of Volume compression ratio ( $V/V_0$ ) for shock pressure $P_{xx} = 3$ GPa, 5 GPa, 7 GPa, 9 GPa, 11 GPa, and 13 GPa along [100] direction for system with 6480 molecules .....	95
Figure 4.19 Time evolution of von Mises Shear stress ( $\tau$ ) for shock pressure $P_{xx} = 3$ GPa, 5 GPa, 7 GPa, 9 GPa, 11 GPa, and 13 GPa along [100] direction for system with 4800 molecules .....	96
Figure 4.20 Time evolution of von Mises Shear stress ( $\tau$ ) for shock pressure $P_{xx} = 3$ GPa, 5 GPa, 7 GPa, 9 GPa, 11 GPa, and 13 GPa along [100] direction for system with 6480 molecules .....	98
Figure 4.21 Comparative analysis of von Mises shear stress for both systems with 4800 molecules and 6480 molecules for shock pressure $P_{xx} = 3$ GPa, 9 GPa, 13 GPa .....	98
Figure 4.22 Volumetric strain of TKX-50 shocked along [100] as a function of shock pressure $P_{xx}$ obtained from Hugoniot simulation for systems with 4800 molecules. The dotted line here representing the approximated HEL while dividing the plot into elastic and plastic region .....	101
Figure 4.23 Final temperature difference of TKX-50 shocked along [100] as a function of shock pressure $P_{xx}$ obtained from Hugoniot simulation for systems with 4800 molecules. The dotted line here representing the approximated HEL while dividing the plot into elastic and plastic region .....	101
Figure 4.24 Snapshots showing shear band in single crystal TKX-50 with 4800 molecules shock loaded along [100] direction for the shock pressure of 13GPa viewed along (a) (001) direction, and (b) (010) direction .....	103
Figure 4.25 Snapshots showing shear band in single crystal TKX-50 with 6480 molecules shock	

loaded along [100] direction for the shock pressure of 13GPa viewed along (a) (001) direction, and (b) (010) direction .....	104
Figure 4.26 Atomic configuration of TKX-50 for [100] shock compression with $P_{xx} = 13$ GPa. The black arrows indicate the slip direction. The black line is to help distinguish the unit cell. The C, N, O atoms are represented by black, green, and, red. ....	105
Figure 4.27 Snapshots showing plastic deformation in single crystal TKX-50 shock-loaded along [100] direction viewed along (010) direction for shock pressure, (a) $P_{xx} = 9$ GPa, (b) $P_{xx} = 11$ GPa, (c) $P_{xx} = 13$ GPa for systems with 4800 molecules viewed along (001) direction .....	107
Figure 4.28 Snapshots obtained from uniaxial Hugoniot simulation for TKX-50 along [100] direction from shock pressure $P_{xx} = 11$ GPa after (a) 5ps (b) 40 ps and (c) 93 ps. ....	108
Figure 4.29 Snapshots obtained from uniaxial Hugoniot simulation for TKX-50 along [100] direction from shock pressure $P_{xx} = 13$ GPa after (a) 5ps (b) 30 ps and (c) 77 ps viewed along (001) .....	109

## **List of Tables**

<b>Table: 4.1 bond lengths (in Å) for various bond types for crystal and optimized structure (Figure 4.3):</b> -----	<b>68</b>
<b>Table 4.2 Energy fluctuation of bistetrazole along with the change of the bond length of C1-C1 bond type.</b> -----	<b>70</b>
<b>Table 4.3 Bond Stretch parameters</b> -----	<b>71</b>
<b>Table 4.4 Energy fluctuation of bistetrazole along with the change of the angle of C1_N4_N3</b>	<b>72</b>
<b>Table 4.5 Angle bending parameters</b> -----	<b>74</b>
<b>Table 4.6: Dihedral torsion parameters</b> -----	<b>77</b>
<b>Table 4.7: Improper torsion parameters</b> -----	<b>78</b>
<b>Table 4.8: Non bonded Forcefield paramters</b> -----	<b>80</b>
<b>Table 4.9 Comparison of crystal, mechanical, and thermodynamic properties of TKX-50, in between Experimental data, QM data, AMBER FF, and our developed FF</b> -----	<b>82</b>
<b>Table 4.10 Elastic Constants</b> -----	<b>86</b>

## **Acknowledgment**

First and foremost, I would like to express my sincere appreciation and thanks to my supervisor, Dr. Mohammad Jane Alam Khan, who was abundantly helpful and offered invaluable assistance, support, and guidance. I would like to convey my gratitude to Bangladesh University of Engineering and Technology for providing financial support and high-performance computing facilities. Special thanks are also due to the numerous teachers and mentors who helped me to compile the software/codes in the high-performance computer. Also, thanks to the Department of Mechanical Engineering, BUET for facilitating all the support. At last, thanks to all the people who have encouraged and helped me in this study both directly and indirectly.

## ABSTRACT

TKX-50 is an emerging energetic material with a high potential. Computational investigations facilitate the understanding of materials' behavior, characteristics, and safety concerns. A proper understanding of the hot spot formation in explosive materials require thorough atomic scale investigations for which an accurate classical forcefield is must. This study examines TKX-50's atomistic structure, thermodynamic characteristics, and mechanical behavior to create an accurate classical forcefield based on quantum chemistry. The ultimate goal is to comprehend TKX-50's performance under extreme situations which led to hot spot formation and detonation and facilitate energetic material development.

This dissertation studies the recently synthesized energetic/explosive material TKX-50 (Dihydroxylammonium-5,5'-bistetrazole-1,1'-diolate) at the atomistic level to develop a classical molecular dynamics forcefield using conventional First Principle Calculation. A post-self-consistent field (SCF) method was used for developing the forcefield for TKX-50 which adds electron correlation effects and improves accuracy over the currently available forcefields. The Electrostatic Potential (ESP) method estimates nonbonded electrostatic potential to maintain charge neutrality and crystal structure integrity. The developed forcefield reproduces the material's crystal structure, cohesive energy, and density very well. Bulk modulus and shear modulus of TKX-50 is further calculated which matches quite well with the experimental values. Thermodynamic investigations are done to evaluate constant volume heat capacity and fares well with experimental results. The elastic constants are estimated, a first which is vital for any continuum scale study. The developed new forcefield is used to investigate the material's behavior under shock to understand deformation characteristics. Constant stress uniaxial Hugoniot shock compression simulations show TKX-50's behavior under extreme conditions by tracking temperature, volume fluctuation, and shear stress. The Hugoniot Elastic Limit (HEL) shock pressure is about 6 GPa with a potential overdriven point about 8 GPa. The shock simulation reveals that TKX-50 undergoes plastic deformation by forming shear bands at high shear. Width of the shear band depends on the shock pressure.

The classical forcefield developed accurately reproduces TKX-50's geometric and thermo-mechanical properties. This research opens the door to machine learning-based forcefields, non-equilibrium molecular dynamics simulations, and multiscale modeling, to understand its sensitivity, ensure its safety and smooth its advancement.

# CHAPTER 1

## INTRODUCTION

### 1.1 Energetic Materials

The quest for energy has been a motivating force behind several scientific and technological achievements in today's ever-changing globe. Among the numerous branches of study dedicated to this goal, the study of energetic materials stands out as an enthralling and critical subject of interest. Energetic materials are a diverse group of chemicals that have outstanding energy release capabilities, making them critical components in a variety of applications such as propulsion, defensive systems, mining, and even pyrotechnics [1]. These materials have the inherent ability to discharge massive amounts of energy in a controlled manner, making them both amazing and potentially hazardous if not handled with extreme caution [2,3].

We will delve into the features, classifications, synthesis methods, and major applications of energetic materials in this detailed examination. Understanding the intriguing world of energetic materials allows us to comprehend the delicate balance that must be struck between harnessing their enormous energy and limiting possible hazards associated with their use.

**Energetic Materials:** Energetic materials are defined as substances that have the ability to rapidly release energy in the form of heat, light, shockwaves, or a combination of these. These materials have various distinguishing properties that set them apart from other substances [1]. One distinguishing feature is their high energy density, which enables them to store and release massive amounts of energy in relation to their mass or volume. Furthermore, energetic materials frequently have a high degree of reactivity, allowing them to perform quick and exothermic chemical reactions under certain conditions.



*Energetic Material Classification:* Energetic materials are classified into numerous categories based on their composition, structure, and intended purpose. Explosives, propellants, pyrotechnics, and reactive materials are the basic classes [4]. Explosives are compounds that decompose quickly, releasing a tremendous quantity of energy in the process. Propellants, on the other hand, are meant to manage the release of energy in order to propel vehicles or projectiles. Pyrotechnics are materials used to create spectacular displays of light, color, and sound. Reactive materials are a different class of substances that are extremely reactive and used for specialized applications such as welding or cutting.

*Energetic Material Synthesis and Development:* The synthesis and development of energetic materials necessitate a thorough understanding of their properties and reactions. Chemical synthesis, mechanical mixing, and formulation methods are among the approaches used by researchers to create these materials. The method of synthesis chosen is determined by the desired qualities and the material's intended application. Creating novel energetic materials frequently necessitates a precise balance of optimizing energy output, stability, sensitivity, and safety.

*Safety Considerations and Energetic Material Handling:* Given the potency of energetic materials, safety precautions and correct handling standards are critical. The sensitivity, stability, and possibility for inadvertent initiation necessitate stringent safety precautions during storage, transportation, and use. To limit dangers and preserve human lives and the environment, strict rules and standard operating procedures control the handling and disposal of hazardous materials.

The fascinating and multifaceted topic of energetic materials integrates chemistry, physics, materials science, and engineering. These extraordinary compounds have played vital role over the years in industry, defense, etc.

## **1.2 Application of Energetic materials**

Energetic materials, often known as explosives or propellants, are used extensively in a variety of industries, including defense, mining, construction, and aerospace. When subjected to controlled initiation, these materials have high energy densities and release a considerable quantity of energy. Their applications span from rocket propulsion to controlled demolition of buildings [3]. We will delve into the diverse applications of energetic materials in this detailed introduction, analyzing their uses, benefits, and accompanying obstacles.

**Applications in Defense and Military:** Energetic materials have long been employed in defense and military applications. In firearms, artillery, and rocket systems, they are the major propellants. Their controlled combustion produces high-pressure gases that launch projectiles at high speeds. Explosives are also used in shaping charges, warheads, and shaped charges for armor piercing, demolition, and breaching purposes.

**Mining and Quarrying:** Explosives are commonly used in mining and quarrying operations. Mining businesses can efficiently recover minerals and ores from the earth's crust by using controlled energy release of energetic materials. These materials are used to break down rock formations and build tunnels [7]. They increase production, lower expenses, and reduce the environmental effect of traditional excavation methods.

**Building and Demolition:** Energetic materials have transformed the construction business. Structures such as buildings and bridges must be demolished with precision and safety. Explosives enable the removal of particular components of a structure while causing minimum harm to neighboring areas [6]. Furthermore, in controlled implosion procedures, energetic materials help buildings collapse into their own footprint, simplifying debris clearance and increasing safety.

**Pyrotechnics and Fireworks:** Pyrotechnics rely primarily on energetic ingredients to create visually dazzling displays. Colorful bursts, sparkles, and flames are produced by the controlled combustion and precise timing of these materials, entralling audiences at diverse events, celebrations, and entertainment displays. Energetic ingredients provide smoke and sound effects, which enhance the whole experience.

**Aircraft and propulsion:** Among the most prominent consumers of energetic materials are the rocketry and aircraft industries. Solid rocket propellants, such as composite propellants, provide the thrust required to launch spacecraft into orbit. They have a high energy density, are stable, and have regulated burn rates. In addition, pyrotechnic equipment such as separation bolts and igniters aid in the separation of rocket stages and the activation of critical systems.

**Propellant Actuated Devices (PAD):** These devices use energetic materials to power mechanical systems. These devices are employed in a variety of applications such as valve actuation, bolt opening and closing mechanisms, and emergency release systems. PADs provide reliable and quick actuation in crucial situations by capturing the energy created by the combustion of energetic materials [8].

**Challenges and Future Developments:** While the usage of energetic materials has numerous advantages, it also has drawbacks. Concerns about safety and security need careful regulation, handling, and storage standards. The possibility of misuse or mishaps emphasizes the significance of training, licensing, and following defined norms [9]. Efforts are also being made to develop energetic materials with improved performance, stability, and lower environmental effect, assuring a safer and more sustainable future.

The use of energetic materials encompasses a wide range of industries and sectors, having a substantial impact on many facets of modern life. From defense and mining to construction and aircraft, these materials offer technological, safety, and efficiency breakthroughs. As ongoing research and development define the sector, the future holds promising advancements in

energetic materials, opening the way for safer and more effective applications in a variety of domains.

### **1.3 Motivation for the study**

The development of accurate force fields is essential for molecular dynamics (MD) simulations because it enables researchers to examine the behavior and properties of complex systems at the atomic level. Understanding the mechanical response of energetic materials, such as TKX-50 [12], under various conditions is crucial for applications ranging from explosives engineering to safety evaluations. However, despite the significance of TKX-50, charge-neutralized and reliable force fields for this energetic substance have been scarce.

The development of force fields for TKX-50, an energizing material created in 2012, has progressed relatively slowly [11]. The only extant MD force field for TKX-50, developed by An et al. in 2015, has a critical flaw: it is not charge-neutralized [10]. When conducting non-equilibrium MD simulations requiring large void sizes, this deficiency presents a significant challenge. The absence of charge neutrality can result in system instability and anomalies, undermining the precision of simulation results. Therefore, it is imperative to address this issue and develop a charge-neutralized force field for TKX-50 to facilitate more accurate and realistic simulations.

The primary objective of this investigation was to address the limitations of the existing force field for TKX-50 and to develop a quantum chemistry-based force field that addresses the charge neutrality issue. Using ab initio calculations, we sought to develop a force field that accurately describes interatomic interactions and captures the fundamental properties of TKX-50. Our force field development process entailed comprehensive quantum chemistry calculations, such as second-order self-consistent field (SCF) methods, which provide greater precision than previous force fields for TKX-50.

In addition, the availability of dependable force fields for other energetic materials such as HMX, RDX, and TATB has demonstrated the significant impact that these force fields can have on a variety of research disciplines [13-20]. Different force fields are tailored to particular properties or phenomena, such as thermal properties, mechanical properties, or crystal structures. However, the lack of a complete and accurate force field for TKX-50 prevents researchers from studying its behavior under different conditions and obtaining insight into its unique properties.

Furthermore, the potential applications of TKX-50 in a variety of industries, including defense, mining, and aerospace, make an accurate comprehension of its mechanical response essential [11]. Simulations of uniaxial shock hugging, designed particularly to collect plasticity data, provide valuable insights into the material's response under dynamic loading conditions. To conduct reliable uniaxial shock hugging simulations for TKX-50, however, a charge-neutralized and robust force field is required. The realization that the availability of a precise force field would allow us to investigate the plasticity and shock response of TKX-50, thereby contributing to a greater understanding of its behavior under extreme conditions, was the impetus for our research.

In summary, the limitations of the existing force field for TKX-50, which lacked charge neutrality and hindered non-equilibrium MD simulations with large void sizes, prompted our investigation. We intended to resolve this issue by developing a force field based on quantum chemistry for TKX-50. Moreover, the lack of comprehensive force fields for TKX-50 compared to other energetic materials, as well as the potential industrial applications of TKX-50, further motivated our research. We aimed to develop a force field that would permit precise predictions of thermal and mechanical properties, facilitate studies of crystal structure, and open the door to non-equilibrium MD simulations. In addition, the objective of our study was to execute uniaxial shock Hugoniot simulations to collect plasticity data and improve our understanding of TKX-50's behavior under extreme conditions.

## 1.4 Statement of Objectives

The following is a list of the most important objectives that this study aims to achieve:

*Objective 1:* The first goal of this project is to create a forcefield for energetic material, TKX-50 that is based on quantum chemistry.

1. Utilizing the concepts of quantum chemistry, construct a forcefield for TKX-50 that is dependable and accurate.
2. Integrate the forcefield into a program that simulates the molecular dynamics of a system.

*Objective 2:* Validation of the Forcefield in order to ensure that the forcefield that has been developed is accurate.

1. Carry out simulations with the help of the LAMMPS molecular dynamics tool, and evaluate the degree to which the results of the simulation and the experiments agree with one another.
2. Determine the thermodynamic and mechanical parameters of the TKX-50 such as constant volume heat capacity, the bulk modulus, the shear modulus, poisson ratio, and the elastic constants.

*Objective 3:* Investigation of deformation characteristics of shocked TKX-50

1. Perform an analysis on how TKX-50 reacts when subjected to shock conditions, paying particular attention to Hugoniot Elastic Limit, Overdriven point, shear stress, shear band formation, as well as slip plane direction.

2. Observe the changes in parameters like stress, volume, and temperature in shocked condition.

Overall, the purpose of this research is to develop a quantum-chemistry based classical forcefield for molecular dynamics simulation followed by validation at atomistic level by estimating thermo-mechanical properties, as well as investigating deformation characteristics of TKX-50 under shock.

## **1.5 Outline of Thesis**

The following structure has been chosen for the dissertation:

In Chapter 1, a general discussion on energetic materials and its application in various fields, motivation of our study, primary objectives of this study have been discussed in detail.

A detailed literature review has been published in Chapter 2 for the purpose of providing a better understanding of earlier computational work on energetic materials, as well as the construction of a classical MD forcefield for use with energetic materials. Additionally, prior works on TKX-50 were the subject of an in-depth discussion.

In Chapter 3, the simulation methodology and background theory that underpins this study have been dissected in great detail.

The relevance of this work to the existing body of published research is the topic of discussion in Chapter 4. The results of all of the computer simulations were analyzed in great detail, and comparisons were drawn with the pertinent literature wherever it was appropriate to do so.

Finally, the recommendations for future work as well as the conclusions drawn from this body of study are presented and addressed in chapter 5.

## CHAPTER 2

### LITERATURE REVIEW

#### 2.1 TKX-50 (Dihydroxulammonium-5,5'-bistetrazole-1,1'-diolate)

TKX-50 is an energetic material that has gotten a lot of attention in the explosives and propellants field because of its unique qualities and possible uses. Tetrakis(hydroxymethyl) phosphonium nitrate, more commonly referred to as TKX-50, is a high-performance explosive chemical that excels in stability, sensitivity, and energy production. It was discovered in the 2012 [12]. This energetic material's potential use in a variety of applications across the military and industrial spheres has been the subject of substantial research.

The structure of TKX-50 consists of four hydroxymethyl groups that are connected to a core phosphonium ion. This phosphonium ion is then bonded to nitrate groups. Because of its molecular structure, TKX-50 possesses outstanding stability, even when subjected to challenging conditions. The presence of hydroxymethyl groups contributes to an increase in the material's thermal stability, which in turn reduces the risk of the substance being ignited by accident. In addition, the phosphonium nitrate core is a significant factor in the high energy content of TKX-50, which helps to explain why it is such a powerful explosive molecule [11].

The fact that TKX-50 is not overly sensitive to stimulation from the outside world is one of its primary selling points. When compared to more traditional explosives such as TNT (trinitrotoluene), TKX-50 demonstrates a far higher level of resistance to the effects of collision, friction, and electrostatic discharge. Because of its property, it is easier to handle, transport, and store, hence lowering the likelihood that it may accidentally detonate. The low sensitivity of TKX-50 also makes it possible to formulate insensitive weapons, which are essential for increasing the safety of military troops and lowering the amount of collateral damage caused by military operations.



The TKX-50 not only has outstanding stability and insensitivity, but it also has a strong energy output. Because of its high detonation velocity, it is well suited for uses that call for the release of a lot of energy in a short amount of time. Because TKX-50 has an energy content that is comparable to that of other powerful explosives, it can be employed either as the primary charge or as a booster in a variety of different types of ammunition and propellant formulations. The tremendous amount of energy that can be generated by TKX-50 makes it an appealing option for use in a variety of military applications, such as those involving explosive devices, warhead fillings, and missile propulsion systems.



*Figure 2.1 First cook off test of TKX-50 [11]*

In spite of the many benefits it offers, using TKX-50 also comes with a few drawbacks. Its susceptibility to moisture is one of the primary causes for concern. The TKX-50 has a propensity to absorb water, which has the potential to negatively impact both its stability and performance. Therefore, appropriate processes for both the handling and storage of the material need to be put into place in order to prevent the introduction of moisture and maintain the material's continued stability over time. In addition, TKX-50 is a recently developed energetic

compound, and the methods involved in its development and manufacture on a big scale are still in the process of being perfected.

In conclusion, TKX-50 is an intriguing candidate for an energetic material since it demonstrates excellent stability, insensitivity, and high energy output. Explosives, propellants, and pyrotechnics are just some of the applications that could benefit from its one-of-a-kind qualities, which make it an appealing choice for a wide variety of industrial and military uses. Because of its high energy content and compatibility with other materials, TKX-50 can be formulated in a wide variety of ways thanks to its remarkable stability and insensitivity. On the other hand, its outstanding stability and insensitivity make its handling and storage significantly more dangerous. TKX-50 has the potential to change the field of energetic materials and contribute to developments in a variety of industries if continuing research and development efforts are made. TKX-50 has the ability to revolutionize the field of energetic materials.

## **2.2 Classical Molecular Dynamics Forcefield for Energetic Materials**

Materials with a lot of energy, like explosives and propellants, are very important in many areas, such as the military, aerospace, and industry. To make safer and more efficient energy systems, it is important to know how these materials behave and what their qualities are at the atomic level. Classical molecular dynamics (MD) simulations have become a strong way to use computers to look into the movement and temperature of energetic materials. The choice of forcefield, which shows how the atoms in the system interact with each other, has a big impact on how accurate and reliable MD models are. This literature review aims to give a full picture of how classical MD forcefields are used in the context of energetic materials, with a focus on the results presented in the paper by Smith et al. [19].

Classical MD Forcefields for Energetic Materials: In classical MD, forcefields are mathematical representations of interatomic potentials that explain the forces and energies between atoms in a system. The properties of these forcefields are based on data from experiments and quantum mechanics. Over the years, scientists have made a number of forcefields that are used to study

energetic materials and try to correctly model their structural, dynamical, and thermodynamic properties.

In the work by Smith et al. [19], a better forcefield for energetic nitroaromatic materials is described. Nitroaromatic compounds are a group of materials that are known for having a lot of energy. The authors fixed the problems with current forcefields by adding new parameters and improving the ones that were already there. Their method was a mix of quantum mechanical calculations, optimization of molecular physics, and testing in the lab.

Smith et al.'s [19] forcefield did a good job of re-creating some of the most important features of nitroaromatic compounds. For example, the forcefield correctly forecast the density, the heat of formation, and the parameters of the crystal lattice. These properties are important for knowing how energetic materials stay stable, fit together, and act in general. The improved forcefield was also more accurate than past ones at predicting vibrational frequencies and lattice energies. This shows that the improved forcefield does a better job of capturing the complicated vibrational and lattice dynamics of nitroaromatic molecules.

The work by Smith et al. [19] shows how important it is to make forcefields that fit the unique properties of each type of energetic material. The authors were able to improve the accuracy and reliability of MD simulations for nitroaromatic compounds by adding new parameters and making changes to old ones. This new discovery helps us learn more about the basic properties and behaviors of energetic materials. This makes it possible to build and improve energetic systems in a more efficient way.

In addition to Smith et al.'s work, other studies have also helped create classical MD forcefields for energetic materials. The AMBER (Assisted Model Building with Energy Refinement) forcefield is a well-known one [19]. It was first made for biomolecular models, but it has since been used to study organic molecules like explosives. The AMBER forcefield uses both bound and non-bonded terms to describe how atoms interact with each other. It has been used a lot to simulate how energetic materials behave [10]. It has been used successfully to study a wide

range of explosive chemicals, and it has shown that it can accurately capture their structure and movement.

The CHARMM (Chemistry at Harvard Molecular Mechanics) forcefield is another well-known forcefield that is often used to study materials with a lot of energy [23]. The CHARMM forcefield was first made to simulate biomolecules. Now, it also has settings for studying materials with high energy. It uses both bound and non-bonded terms, and it has been used to study how explosives and propellants behave [3]. The CHARMM forcefield is a useful tool for learning about the properties and behavior of different explosive chemicals because it can be used in many different ways.

Research is still being done on making and improving standard MD forcefields for energetic materials [24]. Researchers are always looking for ways to make forcefields more accurate and reliable by adding new experimental and theoretical data. Refining forcefields is important for correctly predicting and understanding the structural, dynamical, and thermodynamic properties of energetic materials, which are needed for designing and optimizing safe and effective energetic systems.

In conclusion, classical MD models are a useful way to study the behavior and properties of energetic materials at the atomic scale. The choice of forcefield has a big effect on how accurate and trustworthy MD models are. In their work, Smith et al. [21] describe an improved forcefield for nitroaromatic energetic materials. They also talk about how important it is to have forcefields that are specifically made for the unique properties of these compounds. The forcefield does a good job of recreating key properties and is more accurate than earlier forcefields at predicting vibrational frequencies and lattice energies. In addition to the work done by Smith et al., forcefields like AMBER and CHARMM have been used a lot to study explosive materials. This shows how flexible and useful they are for a wide range of explosive compounds. Keeping up with research and development on forcefields will definitely help us learn more about energy materials and how to use them.

### **2.3 Previous works of TKX-50 and Shock sensitivity study of Energetic Materials**

In their work, An et al. [10] used large-scale molecular dynamics simulations to probe the anisotropic impact sensitivity and shock-induced plasticity of TKX-50 (Dihydroxylammonium 5,5'-bis(tetrazole)-1,1'-diolate) single crystals. The team wanted to know how the material reacted atomically to mechanical stress. Anisotropic impact sensitivity was seen in the TKX-50 specimens; that is, the response to impacts differed depending on the direction of the applied shock pressure, as shown by the study. Shock-induced plasticity, or the ability to undergo plastic deformation in the presence of high pressure, was also shown by the simulations. Understanding TKX-50's mechanical behavior and sensitivity is crucial for determining its safety and developing reliable energetic systems, and this study filled that knowledge gap.

Badgujar and Talawar [25] examined the thermal and sensitivity characteristics of TKX-50 (Dihydroxyl ammonium 5,5'-Bistetrazole-1,1'-diolate)-based melt cast explosive formulations. The objective of the study was to assess the thermal stability and sensitivity of TKX-50-based explosive compositions produced by melt casting. Various parameters, such as thermal behavior, decomposition kinetics, and sensitivity to impact and friction, were evaluated as part of the study. The study revealed that formulations containing TKX-50 exhibited excellent thermal stability, with high decomposition temperatures and low decomposition rates. In addition, the formulations exhibited enhanced sensitivity, exhibiting less sensitivity to impact and friction than conventional explosive formulations. These results demonstrated the potential of TKX-50-based melt cast explosive compositions as safer alternatives with increased stability and decreased sensitivity, paving the way for their potential implementation in explosive systems.

In their article titled "Fabrication of three-dimensional TKX-50 network-like nanostructures by liquid nitrogen-assisted spray freeze-drying method" (Cao et al., 2019) [26], the authors described a novel technique for fabricating three-dimensional nanostructures of TKX-50, an energetic material commonly used in military applications. Utilizing the spray freeze-drying technique aided by liquid nitrogen, they were able to rapidly freeze the TKX-50 suspension

while concurrently spraying it, resulting in the formation of highly porous and network-like nanostructures. Using scanning electron microscopy and X-ray diffraction, the morphological and structural properties of the fabricated TKX-50 nanostructures were confirmed. The investigation revealed that the newly developed method produced TKX-50 samples with superior thermal stability and detonation performance compared to those prepared using conventional methods. Due to their enhanced reactivity and stability, the findings of this study offer promising prospects for the application of TKX-50 nanostructures in numerous military and defense sectors.

The article titled "Effects of carboxymethylcellulose sodium on the morphology and properties of TKX-50, an insensitive high-energy explosive" by Dong et al. (2019) examined the impact of carboxymethylcellulose sodium (CMC-Na) on the morphology and properties of TKX-50 [27], an insensitive high-energy explosive. The researchers intended to improve the efficacy and safety of TKX-50 by modifying its properties with CMC-Na. The authors analyzed the effects of CMC-Na on the morphology, thermal behavior, and sensitivity of TKX-50 through a series of experiments and characterization techniques, such as scanning electron microscopy (SEM), differential scanning calorimetry (DSC), and impact sensitivity tests. The study revealed that the incorporation of CMC-Na altered the morphology of TKX-50 particles, enhanced thermal stability, and decreased impact sensitivity. Utilizing additives such as CMC-Na, these findings have implications for the creation of safer and more effective high-energy explosives.

The article by Dreger et al. (2017b) titled "High-pressure structural response of an insensitive energetic crystal: dihydroxylammonium 5, 5'-bistetrazole-1, 1'-diolate (TKX-50)" examined the structural response of TKX-50, an insensitive energetic crystal, under high-pressure conditions [28]. Researchers sought to comprehend the behavior of TKX-50 under extreme pressures in order to gain insight into its stability and possible applications. The authors analyzed the structural alterations of TKX-50 at various pressure levels through experimental research and computational simulations. According to the findings, TKX-50 exhibited a pressure-dependent phase transition, resulting in modifications to its crystal structure. The findings provide crucial

information regarding the structural response of TKX-50 under high-pressure conditions, which is essential for its practical efficacy and safety.

Fischer et al. (2012) contributed an article titled "TKX-50" to the Proceedings of the sixteenth seminar on novel trends in the study of energetic materials [11]. The authors discussed TKX-50, an energizing material, in light of recent research developments. Although the article lacks specific information about the content, it can be assumed that the authors discuss TKX-50's properties, synthesis, characterization, and potential applications. This article functions as a resource for researchers interested in TKX-50 and its significance in the field of energetic materials.

The article "Estimated detonation velocities for TKX-50, MAD-X1, BDNAPM, BTNPM, TKX-55, and DAAF using the Laser-induced air shock from energetic materials technique" by Gottfried and Witkowski (2017) estimated the detonation velocities of several energetic materials, including TKX-50, MAD-X1, BDNAPM, BTNPM, TKX-55, and DAAF [29]. To ascertain the detonation velocities of these materials, the authors utilized the Laser-induced Air Shock from Energetic Materials (LASEM) method. They obtained estimates of the detonation velocities, which are crucial parameters for comprehending the performance and behavior of these energetic materials, through their experimental investigations. The findings contribute to the understanding and characterization of these materials, providing valuable insights for their application in a variety of disciplines, including propellants, explosives, and pyrotechnics.

The article "Compatibility study of dihydroxylammonium 5, 5'-bistetrazole-1, 1'-diolate (TKX-50) with some energetic materials and inert materials" by Huang et al. (2015a) investigated the compatibility of TKX-50, an energetic material, with a variety of other energetic and inert materials [30]. The authors sought to evaluate the potential dangers and safety concerns associated with combining TKX-50 with various substances. Through their research, they examined the compatibility of TKX-50 with a variety of energetic and inert substances. The results provide insight into the stability and potential reactions of TKX-50 in the presence of

these substances. This study contributes to the comprehension of TKX-50's compatibility and aids in the secure handling and storage of the material for a variety of applications.

The article by Jia et al. (2019) titled "Stability of dihydroxylammonium 5, 5'-bistetrazole-1, 1'-diolate (TKX-50) in solvents" investigated the stability of TKX-50, an energetic material, in various solvents [31]. The authors sought to evaluate the compatibility and potential reactivity of TKX-50 when exposed to various solvents, a crucial aspect of its management and storage. They examined the stability of TKX-50 in a variety of solvents and evaluated factors such as dissolution behavior, thermal stability, and decomposition kinetics through experimental studies and analysis. The results contribute to a greater comprehension of the stability profile of TKX-50, shedding light on its safe handling and potential applications in various solvent systems.

The article "Shock-induced transformations in crystalline RDX: A uniaxial constant-stress Hugoniotat molecular dynamics simulation study" by Bedrov et al. examined the behavior of crystalline RDX (cyclotrimethylene trinitramine) under shock conditions [32]. The authors utilized molecular dynamics simulations with a uniaxial constant-strain Hugoniotat to investigate the shock-induced changes in RDX. They analyzed the structural alterations, phase transitions, and dynamic response of RDX during shock compression in their study. The simulations provided valuable insights into the molecular mechanisms of shock-induced transformations in RDX, casting light on the behavior and response of the material under extreme conditions. This research contributes to a greater comprehension of the shock dynamics of RDX, which is important for the design, development, and application of energetic materials.

The article "Shock-induced shear bands in an energetic molecular crystal: Application of shock-front absorbing boundary conditions to molecular dynamics simulations" by Cawkewell et al. investigated the phenomenon of shock-induced shear bands in an energetic molecular crystal [33]. Using molecular dynamics simulations, the authors focused on investigating the behavior of the crystal under shock conditions. To precisely capture the dynamic response of the crystal, shock-absorbing boundary conditions were implemented. Through simulations, the authors identified and analyzed the formation and properties of shear bands, which play a crucial role



in the deformation and failure of a material when subjected to stress. The research provides valuable insights into the mechanics of shock-induced shear bands in energetic molecular crystals, contributing to a deeper understanding of their behavior and facilitating the development of enhanced materials for a variety of applications.

The article titled "Hot spot formation and chemical reaction initiation in shocked HMX crystals with nanovoids: a large-scale reactive molecular dynamics study" by Zhou et al. examined the formation of hot spots and the initiation of chemical reactions in HMX (cyclotetramethylene tetranitramine) crystals with nanovoids that have been shocked [34]. Through large-scale simulations of reactive molecular dynamics, the authors investigated the behavior of HMX crystals under stress conditions. They were particularly interested in the function of nanovoids in promoting localized heating and initiating chemical reactions. The study provides beneficial insights into the mechanisms of hot spot formation and reaction initiation in energetic materials, allowing for a greater comprehension of their behavior under extreme conditions. The results contribute to the design and development of safer and more effective energetic materials for a variety of applications.

## CHAPTER 3

### BACKGROUND THEORY AND METHODOLOGY

#### 3.1 introduction

Computer simulations that make use of mathematical models play an important part in the process of comprehending complex systems and the characteristics that are inherent to them. These simulations are designed to properly depict the target system while being computationally practical by applying logical assumptions and simplifying approximations. This is accomplished through the use of logic [36]. Traditional experimentation, which frequently includes logistical problems and considerable financial inputs, is limited in comparison to the capabilities of simulations, which may accurately predict and model a wide range of events [35]. To this purpose, computer simulations provide an invaluable resource for carrying out sophisticated research without the costs associated with large-scale experimental setups. However, the accuracy and precision of simulations are strongly dependent on the quality of the underlying "force field," which contains the molecule's energy reaction to key events that are required for its optimal functioning [24]. This is necessary for the molecule to carry out its functions correctly. Sometimes, simplifications are used under certain assumptions in order to alleviate the difficulties involved with simulations. This is done in order to make certain that the core of the real-scale study is not undermined by these simplifications.

The use of mathematical models in computer simulations has given researchers the ability to study and investigate more complicated systems than was previously possible. This has led to the rise of computer simulations as an essential instrument for scientific research. This article examines the ubiquitous influence that computer simulations have had across a variety of academic fields. It focuses on the potential of computer simulations to provide insights and predictions that are frequently impossible or impractical to get through the use of traditional experimental methods.

Mathematical models serve as the basis for computer simulations, making the representation and analysis of a wide variety of different systems much easier. These models are intended to capture the basic traits and behaviors of the target system. This provides researchers with the opportunity to acquire vital insights into the mechanisms that lie behind the surface of the system.

In order to establish a simulation model's trustworthiness and correctness, validation of the model is an absolutely necessary step. This entails determining whether or not the model is capable of accurately describing the system that is the subject of the inquiry, using logical assumptions and simplified approximations as guides. In addition, because of the amount of computing power used to run these simulations, it is necessary to have models that strike a compromise between being easy to understand and being accurate.

Numerous scientific fields, such as physics, astrophysics, environmental science, genetics, biotechnology, climatology, and engineering, have grown to rely heavily on the results of computer simulations. Researchers are able to make accurate predictions and construct accurate models of a variety of phenomena by using the power of simulations. This paves the way for improvements in these domains that were previously unreachable through the use of traditional experimental methods.

The use of computer simulations helps to ease the challenges that are connected with the conduct of experiments, which are frequently difficult, expensive, or impossible due to the limits imposed by logistical considerations. Researchers are able to examine complex research problems without sacrificing accuracy or precision when using simulations as an alternative. Simulations provide an option that is both efficient and cost-effective.

When it comes to molecular simulations, the accuracy of the results is directly proportional to the quality of the "force field" that is used. These force fields provide a description of how the molecule responds energetically to important events that are critical to its correct operation.

When it comes to establishing accurate force fields and improving the fidelity of molecular simulations, having a full understanding of the underlying physics is absolutely necessary.

In the context of simulation modeling, simplifications and assumptions are common. In order to successfully navigate the nuances and complexities that are inherent to simulations, researchers frequently resort to simplifying and making assumptions. These improvements expedite the simulation process without compromising the fundamental components of real-scale analysis. As a result, difficult research issues can now be explored in a way that is both effective and practical.

Research in the scientific community has been profoundly impacted by the introduction of computer simulations, which provide an effective method for gaining an understanding of intricate systems across a wide variety of fields. Researchers are able to transcend the constraints of traditional experimentation and delve into complex research topics with precision and efficiency if they make use of mathematical models, validate their accuracy, and utilize computational feasibility.

The fields of computational mechanics and materials science have been significantly advanced thanks to developments in density functional theory (DFT), ab initio calculations, and molecular dynamics (MD) simulations. This is especially true in the field of research pertaining to the investigation of energetic materials. These computational tools provide extremely useful insights into the behavior, characteristics, and performance of materials on both the atomic and the molecular levels. Researchers are able to study the energetics and reactivity of energetic materials with surprising accuracy thanks to DFT's robust framework for predicting electronic structures and characteristics. DFT is provided by density functional theory (DFT). Calculations known as ab initio, which are founded on the fundamental principles of quantum mechanics, provide a comprehensive understanding of the underlying physics that governs these materials. In addition, MD simulations make it possible to investigate the dynamic behavior and structural changes of energetic materials over the course of time. This provides essential information that is necessary for building energetic materials and enhancing their performance. The

complementary nature of these computational approaches has been a driving force behind recent advances in the field, which has hastened the search for and development of novel energetic materials that have improved stability, sensitivity, and energy release characteristics. Because of this, computational mechanics and materials science have reaped significant benefits from these methods. As a consequence, researchers now have the ability to investigate intricate systems and direct experimental efforts in a manner that is both accurate and effective.

### **3.2 Density Functional Theory**

The density functional theory, also known as DFT, is a computational method that is widely used in the field of quantum mechanics. It offers an effective framework for comprehending the electronic structure and behavior of atoms, molecules, and solids, and it is one of the most popular methods in the field. Instead of depending on the wave functions of individual electrons like in standard wave function-based approaches, this method is based on the notion that the total energy of a system may be represented as a functional of the electron density. This is in contrast to methods that rely on the wave functions of individual electrons [35].

The electron density is the most important idea in density functional theory (DFT) [36]. It is a concept that represents the probability distribution of finding an electron in a specific region of space. DFT enables the calculation of numerous properties, such as total energy, atomic forces, and electronic structure, with exceptional accuracy and computing efficiency. This is accomplished by solving the Schrodinger equation for the electron density. Other properties that may be calculated using DFT include.

The Hohenberg-Kohn theorems are the building blocks upon which the Density Functional Theory (DFT) is constructed [37,38]. These theorems claim that the ground state features of a many-electron system are exclusively dictated by the electron density. These theorems state that the electron-electron interaction can be approximated by an effective potential that is referred to as the exchange-correlation potential. This potential takes into account both the repulsion that exists between electrons and the quantum mechanical exchange effects.

We can solve Schrodinger equation accurately upto one electron problem only. Schrodinger equation for Hydrozen atom is given below:

$$-\frac{\hbar^2}{2\mu} \left[ \frac{1}{r^2} \frac{\partial}{\partial r} \left( r^2 \frac{\partial \psi}{\partial r} \right) + \frac{1}{r^2 \sin \theta} \frac{\partial}{\partial \theta} \left( \sin \theta \frac{\partial \psi}{\partial \theta} \right) + \frac{1}{r^2 \sin^2 \theta} \frac{\partial^2 \psi}{\partial \phi^2} \right] - \frac{Ze^2}{4\pi\epsilon_0 r} \psi = E\psi \quad (3.1)$$

Here,  $\hbar$  is plank's constant,  $r$  is atomic radius,  $Z$  is atomic mass,  $E$  is total energy, and  $\psi$  is wave function. Therefore, some approximation and tricks are required when it comes to system with more than one electron, and in general we deal with systems which consist of many electron. To solve this issue Hohenburg-Kohn provided a theorem, "Electron density of any system determines all ground state property of a system. In this case the total ground state energy of a many-electron system is a functional of the density. So, if we know the electron density functional, we know the total energy of our system.

The main equations of DFT are the Kohn-Sham equations:

$$\left[ -\frac{1}{2} \nabla^2 + V_{ext}(r) + V_H(r) + V_{XC}(r) \right] \varphi_i(r) = \epsilon_i \varphi_i(r) \quad (3.2)$$

First term in (3.2) is kinetic energy term, second one is external potential, third one is Hartree potential, and fourth term in exchange correlation potential. Where the exchange-correlation potential is defined as

$$V_{XC} = \frac{\delta E_{XC}}{\delta n(r)} \quad (3.3)$$

Here,  $E_{XC}$  is exchange correlation functional. In any practical application of the theory, we have to use an approximation to  $E_{XC}$  or  $V_{XC}(r)$ .

Several different approximation approaches are used for the exchange-correlation functional while attempting to solve the equations governing the DFT. These approximations vary from the straightforward local density approximations (LDA) to the more complex gradient-corrected functionals (GGA) and beyond, taking into account both non-local effects and van der Waals interactions.

The capacity of DFT to accurately represent a wide variety of systems, ranging from solitary atoms and molecules to extended solids and surfaces, is one of the most significant benefits offered by this theory. It is possible to anticipate structural qualities, electronic band structures, reaction energies, and a wide variety of other physical and chemical features as a result of this. In addition, DFT has been utilized in a variety of domains, including as materials science, solid-state physics, chemistry, and even biology.

Despite its wide-ranging achievements, DFT is not without its shortcomings. The choice of exchange-correlation functional can have a sizeable effect on the accuracy of computations; yet, there is no one functional that can be used across the board for all different kinds of systems. In addition, it's possible that DFT has trouble adequately representing systems that have substantial electron correlation effects or open-shell systems.

There have been many other advanced variations of DFT developed in order to meet these issues. Some examples of these variants include hybrid functionals, which integrate a percentage of precise exchange, and time-dependent DFT, which permits the analysis of excited states and electronic transitions.

Overall, density functional theory has made significant contributions to the field of computational quantum mechanics. This is because it offers a method that is both flexible and effective for the investigation of the electronic structure and behavior of a diverse variety of systems. DFT is an essential instrument for comprehending and forecasting the behavior of atoms, molecules, and materials in a variety of scientific and technological domains due to the

breadth and depth of its applications as well as the ongoing improvements that have been made to it.

### **3.3 AB Initio Calculation**

AB Initio Calculation, also known as calculations from first principles, are computational methods that are used to examine the properties and behavior of atoms, molecules, and materials from fundamental physical principles, without relying on empirical data or experimental parameters. Ab initio calculations are also sometimes referred to as first principles calculations. The phrase "ab initio" comes from the Latin phrase "from the beginning" and draws attention to the fact that the methodology is based on the fundamental laws of quantum physics [41].

The solution of the Schrodinger equation, which defines the quantum behavior of electrons in a particular system, is the starting point in ab initio calculations. This equation is used to describe the behavior of electrons. Through the process of solving this equation, it is possible to acquire with a high degree of accuracy quantities such as electronic structure, energetics, forces, and other associated quantities.

The Born-Oppenheimer approximation is one of the fundamental ideas that underpin ab initio calculations. This approximation isolates the nuclear motions from the electronic motions of an atom. An assumption made by this approximation is that the motion of atomic nuclei is significantly slower than that of electrons. This makes it possible to determine the electronic structure of a substance while maintaining the same nuclear locations [42].

Calculations made from the very beginning are called ab initio calculations, and they involve the use of various numerical methods and approaches to solve the Schrodinger equation within a particular framework. The Hartree-Fock (HF) approach is a method that is extensively utilized. This method considers electrons to be independent particles and accounts for the effect of electron-electron repulsion by using the mean field approximation. The HF technique offers a decent starting point, but it does not take into account the consequences of electron correlation.



Methods of a more complex nature, such as post-Hartree-Fock techniques, are utilized when it is necessary to take electron correlation into account. Methods such as configuration interaction (CI), linked cluster (CC), and many-body perturbation theory (MBPT) are included in this category. These approaches take electron correlation into systematic consideration and have the potential to produce highly accurate findings; however, they are computationally more demanding.

The Hartree-Fock approximation is

$$\left[ -\frac{1}{2}(\nabla_1^2 + \nabla_2^2) - \frac{Z}{r_1} - \frac{Z}{r_2} + \frac{1}{r_{12}} \right] \psi = E\psi \quad (3.4)$$

The problem with solving equation (3.4) exactly arises from the  $1/r_{12}$  term which makes it impossible to separate the Schrodinger equation for helium into two-electron equations. The impossibility of an analytic solution to poly-electronic atoms and molecules prompted Hartree's approach to calculating wave functions and energy levels for atoms.

Hartree-Fock (HF) approximation is the simplest form of ab initio calculation [43]. The most obvious thing is to assume in this approximation that electrons move independently of each other. Hartree's method was to write a plausible approximate poly-electronic wave function (a "guess") for an atom as the product of one-electron wave functions [44]:

$$\psi_0 = \psi_0(1)\psi_0(2)\psi_0(3) \dots \dots \psi_0(n) \quad (3.5)$$

The function of equation (3.5) is called Hartree product. Here  $\psi_0$  is a function of the coordinates of all the electrons in the atom,  $\psi_0(1)$  is a function of the coordinates of electron 1,  $\psi_0(2)$  is a function of the coordinates of electron 2, etc.; the one-electron functions  $\psi_0(1)$ ,  $\psi_0(2)$ , etc. are called atomic orbitals (molecular orbitals if we are dealing with a molecule). The initial guess  $\psi_0$  is called zeroth approximation to the true total wave function  $\psi$ , as refinement has yet started.; it is based on the zeroth approximation  $\psi_0(1)\psi_0(2)\psi_0$ , etc.

Then we solve for one-electron Schrodinger equation in which the electron-electron repulsion comes from electron one and an average, smeared-out electrostatic field calculated from  $\psi_0(2)\psi_0(3) \dots \dots, \psi_0(n)$ , due to all the other electrons. The only moving particle in this equation is electron one. After solving this equation gives  $\psi_1(1)$ , an improved version of  $\psi_0(1)$ .

We next solve for electron 2, a one-electron Schrodinger equation with electron two moving in an average field due to the electrons of  $\psi_1(1), \psi_1(3), \dots, \psi_1(n)$ . Continuing to electron n moving in a field due to  $\psi_1(1), \psi_1(2), \dots, \psi_1(n-1)$ . This completes the first cycle of calculations and gives

$$\psi_1 = \psi_1(1)\psi_1(2)\psi_1(3) \dots \dots \psi_1(n) \quad (3.6)$$

Repetition of the cycle gives

$$\psi_2 = \psi_2(1)\psi_2(2)\psi_2(3) \dots \dots \psi_2(n) \quad (3.7)$$

This process is continued for k cycles till we have a wavefunction  $\psi_k$  and/or an energy calculated from  $\psi_k$  that are essentially the same (according to some reasonable criterion) as the wavefunction and/or energy from the previous cycle.

This happens when the functions  $\psi(1), \psi(2), \dots, \psi(n)$  are changing so little from one cycle to the next that the smeared-out electrostatic field used for the electron-electron potential has ceased to change. At this stage the field of cycle k is essentially the same as that of cycle k-1, i.e. it is “consistent with” the previous field, and so the Hartree procedure is called the self-consistent-field procedure, which is usually abbreviated as the SCF procedure.

Calculations done from ab initio, require a very specific choice of basis sets and numerical techniques in order to correctly describe wavefunctions and solve the equations that lie beneath

them. The orbitals and wave characteristics of the system are represented by the basis sets, which are comprised of a set of functions that are utilized to expand the wavefunction.

Calculations performed by ab initio calculation have become more useful in a variety of scientific and technological domains. The study of molecular properties, chemical processes, material properties, and surface phenomena are all common applications for these instruments. Calculations performed "from scratch" (abbreviated as "ab initio") can yield extremely specific information about the structure, stability, spectroscopic characteristics, and reaction mechanisms of molecules and materials.

Although ab initio calculations give exceptional precision, performing them requires a significant amount of computing power, particularly for more complex systems. Because of this, approximations and approaches that lower the computational complexity are frequently used in order to make calculations more viable for bigger systems. Some examples of these methods include truncation schemes and effective Hamiltonians.

Overall, ab initio calculations are strong computational methods that enable the examination of molecular and material properties from first principles, without relying on empirical evidence. This is made possible by the fact that ab initio calculations investigate from the ground up. Ab initio calculations, which include finding solutions to the fundamental equations of quantum mechanics, provide information that is both detailed and accurate regarding electronic structures, energetics, and other features. This knowledge contributes to a greater comprehension of the behavior and properties of atoms, molecules, and materials.

### **3.3.1 Self Consistent Field (SCF) method**

The iterative computing method known as the self-consistent field (SCF) method is a technique that is used to address the electronic structure issue in quantum mechanics [45,46]. In order to get a self-consistent solution for the electronic wavefunction and energy, it is utilized in many

different ways for the building of electronic devices, one of which is the Hartree-Fock (HF) method.

The following procedures are included in the SCF method:

The first step of the initialization process is selecting a group of trial wavefunctions or molecular orbitals (MOs). As a representation of the electronic wavefunction, these MOs are often built as a linear combination of basis functions [43,44], such as atomic orbitals. This type of combination is known as a linear combination of basis functions.

Constructing the Fock matrix: The Fock matrix is produced by making use of the MOs that are already available. The Fock matrix is formed by adding up the kinetic and potential energy operators for each electron. This allows the matrix to accurately represent the mean field that is produced by all of the other electrons.

In order to solve the equation for the eigenvalues, the Fock matrix is diagonalized, which results in the generation of a new set of MOs known as the canonical MOs. The occupied and virtual orbitals are the ones that correspond to these orthonormal MOs.

Calculating the electronic energy entails combining the contributions from the potential energy and the electron density into the total energy expression, which is based on the number of occupied MOs. This process determines the electronic energy, which is then used to do calculations.

A convergence check is performed by contrasting the most recently obtained MOs with the MOs from an earlier collection. The calculation is regarded to have converged when the difference between matching MOs is less than a convergence criterion that has been specified beforehand. If this is not the case, the iteration process will continue by returning to step 2.

After the MOs have converged, the electronic energy has been reduced to its minimum, and the self-consistent solution has been attained. The MOs that were produced as a result are, within the bounds of the selected basis set and level of theory, the most accurate representation of the genuine electronic wavefunction.

After that, the SCF method is utilized in more complex electronic structure methods, such as post-Hartree-Fock approaches (for example, configuration interaction, coupled cluster theory), in order to construct upon the initial HF solution and incorporate electron correlation effects.

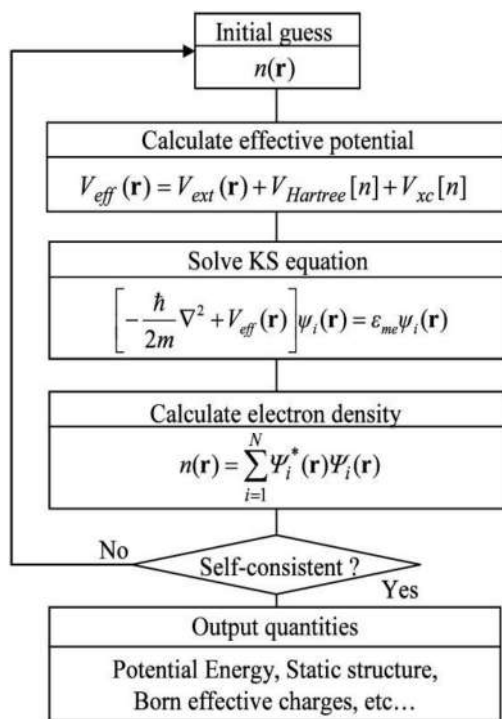


**Figure 3.1** Flow chart of solving Kohn Sham Equation with Self Consistent Field (SCF) method [58]

Overall, the SCF approach is an iterative procedure that seeks to achieve self-consistency between the electronic wave function and the mean-field formed by the electrons. This self-consistency between the two is the end goal of the SCF method. It makes it possible to arrive at an approximation of a solution to the problem of the electronic structure, and it offers vital insights into the characteristics and actions of atoms, molecules, and materials.

### 3.3.2 Post Self Consistent Field Method

Post-self-consistent field methods, also known as post-SCF methods, are more advanced computational approaches that are used to improve upon the results received from the initial calculation of a self-consistent field (SCF). The purpose of these methods is to provide a more accurate representation of the electronic structure by including electron correlation effects, which are omitted in the SCF calculation [49]. The second-order Møller-Plesset perturbation theory, also known as MP2 for short, is a post-SCF approach that is very common [46].

The MP2 approach is a perturbative technique that considers the electron correlation to be a minor disturbance to the wavefunction and energy of the SCF. The Rayleigh-Schrodinger perturbation theory, on which it is based, extends the entire wavefunction and energy as a power series in the perturbation parameter. This theory was developed by John Rayleigh and Erwin Schrodinger.

The following procedures are included in the MP2 method:

1. Calculation of the SCF: The calculation of the SCF is carried out so that an initial estimate of the electronic wavefunction and energy can be obtained. In order to accomplish this, you will need to solve the self-consistent field equations, as was discussed earlier.
2. The perturbation Hamiltonian is a model that takes into consideration the effects of electron correlation and is developed as such. It is obtained by first taking the actual electronic Hamiltonian and then subtracting the HF (SCF) Hamiltonian from it.
3. The electronic wavefunction and energy are extended as a power series inside the perturbation parameter. This is referred to as the "perturbation expansion." The electron-electron repulsion term is the perturbation parameter in MP2, and it is used to illustrate the correlation effects.

4. Terms of the second order: The MP2 algorithm only takes into account terms of the second order or higher in the perturbation parameter. The evaluation of two-electron integrals and the contraction of the perturbation operators using the occupied and virtual orbitals obtained from the SCF calculation are required for the second-order terms.

5. Correction to the energy level Using the second-order terms, one can compute the energy level adjustment that is caused by electron correlation. In order to calculate the MP2 energy, the SCF energy and this adjustment are combined.

6. Correction of the wavefunction: The terms of the second order also make a contribution to the correction of the electronic wavefunction. For the purpose of obtaining the MP2 wavefunction, this adjustment is applied to the MO coefficients that were acquired through the SCF calculation.

Calculations using the MP2 algorithm involve a computing cost that, in most cases, increases as the fourth power of the system size. This makes MP2 algorithms computationally demanding for use with large systems. The fact that MP2 strikes a healthy balance between the amount of processing it requires and the precision it delivers has led to its widespread adoption for medium-sized systems.

It is essential to keep in mind that the MP2 approach is a perturbative one, and it works under the assumption that the perturbation parameter, also known as the electron-electron repulsion term, is relatively modest. Therefore, systems with substantial electron correlation effects, such as transition metal complexes or systems with significant charge transfer, may not be suited for the MP2 method.

In conclusion, the second-order Møller-Plesset perturbation theory, also known as MP2 for short, is a post-SCF technique that incorporates electron correlation effects by considering them as a perturbation to the SCF wavefunction and energy. Calculations based on the MP2 approach have been found to be more accurate than those based on the SCF method. These calculations

are frequently utilized for medium-sized systems in which strong electron correlation effects do not predominate.

### **3.3.4 Basis Functions**

The wavefunctions of electrons in a molecule or atomic system can be approximated by ab initio calculations using basis functions. These calculations are called ab initio computations. The spatial distribution as well as the behavior of the electrons can be described using this collection of mathematical functions that are formed from these basis functions [47]. They are an extremely important factor in establishing the correctness as well as the effectiveness of the calculations. Calculations performed from scratch involve several distinct varieties of basis functions, including the following:

Calculations in quantum chemistry frequently make use of something called Gaussian-type Orbitals (GTOs), which are a form of basis function. A Gaussian function and an angular component form the basis of their mathematical representation as a product. GTOs have the benefit of being mathematically well-behaved and efficiently integrable, which enables faster calculation. This advantage allows GTOs to be used in a variety of applications. However, in order to produce correct results, it may be necessary to use a greater number of basis functions than is the case with other kinds of basis functions.

Orbitals of the Slater type, also known as STOs, are another sort of basis function that is utilized in ab initio calculations. They are modeled theoretically as a single exponential function that has an exponential decay as well as an angular component. In comparison to GTOs, STOs feature properties that are more physically understandable; yet, because it is more difficult to integrate them, STOs are less efficient from a computational standpoint.

Plane Waves: Plane waves are a type of periodic basis function that is frequently utilized in the calculation of solid-state systems. They are able to characterize the behavior of electrical systems that operate in periodic patterns and are shown as complicated exponential functions



that include wavevectors. Computations requiring periodic boundary conditions and computations of band structure lend themselves particularly well to the application of plane wave basis sets. However, in order for them to effectively represent localized electron concentrations, they require a high number of basis functions, which causes them to be computationally expensive.

**Atomic Orbitals** Certain types of calculations can benefit from the utilization of atomic orbitals as basis functions. Some examples of atomic orbitals include the s, p, d, and f orbitals. They offer a picture of the behavior of electrons near individual atoms that is simpler and easier to understand. Atomic orbital basis sets have widespread application in molecular orbital theory as well as in molecular computations, both of which need an accurate description of the localized electron density surrounding atoms.

The choice of basis functions is determined by a number of different criteria, such as the level of accuracy that is sought, the scale of the system, the computational resources that are readily available, and the nature of the problem that is being investigated. When working with bigger and more flexible basis sets, it is often possible to produce more accurate findings; however, this comes at the expense of increasing computing requirements. To achieve more precise results from one's computations, it is possible to gradually enlarge basis sets by include additional basis functions.

In actuality, many ab initio calculations use basis sets that are composed of a combination of multiple types of basis functions. For example, the blend of GTOs and STOs with varying exponents and angular momentum values is an example of such a basis set. These composite basis sets, also referred to as basis set families, offer a compromise between accurate representation and efficient use of computational resources

In a nutshell, basis functions are mathematical functions that are utilized in the process of ab initio computations. These functions are employed to estimate the wavefunctions of electrons. They are available in a variety of forms, including Gaussian-type orbitals, Slater-type orbitals,

plane waves, and atomic orbitals, and each variety has a unique set of benefits and drawbacks. The particular requirements of the computation as well as the characteristics of the system that is being researched should direct the selection of the foundation functions [48].

In our study we have used the aug-cc-pvDz basis set. It is a member of the family of correlation-consistent basis sets with polarization and diffuse functions known as cc-pVXZ, where X indicates the level of electron correlation that was taken into account in the calculation. The word "aug" in aug-cc-pvDz stands for "augmented," which refers to the incorporation of additional diffuse functions to more accurately model the behavior of electrons across extended distances.

To be more specific, the aug-cc-pvDz basis set is comprised of the following three components:

*Core-valence correlation (cc-pVXZ):* The cc-pVXZ component of the basis set gives an accurate description of the electron correlation effects that occur between the core electrons and the valence electrons in a molecule. It contains many basis functions for each type of atomic orbital (s, p, d, etc.), and its accuracy improves as X grows.

*Polarization functions (pVXZ):* The polarization functions take into account changes in electron density that are caused by the presence of additional atoms or interactions between electrons and electrons. They make it possible for the electron cloud that surrounds atoms to be flexible, which in turn enables a more precise representation of the properties of molecules.

*Diffuse functions (DZ):* The diffuse functions in the aug-cc-pvDz basis set were included so that the behavior of electrons that are placed a great distance from the nucleus may be accurately modeled. These functions take into consideration the long-range effects of electron density, which are especially significant when modeling systems that contain charged species, big molecules, or interactions that are not very strong.

The addition of polarization functions and diffuse functions to the aug-cc-pvDz basis set improves the set's ability to accurately characterize the properties of molecules, particularly in the case of systems that have a considerable amount of electron correlation and long-range interactions.

### **3.4 Force Field Parameterization**

The parameters of a force field model can be determined using a process known as force field parameterization, which is derived from ab initio calculations. In molecular dynamics simulations and other forms of computational research, as well as in everyday life, the concept of a "force field" refers to a simplified mathematical representation of the interactions that occur between the atoms or molecules that make up a system.

In most cases, the following procedures are required to complete the process of force field parameterization:

System selection is the initial phase in the process, and it entails choosing the particular system that will have the characteristics of the force field determined for it. This might be a molecule, a substance, or even a more complicated system.

*Ab initio calculations:* In order to do electronic structure calculations for the selected system, ab initio approaches, such as density functional theory (DFT) or coupled cluster theory, are utilized. These computations provide correct information about the electronic structure, energetics, and forces by offering a solution to the Schrodinger equation, which starts from basic principles.

*Attaining Potential Energy Surface (PES),* or ground state energy level of the molecular system. Information regarding the forces that are acting on the atoms and the stability of various configurations can be obtained from the PES.

A force field model that is appropriate for the system under inquiry is selected. This step is known as the selection of the force field model. The mathematical equations that make up force field models often explain the interactions between atoms or molecules. These interactions can include bond stretching, angle bending, torsional rotation, and nonbonded interactions.

Adjustments are made to the parameters of the force field so that they can accurately recreate the results that were obtained from the ab initio calculations. The energy, forces, and other parameters acquired from the ab initio calculations need to be matched up with those predicted by the force field model at this point.

*Optimization:* To repeatedly enhance the force field parameters, various optimization techniques, such as least-squares fitting or genetic algorithms, may be utilized. Finding a set of parameters that minimizes the disparities between the findings obtained from ab initio calculations and the predictions made by the force field model is the purpose of this endeavor.

*Validation and improvement:* The parameterized force field is validated by comparing its predictions to either experimental data or computations that are more accurate, if any are available. In order to increase the force field's accuracy and dependability, further adjustments or refinements could be made to it depending on the findings of the validation.

It is essential to keep in mind that the process of force field parameterization based on ab initio calculations is a difficult endeavor. It may be required to use simplifications or approximations in order to make the process practicable due to the high computing cost associated with ab initio calculations, which are especially problematic when applied to large systems [20,21]. In addition, force fields are empirical models, which means that they automatically include some amount of approximation and may not capture all of the complexity of the system they are describing.

However, force field parameterization through the use of ab initio calculations is a useful method for developing accurate force field models. These models may be utilized to simulate

and investigate the behavior of complex systems in molecular dynamics simulations as well as other computational investigations.

### **3.5 Population Methods for Estimating Partial Atomic Charges**

In many different simulations and calculations involving molecules, estimating the partial atomic charges is a step that is required. In order to assign partial charges to the atoms that make up a chemical system, one can use any one of a number of distinct population analysis approaches. These techniques are designed to divide the total charge of the molecule among its constituent atoms in a manner that is reflective of the individual atoms' contributions to the electronic structure and chemical properties of the molecule as a whole. The following are some ways of population that are regularly used:

**Analysis of the Mulliken Population** The Mulliken population analysis gives atoms their partial charges based on the electron density distribution that is derived from quantum mechanical calculations [51]. The atomic charge is determined by dividing the electron density of linked atoms using the overlap of their respective atomic orbitals as the basis for the calculation.

The Hirshfeld Population Analysis is a more contemporary method that assigns partial charges based on the electron density that is acquired from quantum mechanical calculations [52]. This method was developed by Hirshfeld. It does this by employing the idea of the Hirshfeld surface, which divides the electron density into different parts dependent on the distance that each point on the surface is from the closest atomic nucleus.

Natural Population Analysis (NPA) is a technique that seeks to assign charges in a manner that is congruent with the natural atomic populations present in a molecule. This congruence is the end goal of the Natural Population Analysis technique [53]. In order to determine the atomic charge distributions, this method requires performing a linear transformation on the molecular orbital coefficients acquired from the quantum mechanical calculations.

ESP Methods of Charge Equilibration methods apply partial charges to a system in a way that minimizes the amount of electrostatic potential energy it possesses [54,55]. In order to distribute charges in a manner that is internally consistent, these approaches take into account the connectivity and shape of the molecular system.

RESP, which stands for "Restrained Electrostatic Potential," is a method that is frequently used in the parameterization of force fields for biomolecular simulations. RESP was developed by the University of Maryland [56]. It entails fitting partial atomic charges to replicate the electrostatic potential resulting from quantum mechanical calculations, with extra restrictions being added to ensure smooth charge distributions. This is done with the intention of producing an accurate representation of the electrostatic potential.

Electronegativity Equalization Method (also known as EEM): The EEM is predicated on the idea of electronegativity equalization, which states that atoms in a molecule will change their charges in order to produce electronegativities that are comparable to one another [57]. Charges are assigned to atoms in a molecule according to their electronegativity and the degree to which they are connected to other atoms.

These are just a few examples of the several population approaches that can be used to estimate partial atomic charges. There are many more. Each approach has a unique set of benefits, drawbacks, and assumptions, and the selection of a method is contingent on the particular requirements of the investigation or simulation that is being carried out. Due to the fact that they are simplifications of the actual electronic structure of a molecule, it is essential to keep in mind that partial atomic charges are merely model parameters, which means that their interpretation requires extreme caution.

In this study we have used electrostatic potential (ESP) method for generating partial atomic charges for the TKX-50 molecule.

### **3.5.1 Electrostatic Potential (ESP) Method:**

The electrostatic potential (ESP) method is a common strategy that is utilized for the purpose of determining the partial atomic charges that are present in molecular systems. It does this by making use of the information that is gained from the electrostatic potential of the molecule in order to assign charges to specific atoms. The electrostatic potential at the surface of a molecule is assumed to have a direct correlation to the charge distribution within the molecule by the ESP technique, which operates under the presumption that this relationship exists [54,55].

The following procedures are included in the ESP method:

**Calculation Utilizing Quantum Mechanics** In order to determine how the electrons are distributed throughout the molecule, a calculation using quantum mechanics is carried out. In most cases, this is accomplished by the use of strategies like the density functional theory (DFT) or the Hartree-Fock theory.

**Electrostatic Potential Calculation:** The molecule electrostatic potential is determined by using the electron density distribution that was acquired from the quantum mechanical calculation. The electrostatic potential is the potential energy that would be encountered by a positive test charge if it were to be positioned at a number of different sites in close proximity to the molecule.

**Assignment of Charges** The electrostatic potential is utilized in the process of assigning partial charges to the individual atoms that make up the molecule. This is accomplished by adjusting the electrostatic potential so that it corresponds to the charges that are carried by the atoms and then optimizing the charge distribution in order to reduce the amount of variance that exists between the calculated potential and the fitted potential.

**Optimization of Charges:** In order to achieve a greater degree of congruence between the predicted and measured electrostatic potentials, the assigned charges are subjected to a process

of iterative refinement known as optimization. In order to fine-tune the charges, one may make use of a wide variety of optimization strategies, such as least-squares fitting or charge equilibration approaches.

The ESP approach offers a number of potential benefits. Because it establishes a clear connection between the electrostatic potential of molecules and the partial atomic charges, it is both physically obvious and straightforward to understand how it works. The charges that are produced through the use of the ESP method are transferable, which means that they can be employed in a variety of different molecular settings without requiring major readjustment.

Nevertheless, it is essential to keep in mind that the ESP method does have a few restrictions. It disregards factors such as polarization and charge transfer, assuming instead that the charge is distributed in a manner that is unchanging and nonpolarizable. The quality of the quantum mechanical computation, the basis set that is applied, and the precision of the electrostatic potential fitting operation all contribute to the level of accuracy that may be achieved using the ESP approach.

In conclusion, the ESP method is a strategy that is utilized frequently in order to estimate the partial atomic charges present in molecular systems. Assigning charges to individual atoms is accomplished by the utilization of the molecular electrostatic potential that is generated from quantum mechanical computations.

### **3.6 ORCA**

In this study ORCA was used as primary ab initio calculation tool where all the SCF and post SCF calculations for geometry optimization and geometry scanning were done.

The Open Roothan Chemistry program, also known as ORCA, is a calculating tool for quantum chemistry that is both flexible and potent as a piece of software. It provides a wide variety of computational approaches for researching the electrical structure of molecules as well as their



properties [58]. ORCA offers precise computations at multiple levels of theory thanks to its support for both density functional theory (DFT) and wavefunction-based approaches. These methods include Hartree-Fock, Moller-Plesset perturbation theory, and coupled-cluster theory. It includes a broad variety of basis functions, including those with polarization and diffuse functions, which enables precise representation of electron correlation and long-range interactions. These functions include those with polarization and diffuse functions.

*SCF Method:* This is a popular numerical iterative method for solving Schrodinger equations, where electron-electron correlation effect is not considered.

*Moller-plesset perturbation theory:* This is post SCF method, where electron-electron correlation effect is introduced by perturbing some ground state electrons to excited states.

*Basis Functions/sets:* They are sets of trial functions which are used to solve the complex shrodinger equations by numerical approach.

ORCA is a valuable tool for researching molecular characteristics, reaction mechanisms, and solvent effects since it provides capabilities for spectroscopic calculations, reaction route investigation, and solvation modeling. ORCA is a popular choice among academics working in the field of computational chemistry due to its user-friendly graphical interface, powerful visualization features, and effective parallelization for high-performance computing. In addition, ORCA is able to support a wide variety of applications in both the academic and industrial sectors.

### **3.7 MultiWfn**

Partial atomic charges were calculated in MultiWfn tool using the out put data from ORCA tool [59]. For the purpose of analyzing wavefunction files in quantum chemistry, the powerful and flexible software package known as Multiwfn is utilized. It offers a wide variety of functions and may be used with a number of different quantum chemistry software packages, one of

which being ORCA. Multiwfn's capacity to create partial atomic charges for a molecular system based on output files obtained from ORCA calculations is one of the program's most impressive features. These output files are obtained from the calculation program.

The actions listed below must be carried out in order for partial atomic charges to be generated by using Multiwfn:

1. In order to get ready, make sure that you have the output file from the ORCA calculation (for example, a file ending in.out or.gbw) which contains the information on the wavefunction of the system.
2. Open Multiwfn and load the ORCA output file before beginning the launch of Multiwfn.
3. Calculating the Partial Atomic Charges To calculate the partial atomic charges, use the "Charge Analysis" option found in the Multiwfn program. This choice gives users access to a variety of charge analysis methods, some of which are the Mulliken population analysis, the Hirshfeld population analysis, the Natural population analysis (NPA), and the Merz-Kollman population analysis. Choose the approach that best suits your needs to compute the partial atomic charges.
4. Set the output options to specify the format and location for recording the calculated partial atomic charges. This is done under the "Specify Output" heading.
5. Start the computation in Multiwfn to generate the partial atomic charges based on the specified analytical method, and then press the "Execute Calculation" button. The required calculations will be carried out by the software, and the results will be sent in accordance with your specifications.

Overall, Multiwfn is a useful tool that can supplement ORCA computations by giving additional analysis capabilities. These capabilities include the production of partial atomic charges, which is only one example. Both the comprehension of molecular systems and the interpretation of the results of quantum chemistry are improved as a result of this.

### **3.8 Avogadro**

Avogadro is a sophisticated quantum chemistry tool that gives scientists and researchers access to a wide variety of computational resources for investigating molecular systems. This program, named after the great Italian chemist Avogadro, is a quantum mechanical toolkit for investigating and analyzing molecules and their properties, processes, and structures [58].

Avogadro's capacity to display molecular structures in three dimensions is one of its most notable qualities. It has a simple and straightforward interface that anyone can pick up and use to form molecules by rearranging atoms and bonds and viewing the results in real time. The software is compatible with many other computational chemistry tools since it supports a large variety of molecular file types.

Multiple high-powered computing engines dedicated to quantum chemistry calculations are also included in Avogadro. Molecular mechanics, semi-empirical approaches, and ab initio methods such as Hartree-Fock theory and density functional theory (DFT) are only some of the computational methods it supports. Scientists can use these computations to learn about the molecular structure, including its energy level, electron distribution, orbital configuration, and vibrational frequency.

Avogadro's suite of analysis tools includes graphical representations of structures and quantum chemical computations. Surfaces, electrostatic potentials, and molecular characteristics such as dipole moments and polarizabilities can all be calculated. The software also gives capabilities for doing molecular dynamics simulations, improving molecular geometries, and studying

reaction processes. Because of these capabilities, Avogadro can be used to investigate many facets of complex molecular systems.

Avogadro's open-source nature and thriving development community have helped it earn widespread acceptance in the scientific world. This makes it possible for researchers to tailor the program to their own needs. Avogadro also works well with other computational chemistry software, allowing for streamlined processes and increased opportunities for teamwork.

Together, Avogadro's molecular imaging, computational engines, and analytical capabilities make it a powerful quantum chemistry instrument. It allows scientists to get vital insights into the behavior and properties of molecules through quantum-level investigation and analysis.

### **3.9 Molecular Dynamics Simulations**

The Newton's equation of motion and the rules of classical mechanics are numerically solved for each particle at each time step in molecular dynamics. The following time evolution of the system may be accurately predicted for the initial locations and velocities of all the particles in the simulation region [62]. In more visual terms, when the atoms move around the simulation area and collide with one another, Newton's law is used to calculate the acceleration of each particle based on the force exerted on it by other atoms in the system. The velocity and new position of each particle are then determined at each time step by numerically integrating their acceleration. The velocity and position of each particle are used to compute the temperature and all other system parameters, including potential and kinetic energy.

### 3.9.1 General Procedure of Molecular Dynamics Simulation

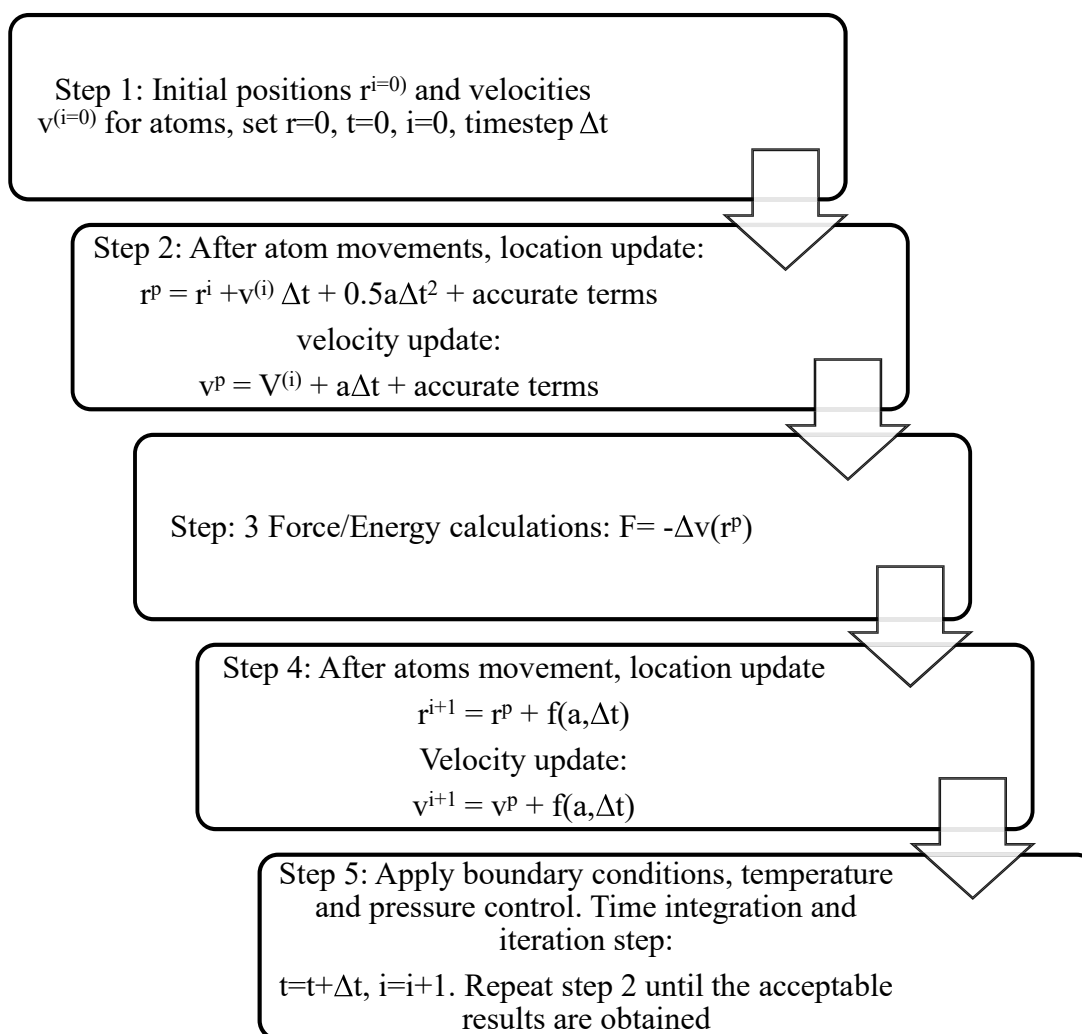


*Figure 3.2 Schematic diagram of a basic MD simulation*

### **3.10 Equilibrium Molecular Dynamics and Non-Equilibrium Molecular Dynamics**

In Equilibrium Molecular Dynamics Simulation, the system must be equilibrated thermodynamically [60,61]. A first sign that the system is in equilibrium is that it has a convergence of some parameters like energy, pressure or temperature depending on the simulation ensemble. In Non-equilibrium Molecular Dynamics Simulation, the system is generally evolving after a perturbation. EMD is statistical mechanics-based method. With a view to having a better understanding of EMD, it is necessary to introduce very important concept of ensemble. An ensemble is a collection of all possible system which has different microscopic state but have an identical macroscopic or thermodynamic state. Several ensembles are used to perform the MD simulations. The constant NVE ensemble also called micro-canonical ensemble, has  $N$  particles in volume  $V$  and the total energy  $E$  is a constant.

Besides, the constant- NPT ensemble has  $N$  particles with a constant pressure  $P$  and a temperature  $T$ . The constant-NVT ensemble has a constant particle number  $N$ , a volume  $V$  and a temperature  $T$ . It would be quite difficult to perform MD simulations in ensembles other than the canonical due to the difficulty to maintain the MD simulations at either a constant temperature or a constant pressure [61]. Two probable solutions of this problem have been proposed. The first solution is based on the idea that dynamical simulation of other ensembles is possible by mixing Newtonian MD with certain MC moves. The second approach is completely dynamical in origin: it is based on a reformulation of the Lagrangian equations of motions of the system. The Nose equations of motions have been further simplified by Hoover with real-variable formulation. The Nose scheme in the formulation of Hoover is the commonly used Nose- Hoover thermostat. However, for solids, the Nose-Hoover thermostat can lead to problems, which are solved by so-called Nose-Hoover chains. In the same spirit, the Nose-Hoover barostat can be formed to maintain constant pressure [60]. For NEMD simulations, non-translational kinetic energy (heat) is added to a group of atoms while the same amount of heat is subtracted from another group of atoms to establish a temperature gradient across a simulation domain while the total energy of the system is conserved.

NEMD method is also known as “the direct method” because it is directly analogous to the way thermal conductivity is measured experimentally in macroscopic materials. Two different approaches have been taken to create the non-equilibrium heat transfer conditions: imposing a temperature difference to calculate the heat flux or imposing a heat flux to calculate the resulting temperature distributions [60]. The key issue is how to impose the hot and cold reservoirs. NEMD, like EMD depends on time-reversible equations of motion, Newton’s equation. In context of equilibrium molecular dynamic, non-equilibrium molecular dynamics is just another mean of computing transport coefficient. NEMD simulation also has a better efficiency in calculation.

### **3.11 Buckingham Potential**

In theoretical chemistry, the Buckingham potential is a formula proposed by Richard Buckingham which describes the Pauli exclusion principle and van der Waals energy for the interaction of two atoms that are not directly bonded as a function of the interatomic distance  $r$ . It is a variety of interatomic potential [61].

Observing Figure 3.3 Let's say there is no force acting on the two rubber balls and they are separated by a great distance. Due to their great distance from one another, there is no force acting between them in the first condition. Now, as the two balls move in close proximity to one another, they will interact. Once they are gathered, an attractive force will begin to unite them. The two things will be quite close together thanks to this force of attraction. They will eventually come to an equilibrium distance and the lowest bonding potential. The balls will merge if the gaps between them are reduced still further, at which point repulsive force will begin to operate. The balls will separate due to this repellent force. The Buckingham potential is the ideal way to describe this kind of phenomenon because it applies to neutral atoms and molecules as well.

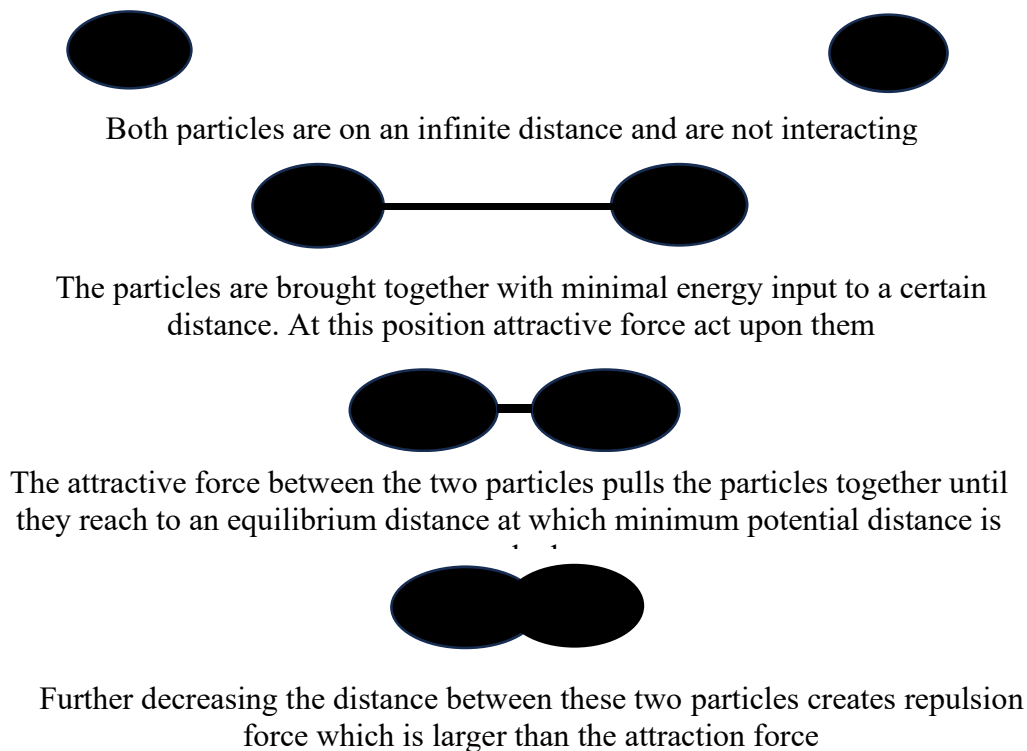


**Figure 3.3** Particle's interaction according to Buckingham model

The Buckingham Potential is given by the following equation:

$$\Phi_{12}(r) = A \exp(-Br) - \frac{C}{r^6} \quad (3.9)$$

Here, A, B and C are constants. The two terms on the right-hand side constitute a repulsion and an attraction because their first derivatives with respect to r are negative and positive, respectively.

As explained in Buckingham's original paper [81], the repulsion is due to the interpenetration of the closed electron shells. "There is therefore some justification for choosing the repulsive



part as an exponential function”. The Buckingham potential has been extensively used in molecular dynamics simulation.

Because the exponential term converges to a constant as  $r$  towards 0, while the  $r^{-6}$  term diverges, the Buckingham potential becomes attractive as  $r$  becomes small. This may be problematic when dealing with very short interatomic distances, as any nuclei that cross a certain threshold will become strongly bonded to one another at a distance of zero.

### **3.12 Cut-off Radius**

The force calculation is the most rigorous step in a molecular dynamics simulation since force on each atom  $i$  by all other  $N-1$  atoms in the simulation domain is calculated. Moreover, at each time step the force on each and every atom from all remaining atoms in the simulation domain has to be calculated. The force calculation grows as  $O(N^2)$  in a molecular dynamics simulation of  $N$  atoms. In order to save some computation time, a cut-off radius,  $r_{\text{cut off}}$  is used and for atom  $i$  the interaction by atoms which fall outside a sphere of radius,  $r_{\text{cut off}}$  is neglected. Commonly used cut-off radius for Lennard-Jones potential is  $2.5\sigma - 3.2\sigma$  [62]. The definition of  $\sigma$  is defined in article 3.11.

### **3.13 Integration of Equations of Motion**

At every time step, the force on each atom is calculated and then using Newton’s law, the acceleration of the particle is calculated. At each time step equation of motion for each atom is then integrated numerically to find their velocities. The velocities are used to advance the atoms and their new positions are calculated by numerically integrating the velocities. A good integration algorithm should have the following characteristics:

1. Small propagation error (allowing large time step)
2. Small velocity propagation error
3. Time reversibility
4. Energy conservation

Some of the time integration algorithm schemes which are frequently used in MD simulation are discussed below:

### 3.13.1 Verlet Algorithm:

In this simple integration scheme [70], position of atoms at  $t + \Delta t$  is calculated based on the current positions,  $r(t)$  and forces,  $F(t)$  and the previous positions,  $r(t - \Delta t)$ . From the Taylor series expansion for  $r(t + \Delta t)$  and  $r(t - \Delta t)$  are:

$$r(t + \Delta t) = r(t) + \Delta t v(t) + 0.5 \Delta t^2 a(t) + \dots \quad (3.10)$$

$$r(t - \Delta t) = r(t) - \Delta t v(t) + 0.5 \Delta t^2 a(t) + \dots \quad (3.11)$$

Summing these two equations yield,

$$r(t + \Delta t) \approx 2r(t) - r(t - \Delta t) + \Delta t^2 a(t) \quad (3.12)$$

The estimation of the new position contains an error that is of order  $\Delta t^4$ , where  $\Delta t$  is the time step in MD scheme. Once the trajectory is known, the velocities can be derived using the following equation:

$$v(t) = \frac{r(t + \Delta t) - r(t - \Delta t)}{2\Delta t} \quad (3.13)$$

This expression contains an error that is of order  $\Delta t$ .

### 3.13.2 Leap-Frog Algorithm

To obtain both the positions and velocities from readily available quantities, the leap-frog scheme can be applied. The equations are:

$$v\left(t + \frac{\Delta t}{2}\right) = v\left(t - \frac{\Delta t}{2}\right) + \Delta t a(t) \quad (3.14)$$

$$r(t + \Delta t) = r(t) + v\left(t + \frac{\Delta t}{2}\right) \Delta t \quad (3.15)$$

The velocities are updated at half time steps and ‘leap’ ahead the positions. The current velocities can be obtained from the following equation.

$$v(t) = \frac{v\left(t + \frac{\Delta t}{2}\right) + v\left(t - \frac{\Delta t}{2}\right)}{2} \quad (3.16)$$

### 3.13.3 Velocity-Verlet Algorithm

An algorithm that yields the positions, velocities and forces at the same time is given by the Velocity-Verlet scheme [62]. After calculating the force acting on each atom  $i$  from the potential function, using the acceleration, the position and velocities are obtained via the integrator method for time  $t + \Delta t$ . The positions and velocities are updated according to the following equations:

$$r(t + \Delta t) = r(t) + \Delta t v(t) + \left(\frac{1}{2}\right) \Delta t^2 a(t) \quad (3.17)$$

$$v(t + \Delta t) = v(t) + \left(\frac{1}{2}\right) [a(t + \Delta t)] \Delta t \quad (3.18)$$

Firstly, the new positions at time  $t + \Delta t$ , are calculated. After that, the velocities are calculated at half step using:

$$v\left(t + \frac{\Delta t}{2}\right) = v(t) + \left(\frac{1}{2}\right) a(t) \Delta t \quad (3.19)$$

The forces and accelerations are then calculated at time  $t + \Delta t$ , and the velocities are calculated at full step:

$$V(t + \Delta t) = v\left(t + \frac{\Delta t}{2}\right) + \left(\frac{1}{2}\right)a(t + \Delta t) \Delta t \quad (3.20)$$

At this point, the positions and velocities at time  $t + \Delta t$  are completed, and the system will be advanced to the next time step and repeated. Velocity Verlet algorithm is seen to require less computational amount as only one set of positions, velocities and forces need to be carried out at one time.

### 3.14 Periodic Boundary Conditions

In this particular research endeavor, the molecular dynamics simulation was carried out using a periodic boundary condition. The distinction between a finite system and an infinite system is quite significant. As a result, there is no one correct response to the question of what the size of a relatively small system needs to be in order to produce outcomes that truly mirror the behavior of an infinite system. There are many different kinds of boundary conditions that can be used to simulate a simulation that is taking place inside a container. You have the option of modeling the wall of the simulation box as either fixed or periodic, as well as fixed wrapped or fully wrapped. A finite system can be treated as an infinite system by applying periodic boundary conditions. This is possible. The periodic boundary condition presupposes that there are particles of the same kind located beyond the boundaries of the simulation box. As a result, even if only one atom leaves the box, another atom will immediately enter it from the outside. In the event that the fixed boundary condition is applied, the wall will remain immobile both in terms of time and space. In the case of a wrapped boundary condition, the simulation box or a particular wall can be made to stretch along with the moving particle. In the case of a fixed wrapped boundary condition, the simulation wall will extend; however, it will only do so to a set point before stopping. A representation of the periodic boundary condition can be found in Figure 3.4.

A system that is bounded but free of physical walls can be constructed by resorting to periodic boundary conditions. By using periodic boundary condition, a finite system can be modeled as infinite system. Periodic boundary condition assumes that there are similar types of particles outside the simulation box. The introduction of periodic boundaries is equivalent to considering an infinite, space filling array of identical copies of the simulation region. There are two effects of assuming it. The first one is that an atom that leaves this simulation region through a particular bounding face immediately reenters the region through the opposite face. The second one is that atoms lying within a distance  $r_{\text{cutoff}}$  of a boundary interact with atoms in an adjacent copy of the system.

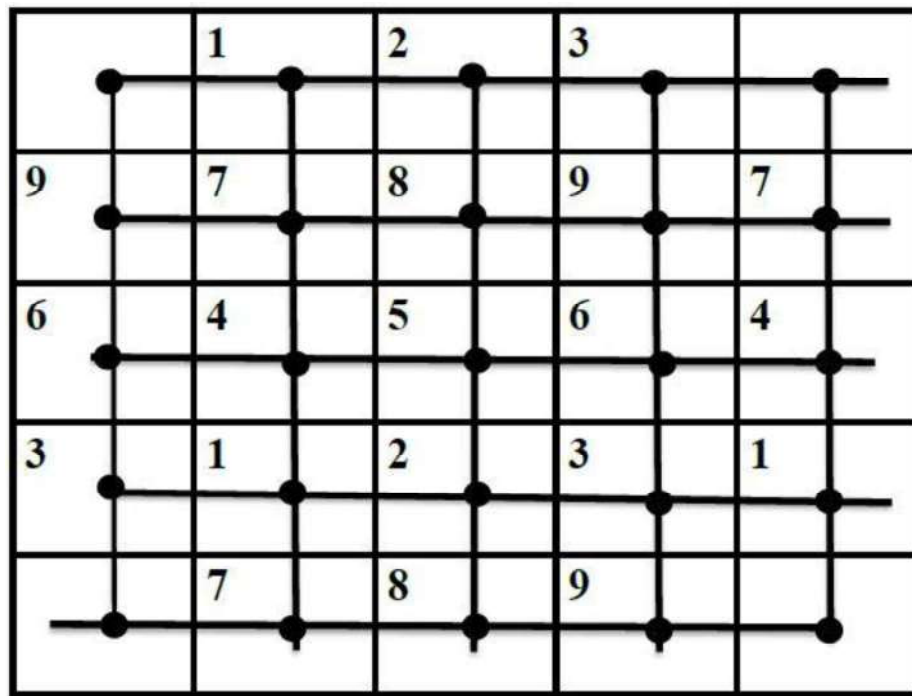


*Figure 3.4 Periodic boundary condition [73]*

### 3.15 LAMMPS

Large-scale Atomic/Molecular Massively Parallel Simulator (LAMMPS) is a molecular dynamics program from Sandia National Laboratories [62]. LAMMPS

makes use of Message Passing Interface (MPI) for parallel communication and is free and open-source software, distributed under the terms of the GNU General Public License [62]. The year of its initial release is 1995. This simulation tool has a great contribution in heat transfer, fluid mechanics, fracture mechanics, composite materials, DNA and RNA synthesis, drug preparation and biological science. It can be run in Cross-platform: Linux, OS X, and Windows. The code was initially developed in C++.

LAMMPS was originally developed under a Cooperative Research and Development Agreement (CRADA) between two laboratories from United States Department of Energy and three other laboratories from private sector firms. LAMMPS has very good computation effectiveness. For this computation efficiency, it uses neighbor lists (Verlet lists) to make a trace to the neighboring atoms. Based on the system of simulation LAMMPS optimize the neighbor list. In case of parallel computing, spatial-decomposition techniques are being used. In this technique, LAMMPS creates to partition in the simulation domain and assign the specific sub domain to different processors. Processors communicate and store ghost atom information for atoms that border their subdomain [65].

### **3.16 OVITO**

OVITO means Open Visualization Tool. It is freely available visualization and data analysis software for atomistic datasets as output by large-scale molecular dynamics/statics and Monte-Carlo simulations. The main goal of developing this tool is to ensure flexibility and reliability in in visualization. Molecular dynamics (MD), molecular statics and Monte-Carlo based simulations are nowadays standard methods for modeling materials with atomic-scale resolution [63]. These types of atomistic models basically generate a three-dimensional atomic configuration and the trajectories of atoms are monitored. For such kind of sophisticated atomistic model, a powerful analysis and visualization tool is needed because a powerful visualization tool play a key role in larger and complex simulated systems. Without a proper visualization tool, key information will remain undiscovered, inaccessible and unused. The main purpose of the visualization packages OVITO is to, convert some raw data files to a meaningful atomic representation so that exact insight of the simulation is revealed. OVITO is

written in C++ that runs on all major operating systems, including Microsoft Windows, MacOS and Linux. The major features of OVITO are given below:

Features of OVITO:

1. CNA Analysis
2. Analysis of Bond and Angle
3. Coordination number analysis
4. Finding Radial distribution function
5. Calculation of Displacement vector
6. Atomic strain tensors calculation
7. Histogram, scatter plot, and bin-and-reduce functions

### **3.17 VMD**

The VMD (Visual Molecular Dynamics) program is a robust piece of software for viewing and analyzing results from molecular dynamics simulations. Researchers in computational chemistry and structural biology use it frequently to investigate the atomic-level behavior and characteristics of biomolecules [64].

VMD offers a full suite of functionalities for viewing and modifying complicated molecular systems. It's compatible with many other simulation programs thanks to its support for a wide variety of file formats, such as PDB (Protein Data Bank), CHARMM, AMBER, and GROMACS. This flexibility allows scientists to compare and contrast results from a wide variety of simulations.

VMD's strength lies in its capacity to render accurate images of molecular structures. It has several rendering choices, letting users change the look and color of atoms, bonds, and other chemical components. Understanding the structure, behavior, and interactions of biomolecules is greatly aided by VMD's visualization tools.

VMD offers many different kinds of analytical tools in addition to displaying molecular structures. Distances, angular and torsion angles, hydrogen bonds, and secondary structure elements are only some of the many properties that may be computed and viewed. Researchers can make more precise observations about biomolecular systems with the aid of these analysis tools.

Trajectory analysis and cross-correlation analysis are only two examples of the sophisticated analysis tools that may be used with VMD. Time-series analysis of molecular systems, visualized conformational changes, and analyzed protein folding and binding processes are all possible with the help of trajectory analysis. Insights into the collective behavior and dynamics of biomolecules can be gained through the use of cross-correlation analysis, which identifies correlated motions between distinct regions of a molecule.

In addition, users can take advantage of VMD's scripting features in Tcl to do automated operations, develop their own analysis tools, and expand the program's capabilities. VMD's scripting capabilities add versatility and personalization, making it a useful resource for a wide variety of scientific endeavors.

In the overall scheme of molecular dynamics simulations, VMD is an indispensable, all-encompassing instrument. Researchers researching the behavior and properties of biomolecules will find it indispensable because to its robust visualization and analytic capabilities, compatibility with a wide range of file formats, and scripting capabilities.

### **3.18 Elastic Constants and Mechanical Properties**

In molecular dynamics simulations, the computation of elastic coefficients requires the use of linear elasticity theory. Stress-strain relation in an orthotropic monoclinic crystal can be defined by the independent elastic stiffness parameter [74,75]:



$$\begin{bmatrix} \sigma_{11} \\ \sigma_{22} \\ \sigma_{33} \\ \sigma_{12} \\ \sigma_{13} \\ \sigma_{23} \end{bmatrix} = \begin{bmatrix} c_{11} & c_{12} & c_{13} & 0 & c_{15} & 0 \\ c_{12} & c_{22} & c_{23} & 0 & c_{25} & 0 \\ c_{13} & c_{23} & c_{33} & 0 & c_{35} & 0 \\ 0 & 0 & 0 & c_{44} & 0 & c_{46} \\ c_{15} & c_{25} & c_{35} & 0 & c_{55} & 0 \\ 0 & 0 & 0 & c_{46} & 0 & c_{66} \end{bmatrix} \begin{bmatrix} \varepsilon_{11} \\ \varepsilon_{22} \\ \varepsilon_{33} \\ \gamma_{12} \\ \gamma_{13} \\ \gamma_{23} \end{bmatrix} \quad (3.21)$$

where  $\sigma$  represents the normal stress and shear stress in each direction;  $\varepsilon$  and  $\gamma$  are the normal strain and shear strain in each direction respectively.

For monoclinic crystal structure, elastic constants include  $C_{11}$ ,  $C_{22}$ ,  $C_{33}$ ,  $C_{12}$ ,  $C_{13}$ ,  $C_{23}$ ,  $C_{44}$ ,  $C_{55}$ ,  $C_{66}$ ,  $C_{15}$ ,  $C_{25}$ ,  $C_{35}$ , and  $C_{46}$ . The criteria for mechanical stability are given by Wu et. Al [76]:

$$c_{ii} > 0 \quad (i = 1, 2, 3, 4, 5, 6) \quad (3.22)$$

$$(c_{44}c_{66} - c_{46}^2) > 0 \quad (3.23)$$

$$(c_{33}c_{55} - c_{35}^2) > 0 \quad (3.24)$$

$$[c_{11} + c_{22} + c_{33} + 2(c_{12} + c_{13} + c_{23})] > 0 \quad (3.25)$$

$$(c_{22} + c_{33} - 2c_{23}) > 0 \quad (3.26)$$

By applying Voigt-Reuss-Hill approximation [77] it is possible to calculate a material's resistance to compression by utilizing an equation that goes as follows: the bulk modulus, denoted by "K,"

$$K = \frac{c_{11} + c_{22} + c_{33} + 2(c_{12} + c_{13} + c_{23})}{9} \quad (3.27)$$

The shear modulus, denoted by the letter G, is an indicator of the resistance of a material to shear deformation. It is determined by the equation:

$$G = \frac{(C_{11} + C_{22} + C_{33}) - (C_{12} + C_{13} + C_{23}) + 2(C_{44} + C_{55} + C_{66})}{12} \quad (3.28)$$

Additionally, Poisson's ratio ( $\nu$ ), which describes the ratio of lateral strain to axial strain, can be determined as

$$\nu = \frac{3K - 2G}{2(3K + G)} \quad (3.29)$$

The mechanical behavior of materials can be characterized by the elastic coefficients, and these equations make it possible to calculate those coefficients. Noting that these equations make the assumption of isotropy and ignore any anisotropic behavior that may be present in the material is a crucial point to keep in mind. The incorporation of these equations into the research work that is being done on molecular dynamics gives a solid platform for researching and comprehending the elastic properties of various materials.

### **3.19 Volume Fluctuation Formula for generating Heat Capacity by MD simulation**

The formula for volume fluctuation is a mathematical statement that links the changes in volume of a system to the thermodynamic features of that system. Simulations of statistical mechanics and molecular dynamics frequently make use of it because it reveals how the volume of a system shifts over the course of time and offers other useful information [76].

According to the formula for volume fluctuation, the squared fluctuation in volume is directly proportional to the temperature of the system, the volume of the system, and its isothermal compressibility. This suggests that a higher temperature or a material with a greater compressibility equates to a volume change that is greater in magnitude. The formula is of the following form [61].

$$C_V = \frac{1}{\kappa_B T^2} (\langle E^2 \rangle_{NVT} - \langle E \rangle_{NVT}^2) \quad (3.30)$$

Here,

$C_V$  = Constant Volume Heat Capacity

$\kappa_B$  = Boltzaman Constant

$\langle E^2 \rangle$  = Average value of square of total energy

$\langle E \rangle^2$  = Square of the average value of total energy

$\langle E^2 \rangle_{NVT} - \langle E \rangle_{NVT}^2 = \Delta \langle E^2 \rangle =$  mean square fluctuation of energy

Calculating thermodynamic parameters, such as the constant volume heat capacity ( $C_V$ ) and the constant pressure heat capacity ( $C_p$ ), is typically accomplished with the help of the volume fluctuation formula in molecular dynamics simulations. These heat capacities can be established by measuring the fluctuations in volume that occur during the simulation and then applying the formula. This provides insight into how the system reacts to changes in both temperature and pressure.

Researchers are able to analyze the thermodynamic properties of materials and study their response to various conditions as a result of the volume fluctuation formula, which acts as a fundamental equation for understanding and characterizing the dynamic behavior of systems. In general, the volume fluctuation formula serves this purpose.

### 3.20 Hugoniot Shock Simulation

A computational method known as uniaxial hugoniot shock simulation is utilized for modeling and analyzing the behavior of materials when they are exposed to high-pressure shock waves. It is a key tool in a variety of domains, including materials science, geophysics, astrophysics, and engineering, where it is crucial to understand how materials react when subjected to extreme conditions [65].

In order to complete the simulation, you will need to solve the equations of fluid dynamics, more especially the Euler equations. These equations outline the principles of mass conservation, momentum conservation, and energy conservation within a fluid medium. The equations are then supplemented with constitutive relationships, which characterize the behavior of the substance that is the subject of the investigation. Under extreme conditions, these relationships generally include equations of state, which relate the thermodynamic parameters of the material, such as density, pressure, and temperature.

For one-dimensional steady flow, the conservation of mass, momentum, and the energy across a planar shock front connecting the initial unshocked and final shocked states lead to Rankine-Hugoniot jump conditions:

$$\text{mass: } \rho_s = \rho(u_s - u_p) \quad (3.31)$$

$$\text{momentum: } P_{xx} = P_0 + \rho_0 u_s u_p \quad (3.32)$$

$$\text{Energy: } E_H = E_0 + \frac{1}{2}(P_{xx} + P_0)(V_0 - V) \quad (3.33)$$

Here, the subscript 0 refers to those qualities in the unshocked initial state.  $P_{xx}$  is the normal component of the stress tensor in the shocked direction (chosen to be the x direction),  $\rho=1/V$  is the mass per unit volume,  $u_s$  is the shock velocity, and  $u_p$  is the particle velocity. Equation (3.26), (3.27), (3.28) lead to the following relations:

$$\frac{u_p}{u_s} = 1 - \frac{V}{V_0} \quad (3.34)$$

$$u_s = \sqrt{\frac{P_{xx} - P_0}{V_0 - V}} V_0 \quad (3.35)$$

$$u_p = \sqrt{(P_{xx} - P_0)(V_0 - V)} \quad (3.36)$$

The Hugoniot method is conceptually comparable to the conventional isobaric-isothermal simulation protocols proposed by Nosé and Hoover [61] in the sense that it couples, via a set of additional degrees of freedom and in the equations of motion, a system of particles to an external bath in a manner that drives the system toward the thermodynamic state and statistical mechanical ensemble of interest. The Rankine–Hugoniot relations [65], which ensure the conservation of mass, momentum, and energy in both the pre- and post-shock phases of the material, are used here to specify the thermodynamic state of the system. The additional degree of freedom  $i$  corresponds to a dimensionless strain rate and acts as a piston or barostat to maintain the component of stress in the direction of wave propagation  $i$  at the appropriate value  $P_{ii}$ . This is accomplished by ensuring that the extra degree of freedom  $i$  plays its part. The remaining degree of freedom is the dimensionless heat-flow variable the ergostat, which ensures that the internal energy of the system satisfies Hugoniot relation for energy.

In order to carry out a uniaxial Hugoniot shock simulation, it is customarily necessary to follow a series of stages. To begin, the beginning circumstances of the material are specified. These conditions include the density, pressure, and temperature of the substance at the outset. In most cases, the selection of these criteria is based on the results of experiments or on theoretical predictions. The fluid dynamics equations are then solved numerically by employing computational methods such as finite difference, finite volume, or finite element techniques. These techniques partition the space occupied by the fluid into a grid or mesh and then use discrete difference approximations to come up with a close approximation of the equations' derivatives.

During the simulation, the material is exposed to a uniaxial shock wave, which is normally delivered by forcing an abrupt rise in pressure on the boundary of the material. This causes the wave to travel in a direction perpendicular to the direction of the simulation. As the shock wave travels through the material, it causes the material to undergo fast compression as well as heating and deformation as it moves through the material. The simulation follows the development of the shock wave and the response of the material through time. This enables researchers to explore phenomena such as the propagation of shock waves, the failure of materials, phase transitions, and the formation of secondary waves.

The resolution of the computational grid or mesh, the choice of equations of state, and the numerical methods that are used all play a role in determining how accurate and reliable the uniaxial Hugoniot shock simulation will be. In addition, testing the outcomes of the simulation against the actual data collected in the experiment is essential in order to validate the prediction capabilities of the model. Researchers are able to increase the accuracy of future simulations by comparing the outcomes of simulations to those of experiments, which helps them modify the constitutive models.

The understanding that may be obtained by uniaxial Hugoniot shock simulations can be applied in a variety of contexts. These simulations can provide useful information on the behavior of materials under extreme conditions, which can help in the creation of more durable and resilient materials for applications such as armor, aircraft components, and high-pressure tests. In the field of materials science, this knowledge can be found in simulations. The simulations enable researchers in geophysics and astrophysics understand the behavior of materials within the interiors of planets, as well as the behavior of supernova explosions and impact events. In addition, uniaxial Hugoniot shock simulations contribute to the creation of safer and more effective engineering systems. These engineering systems include shock absorbers, structures that are resistant to blasts, and high-speed impact protection.

In conclusion, uniaxial Hugoniot shock simulation is an effective computer method that gives researchers the opportunity to investigate the behavior of materials when subjected to extreme conditions. These simulations provide useful insights into the reaction of materials to high-pressure shock waves by solving the equations of fluid dynamics and adding constitutive relationships. These simulations can be found here. The findings that were acquired from these simulations contribute to developments in a variety of domains, such as materials science, geophysics, astrophysics, and engineering. These advancements, in turn, ultimately lead to the creation of better materials and greater safety measures in high-pressure situations.

## **CHAPTER: 4**

### **RESULTS AND DISCUSSIONS**

#### **4.1 Forcefield Development for TKX-50**

##### **4.1.1 Geometry Optimization**

Accurate parameterization of force fields is essential for reliable molecular simulations. Geometry optimization, which involves identifying the most stable molecular configuration, plays a pivotal role in this process. In this study, we focus on the geometry optimization of TKX-50, a high-performance energetic material, to determine its ground state energy and atomic conformation. The obtained ground state energy level serves as a reference for subsequent parameterization of the bonded force field parameters. Through rigorous computational analyses, we aim to establish a robust force field model that accurately captures the behavior and properties of TKX-50 at the atomic scale.

##### **4.1.2 Data Acquisition**

In order to get started with our investigation, we acquired crystal structure information from the Cambridge Crystallographic Data Centre (CCDC) about the molecular conformation of dihydroxylammonium 5,5'-bistetrazole-1,1'-diolate (TKX-50) [10]. During the selection procedure, conformations are extracted at a temperature of 298K. The unit cell of TKX-50 is monoclinic crystal in  $P 2_1/c$  space group. This is done to ensure that a representative sample of the molecule's behavior was obtained. The information that was collected is in the format known as CIF (Crystallographic Information File), which is then changed to the format known as PDB (Protein Data Bank) by making use of the tool known as VMD (Visual Molecular Dynamics). The procedure of conversion ensures that the subsequent analysis and calculations would be compatible with the results.

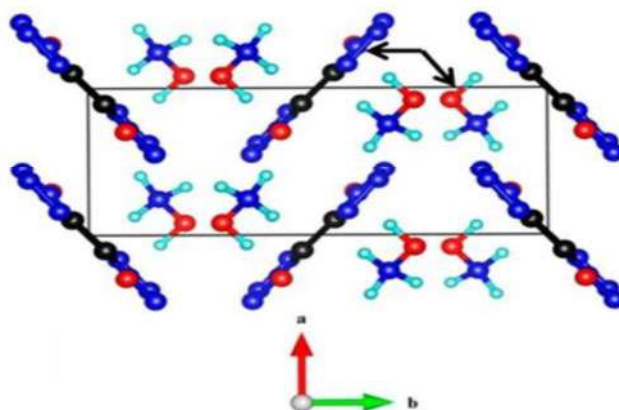


**Figure 4.1:** Unit cell of TKX-50 with periodic conformation collected from the CIF file of CCDC [10]

### 4.1.3 Format Conversion for the XYZ System

In order to carry out calculations involving quantum chemistry, the PDB file is further processed with the Avogadro tool, which results in the file being converted to the XYZ format. A clear and concise representation of the molecule's conformational coordinates can be obtained through the use of the XYZ format. During the process of conversion, the necessary adjustments and validations are carried out to ensure the accuracy of the resulting XYZ file, which contained the precise coordinates of TKX-50's molecular conformation. These modifications and validations are undertaken to ensure the accuracy of the resulting XYZ file.

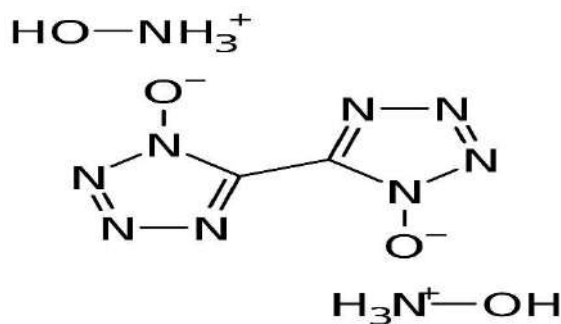


**Figure 4.2:** Molecular Formula of TKX-50 [71]



#### **4.1.4 Calculation of Quantum Chemistry**

The Orca software package is used to perform the quantum chemistry calculations because of its powerful capabilities in ab initio calculations. This software package is selected for its versatility. The optimization of TKX-50's three-dimensional geometry is the primary focus of this stage's work. In order to accomplish this, we utilize the Second Order Moller-Plesset Perturbation Theory (MP2) approach for the calculation of the post self-consistent field (SCF). It is determined after several trials and errors that the aug-CCPvdZ basis set would provide the most accurate description of the molecule's electron density. This basis function is an augmented functions which includes core-valence electrons interaction, electron-electron polarization and diffusion effects.

#### **4.1.5 Optimization and Acceleration of the Simulation**

This study makes use of the Resolution Integration strategy that was contained within the Orca software in order to speed up the process of optimization. By approximating specific integrals within the calculations, this method permits efficient computations. The end result is a significant reduction in the amount of time needed to perform the computations, while the accuracy is maintained to a satisfactory level.

To accomplish the optimization of the geometry, the potential energy surface of TKX-50 is made as small as possible in an effort to find the most stable conformations at the lowest possible energy levels. Adjusting the molecule coordinates through a series of repetitive steps is required for the optimization process. This is done until a global minimum on the potential energy surface (PES) is reached, which indicated a stable conformation.

#### **4.1.6 Observations and Discussion**

After finishing up with the geometry optimization, we are able to get our hands on the potential energy surface of TKX-50. This surface offers crucial topological information on the stable conformations of the molecule as well as the energy levels associated with each of those

conformations. Through in-depth study of the potential energy surface, we are able to determine the conformations of the molecule that are the most stable and had the lowest energy levels. This gives us insight into the behavior and attributes of the molecule.

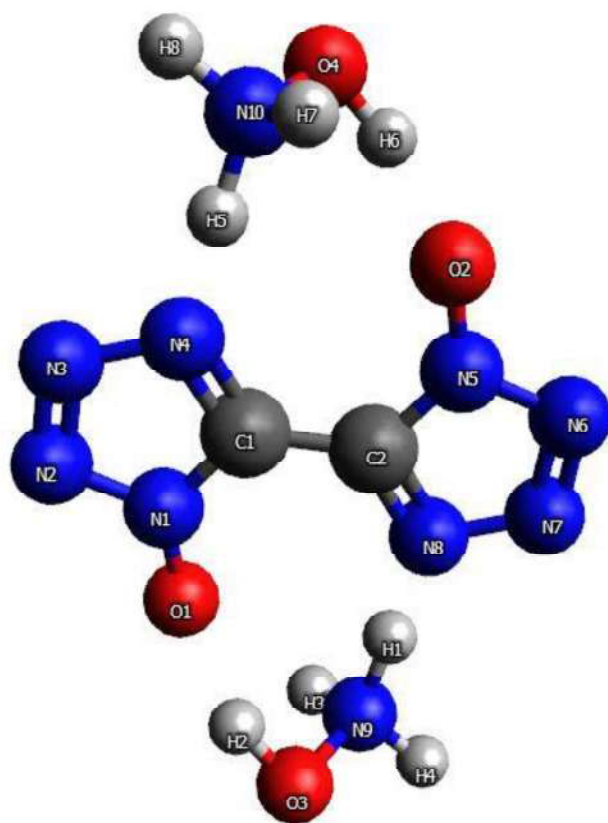


**Figure 4.3** *Optimized Molecular structure of TKX-50*

The above Figure 4.3 shows the stable molecular conformation of TKX-50. The atomic ID depicted in the Figure 4.3 will be used as the reference throughout this study. The comparison

of crystal bond length and optimized bond length at PES (Potential Energy Surface) are provided in the Table 4.1.

**Table: 4.1** bond lengths (in Å) for various bond types for crystal and optimized structure (Figure 4.3):

Bond type	Crystal (exptl at 298K)	Optimized Structure at PES
<b>C1-C2</b>	1.449	1.456
<b>C1-N1/C2-N5</b>	1.34	1.381
<b>C1-N4/C2-N8</b>	1.336	1.357
<b>N1-O1/N5-O2</b>	1.325	1.286
<b>N1-N2/N5-N6</b>	1.343	1.367
<b>N2-N3/N6-N7</b>	1.309	1.3584
<b>N3-N4/N7-N8</b>	1.358	1.355
<b>O3-H2/O4-H6</b>	0.91	0.978
<b>O3-N9/O4-N10</b>	1.409	1.407
<b>N9-H1</b>	0.92	1.032

#### 4.1.7 Forcefield Parameterization

We have learned the detail of geometry optimization in Article 4.1.6. After the optimization of the molecular configuration we start the forcefield parameterization. For our forcefield the potential energy function stands as following:

$$\begin{aligned}
E = & \sum_{bonds} \frac{1}{2} K_r (r - r_0)^2 + \sum_{angles} \frac{1}{2} K_\theta (\theta - \theta_0)^2 + \sum_{torsions} A_n \cos^n(n\varphi) \\
& + \sum_{impropers} \frac{1}{2} K_\chi (\chi - \chi_0)^2 + \sum_{i < j}^{atoms} \left( A_{ij} e^{-B_{ij} r_{ij}} - \frac{C_{ij}}{r_{ij}^6} \right) + \sum_{i < j}^{atoms} \frac{q_i q_j}{r_{ij}} \quad (4.1)
\end{aligned}$$

Here, the six terms include the energies of bond stretching, angle bending, torsional motion, improper torsion, van der Waals interactions, and electrostatic Coulomb interaction. Detailed explanations of the parameters in equation (4.1) can be found elsewhere [67].

In this computational study we used Orca as a primary tool for optimizing the geometry and scanning the geometry for different topological information. Here, we have optimized the anion bistetrazole and the cation hydroxylammonium separately. During optimization the structure we carefully monitor the frequency. If any negative frequency appears in the Orca output file, that indicated as the structure not reaching the Potential Energy Surface (PES), but a saddle point. In that case, we adjust the structure with the help of Avogadro tool before conducting the optimization again. In this way we got global PES for the cation (bistetrazole) and anion (hydroxylammonium).

After this Geometry scanning is done for all the topological (bond stretch, angle bending, torsional moment, improper torsional moment) information. All the quantum calculation is done at second order Moller-Plesset perturbation theory with the similar basis set (aug-ccPVDZ) as described in article 3.3.2.

#### 4.1.7.1 Bond Stretch Parameterization

From the PES of bistetrazole we gather the optimized bond length for each bond type. Say for bond type C1-C1, we get the optimized bond length of 1.45613. Then we start geometry scanning for this particular bond type keeping the other topological information same. We fluctuate the bond length for C1-C1 in the range of  $-0.02 \leq \Delta r \leq +0.02$ . We get the following

deviation of energy in terms of deviation of bond length for C1-C1 type bond presented in Table 4.2.

**Table 4.2** Energy fluctuation of bistetrazole along with the change of the bond length of C1-C1 bond type.

Bond length (Å)	Energy difference, $\Delta E$ (Kcal/mol)
1.436127	0.172364
1.440127	0.11063
1.444127	0.061377
1.448127	0.026744
1.452127	0.006357
1.456127	0
1.460127	0.00716
1.464127	0.027849
1.468127	0.061527
1.472127	0.107988
1.476127	0.166177

After that, we conform the data for this bond type to the harmonic function that we have introduced in equation (4.1) and that is going to be a part of our forcefield. To derive the parameter that would be used for the proposed forcefield, we employ the Python programming language and its libraries like matplotlib, scipy, and numpy to fit the curve to the function. Figure 4.4 is the fitted curve for bond type C1-C1.

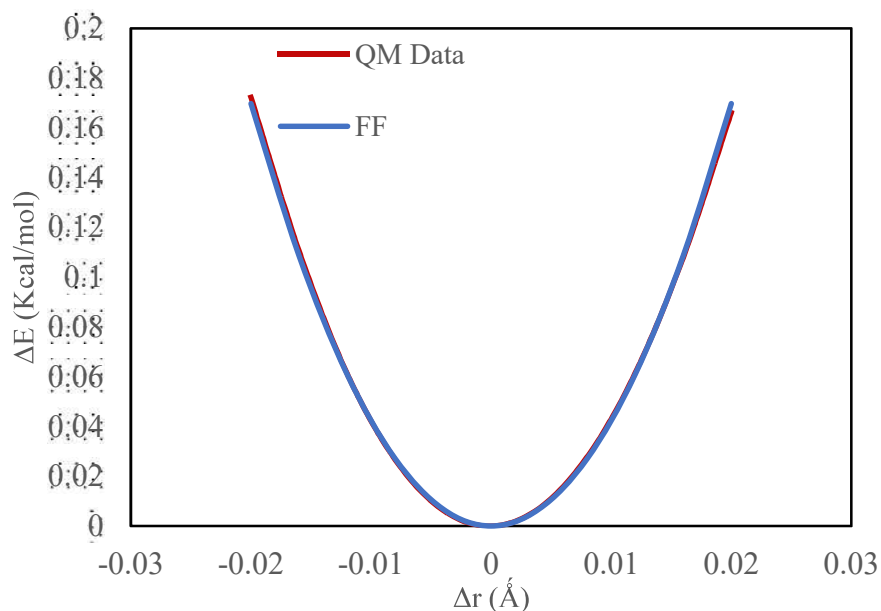


**Figure 4.4** Comparison of the bond stretch of C1\_C1 bond type for FF and QM

Similar calculations are done for all the other ten type of bonds. The parameters are given in Table 4.3.

**Table 4.3** Bond Stretch parameters

Bonded stretches, $U = \frac{1}{2} K^s (r_{ij} - r_{ij}^0)^2$		
Bond type	$K^s$ (Kcal/mol.angstrom <sup>-2</sup> )	$r_{ij}^0$ (angstrom)
C-C	409.522	1.456
C-N1	461.837	1.357
C-N4	461.837	1.357
N1-N2	514.539	1.381
N2-N3	454.917	1.032
N3-N4	526.2	0.978
N1-O1	503.213	1.355
O2-H2	815.891	1.3584
N5-O2	784.903	1.376
N5-H1	541.754	1.286
N5-H3	340.476	1.407
N5-H4	409.522	1.456

### 4.1.7.2 Angle Bending Parameterization

From separate geometry optimization simulations of anion bistetrazole and cation hydroxylammonium topological information are gathered at PES.

For angle type C1\_N4\_N3 optimized value of angle is found 106.5°. Then we start geometry scanning for this particular type of angle keeping the other topological information same. We fluctuate the angle value for C1\_N4\_N3 in the range of  $-20^\circ \leq \Delta\theta \leq +20^\circ$ . We get the following deviation of energy in terms of deviation of angle for C1\_N4\_N3 type angle presented in Table 4.4.

**Table 4.4** Energy fluctuation of bistetrazole along with the change of the angle of C1\_N4\_N3

Angle (°)	Energy difference, $\Delta E$ (Kcal/mol)
86.5	33.56851
90.5	21.43765
94.5	11.93892
98.5	5.21679
102.5	1.266144
106.5	0
110.5	1.284122
114.5	4.924735
118.5	10.70619
122.5	18.3725
126.5	27.65907

After that, we conform the data for this angle type to the harmonic function that we have introduced in equation (4.1) and that is going to be a part of our forcefield. To derive the parameters that would be used for the proposed forcefield, we employ the Python programming language and its libraries like matplotlib, scipy, and numpy to fit the curve to the function. Figure 4.5 represents the fitted curve for angle type C1\_N4\_N3.

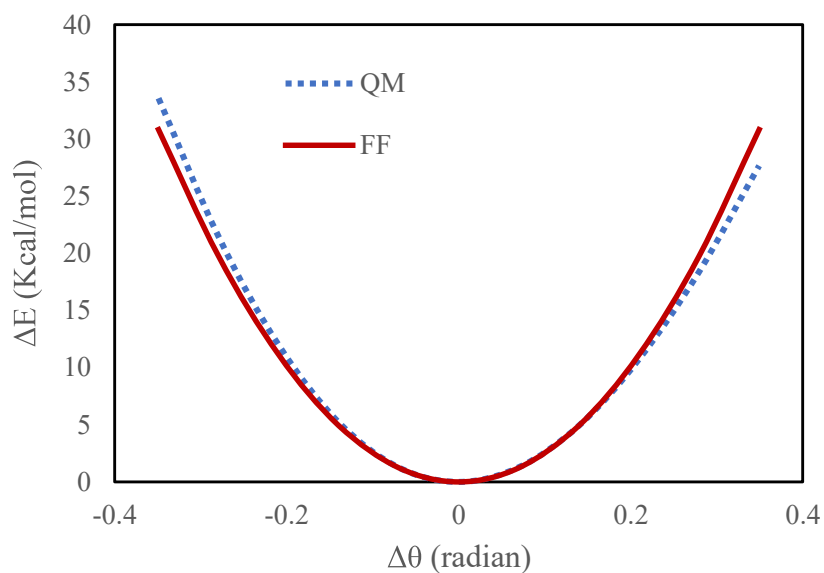


**Figure 4.5** Comparison of the angle bending stretch of C1\_N4\_N3 angle type for FF and QM

Similar calculations were done for all the other types of angles. The parameters are given in the Table 4.5.



**Table 4.5** Angle bending parameters

Angle bending stretches, $U = \frac{1}{2} K_{ijk}^b (\theta - \theta^0)^2$		
Angle type	$K^b$ (Kcal/mol.rad <sup>2</sup> )	$\theta_{ij}^0$ (degree)
C1-C1-N1	60.768	126.5
C1-C1-N4	76.608	124.868
C1-N1-N2	237.018	106.5
C1-N1-O1	237.018	106.5
C1-N4-N3	259.98	107.816
H2-O2-N5	130.529	129.018
H1-N5-H3	38.42	108.9
H1-N5-H4	46.232	104.5
H1-N5-O2	56.28	106.7
H3-N5-H4	31.4074	100.2234
H3-N5-O2	243.1	108.6
H4-N5-O2	259.64	110.708
N1-C1-N4	272.394	106.4055
N1-N2-N3	112.922	123.2
N2-N1-O1	60.768	126.5
N2-N3-N4	76.608	124.868

### 4.1.7.3 Torsional moment Parameterization

From the PES of bistetrazole and hydroxylammonium optimized dihedral information are gathered. To fit the torsion barrier of N1\_C1\_C1\_N1 and N1\_C1\_C1\_N4 (in bistetrazole anion) we scan the geometry from 0 to 360° with 20° interval. For H1\_N9\_H3\_O2 (in hydroxylammonium) geometry is scanned from -120° to 240° with 40° interval.

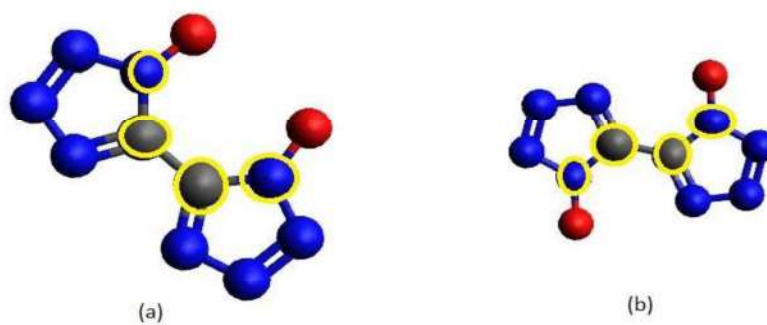


**Figure 4.6:** The configuration of  $0^\circ$ (Figure (a)) and  $180^\circ$ (Figure(b)) are shown here. Here yellow circles show the torsion barrier of  $N1\_C1\_C1\_N1$ .

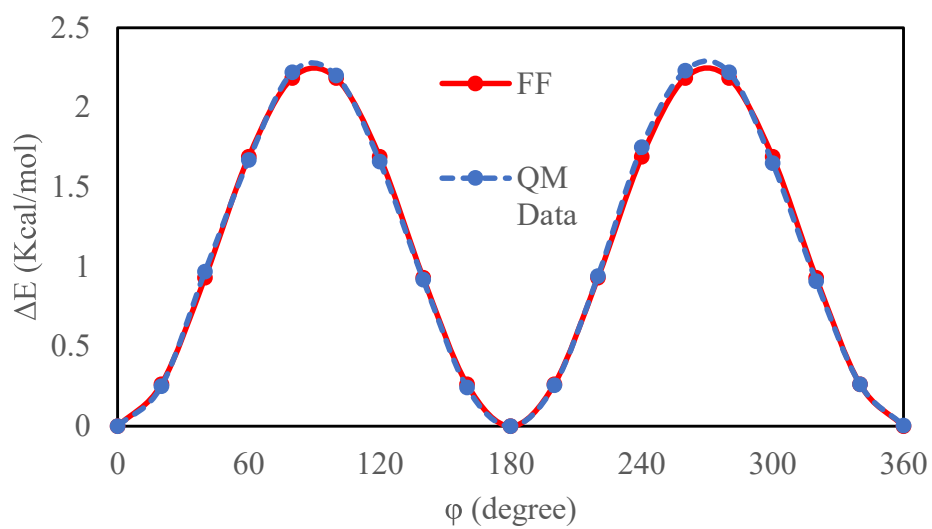


**Figure 4.7:** Comparison of  $N1\_C1\_C1\_N1$  torsion barrier (in kcal/mol) between FF and QM. The blue dots are from QM data and the red line is from FF.

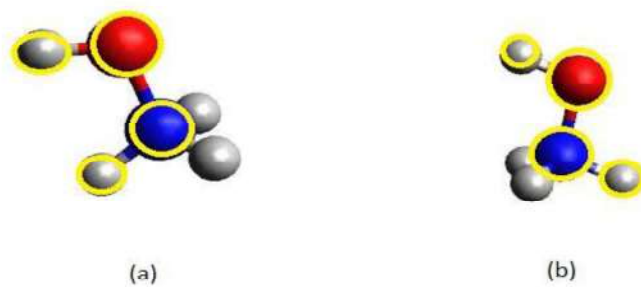


**Figure 4.8:** The configuration of  $-120^\circ$  (Figure (a)) and  $+60^\circ$  (Figure (b)) are shown here. Here yellow circles show the torsion barrier of H4\_N9\_O3\_H2.

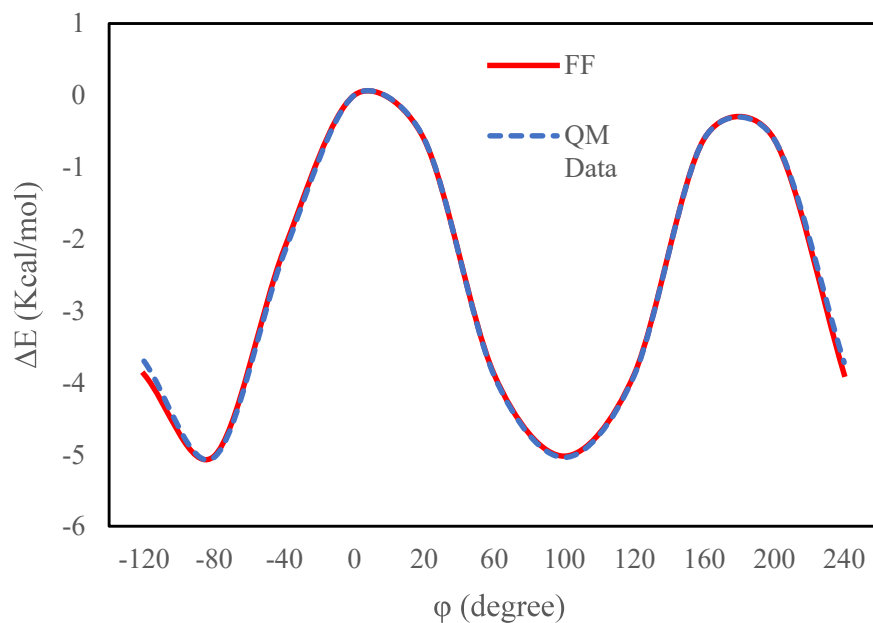


**Figure 4.9:** Comparison of H4\_N9\_O3\_H2 torsion barrier (in kcal/mol) between FF and QM. The blue dots are from QM data and the red line is from FF.

The dihedral parameters are given in Table 4.6

**Table 4.6:** Dihedral torsion parameters

<i>Dihedral torsion potential, <math>U = \sum_1^n A_n \cos^n(n\varphi)</math></i>								
<b>Dihedral type</b>	<b>n</b>	<b>K<sub>1</sub> (Kcal/mol)</b>	<b>K<sub>2</sub> (Kcal/mol)</b>	<b>K<sub>3</sub> (Kcal/mol)</b>	<b>K<sub>4</sub> (Kcal/mol)</b>	<b>K<sub>5</sub> (Kcal/mol)</b>	<b>K<sub>6</sub> (Kcal/mol)</b>	<b>K<sub>7</sub> (Kcal/mol)</b>
<b>C1-C1-N1-N2</b>	4	45.123	76.977	41.479	13.621			
<b>C1-C1-N1-O1</b>	5	195.264	351.324	268.226	230.061	115.804		
<b>C1-C1-N4-N3</b>	4	94.847	-126.94	42.003	-16.295			
<b>C1-N4-N3-N2</b>	4	175.734	-222.628	32.931	9.977			
<b>C1-N1-N2-N3</b>	6	195.507	-39.145	-141.581	12.116	10.836	-42.614	
<b>C1-N1-O1-H2</b>	4	-3.4852	-0.00002	-0.5148	-1e-06			
<b>H1-N9-O3-H2</b>	4	-9.1792	0	5.1792	0			
<b>H2-O1-N1-N2</b>	4	-2.7904	0	-1.2096	0			
<b>N4-C1-C1-N8</b>	7	-3.736	1.133	-0.945	-7.313	7.534	13.019	-4.613
<b>N4-C1-C1-N5</b>	7	-4.114	-0.834	7.296	3.957	-12.906	-5.385	13.179
<b>N4-C1-N1-N2</b>	3	139.424	-189.511	46.134				
<b>N4-C1-N1-O1</b>	4	56.649	76.511	21.927	6.065			
<b>N4-N3-N2-N1</b>	4	47.43	605.088	-944.951	287.768			
<b>N8-C1-C1-N4</b>	7	-3.736	1.133	-0.945	-7.313	7.534	13.019	-4.613
<b>N8-C1-C1-N1</b>	7	-4.114	-0.834	7.296	3.957	-12.906	-5.385	13.179
<b>C1-C1-N1-N2</b>	3	139.424	-189.511	46.134				
<b>C1-C1-N1-O1</b>	4	56.649	76.511	21.927	6.065			
<b>C1-C1-N4-N3</b>	4	157.745	-187.302	2.921	22.662			

Similarly, we develop the potential parameters for improper torsion barriers of two different types of improper atoms for bistetrazole anion and one improper type for hydroxylammonium cation. The improper parameters are given in Table 4.7.

**Table 4.7:** *Improper torsion parameters*

<b>Improper torsional potential, <math>U = \frac{1}{2}K_{\chi}(\chi - \chi^0)^2</math></b>		
<b>Improper type</b>	$K_{\chi}$ (Kcal/mol.rad <sup>2</sup> )	$\chi^0$ (degree)
<b>C-N1-C-N4</b>	0.011	0
<b>N1-N2-O1-C</b>	0.02	0
<b>N5-H1-O3-H3</b>	0.023	32.7

#### 4.1.7.4 Nonbonded parameters and partial atomic charge derivation

The Buckingham-Hill potential repulsion/dispersion parameters are taken from previous work of Smith et. al [11]. The parameters for ten types of carbon, hydrogen, nitrogen, and oxygen atoms are provided in Table 4.8. The interaction between Heterogenous atoms is computed using modified Walder-Hagler combining rules [80]:

$$A_{ij} = \sqrt{A_{ii}A_{jj}} \frac{B_{ij}^6}{B_{ii}^3 B_{jj}^3}; B_{ij} = \left( \frac{2}{B_{ii}^{-6} + B_{jj}^{-6}} \right);$$

$$C_{ij} = \sqrt{C_{ii}C_{jj}} \quad (4.2)$$

The repulsive terms and attractive terms are scaled by 1.65 and 2.3 respectively to reproduce the crystal parameters a, b, c,  $\alpha$ ,  $\beta$ ,  $\gamma$ , and density.

A factor of 0.5 is applied to scale down the electrostatic and van der Waals interactions between next-next nearest neighbors (1-4 interactions). Interactions on the 1-2 and 1-3 levels are scaled by a factor of 0.

The partial atomic charges were determined by fitting to the electrostatic potential at a grid of points formed from the MP2/aug-ccPvDZ wave functions. ORCA was used to obtain the optimum output from the wavefunction that was presented earlier. After that, the information from the ORCA output file along with its hessian matrix is extracted in order to carry out the task of doing the partial atomic charge calculation. The tool known as MultiWfn is used to perform the electrostatic potential (ESP) population calculation. Throughout the procedure of fitting, the width of the grid was 0.1 angstroms, and it had roughly 125,000 points in total. The box's dimensions are expanded to a total of 5 square inches. It has been determined that the dipole moment caused by the partial atomic charges has a value of 0.002332 D. This value is in great agreement with the quantum chemical analysis, which had a value of 0.00237 D. Additional alterations are made to these partial atomic charges in order to guarantee that the forcefield accurately reproduced the crystal structure. In addition to this, it is ensured that the molecular system stays charge neutral.

In Table 4.8 electrostatic and van der Waals parameters are provided. Figure 4.3 should be regarded as the reference to the respective atomic id.

**Table 4.8:** Non bonded Forcefield parameters

Atom type	charge	$A_{ij}$ (kcal/mol)	$B_{ij}$ ( $\text{\AA}^{-1}$ )	$C_{ij}$ (kcal mol <sup>-1</sup> $\text{\AA}^6$ )
O1	-0.57888	125143.92	0.246123	917.47
C1	0.65664	24710.4	0.3236	1473.84
N1	-0.109728	100375.935	0.26596	269.215
N2	-0.113184	100375.935	0.26596	269.215
N3	-0.095904	100375.935	0.26596	269.215
N4	-0.452736	100375.935	0.26596	269.215
N9	-0.468288	100375.935	0.26596	269.215
O3	-0.663552	125143.92	0.246123	917.47
H3	0.54432	4372.005	0.26738	63.02
H2	0.422496	4372.005	0.26738	63.02

#### 4.1.8 Forcefield Validation and predicted Mechanical and Thermodynamic Properties

By employing the newly constructed forcefield in conjunction with the Molecular Dynamics (MD) simulation, the mechanical and thermodynamic properties of TKX-50 are determined. The LAMMPS package is utilized in order to do the MD simulations. The particle particle particle mesh (PPPM) approach [61] was applied here for the purpose of achieving an accuracy of  $10^{-6}$  for the electrostatic interactions. Both the coulomb and the vdW cut-offs are set to  $10 \text{ \AA}$  at the beginning.

#### 4.1.8.1 Simulation Protocol

The time step for the MD calculation is set to 1 fs. During the MD simulations, we use a variety of ensembles, such as microcanonical (NVE), canonical ensemble (NVT), and isothermal-isobaric ensemble (NPT). The Nose-Hoover style is utilized for both the thermostat and the barostat. The damping constants for the temperature are set at 100 femtoseconds, while the damping constants for the pressure were set at 1000 femtoseconds.

A supercell of size 6x3x5 unit cell is created by replicating the experimental unit cell in order to compute the crystal structure as well as some thermodynamic and mechanical properties. The conjugate gradient (CG) approach is initially utilized in order to do an initial structural minimization. To obtain a local energy minimum for the system, minimization is utilized. This is often done to relax the initial configuration or reduce overlaps between atoms. It is decided that quadratic interpolation would be used for the line search so that convergence could be improved while minimization is being performed. Both the force convergence tolerance and the potential energy tolerance are set to  $1e-40$ . The potential energy tolerance is also set to  $1e-40$ . The minimization procedure is configured to allow for a maximum number of iterations of 100,000.

After the minimization, a MD simulation is performed at 100K for 20 picoseconds by canonical ensemble. After that, we heat the system using simulations called cook-off to get it from 100 K to 400 K uniformly within 20 picoseconds. Next, the system is equilibrated at various temperatures by running an isothermal-isobaric ensembled simulation for 400 picoseconds. This annealing process allows us to forecast the densities as well as the cell properties by utilizing the averages over the last 100 ps. The optimized geometry with the developed forcefield shows good agreement to the experimental crystal structure. The cohesive energy is found to be better agreement with the existing experimental value with 25% more accuracy than existing forcefield. Crystal structure, volume, and density are within 3% deviation. B is found to be much better agreement with experimental crystal than the existing forcefield's estimation. These data are provided in the Table 4.8 with proper comparison to experiment and AMBER forcefield.



#### 4.1.8.2 Crystal, Mechanical and Thermodynamic properties

In Table 4.9 comparison of various crystal, thermodynamic, and mechanical properties from the FF and QM with experimental are given.

**Table 4.9** Comparison of crystal, mechanical, and thermodynamic properties of TKX-50, in between Experimental data, QM data, AMBER FF, and our developed FF

Properties	Experimental/QM	Amber FF	Developed FF
<b>a</b> (Å)	5.4408	5.25	5.61
<b>b</b> (Å)	11.7514	12.11	11.35
<b>c</b> (Å)	6.5612	6.6	6.58
<b><math>\alpha</math></b> (deg)	90	90	90
<b><math>\beta</math></b> (deg)	95.07	93.5	94.9
<b><math>\gamma</math></b> (deg)	90	90	90
<b>Volume</b> (V, Å <sup>3</sup> )	417.86	418	417.3
<b>Density</b> ( $\rho$ , g.cm <sup>-1</sup> )	1.877	1.875	1.879
<b>Lattice energy</b> (kJ.mol <sup>-1</sup> )	-1506	-756	-1055.29
<b>Bulk Modulus</b> (K,Gpa) (at 298.15 K)	21.9	32.72	23.92
<b>Shear Modulus</b> (G, GPa)	9.067 (QM value)	12.385	11.2
<b>Heat capacity</b> (C <sub>v</sub> ,J/mol-K) (at Room temp. and 1 atm pressure)	265.2	292	246.02
<b>Poisson ratio</b> ( $\nu$ )	0.33	Not reported	0.329

### **4.1.8.3 Elastic constant, shear, bulk modulus calculation**

In the field of materials science and engineering, understanding the mechanical properties of materials is of paramount importance. Elastic coefficients, bulk modulus, shear modulus, and Poisson's ratio are key parameters that describe a material's response to external forces and deformation. Molecular dynamics simulations, such as those performed using LAMMPS (Large-scale Atomic/Molecular Massively Parallel Simulator), provide a powerful tool for investigating the mechanical behavior of materials at the atomic scale. In this section, a detailed description of the simulation done to estimate various mechanical properties like elastic constants, bulk and shear modulus, poisson ratio is provided.

#### *Simulation Setup:*

The simulation is begun by setting up the environment. The temperature of the system is set to 298.15 Kelvin. The simulation is divided into two parts, with the first part consisting of 5000 picoseconds of compression and the second part consisting of 10,000 picoseconds of expansion. The system is initialized with atoms assigned random velocities according to a Gaussian distribution.

#### *Equilibration:*

To ensure the stability and equilibration of the system, the system is first thermalized by microcanonical ensemble. This is followed by the application of the Langevin thermostat, which controls temperature fluctuations. The Langevin thermostat is applied with a temperature of 298.15 Kelvin, as well as a damping coefficient of 100.0 femtoseconds. The simulation is continued for 1000 timesteps to allow the system to reach equilibrium.

### *Box Relaxation and Minimization:*

In order to obtain the initial state of the system, the crystal structure is relaxed by adjusting the box dimensions and atom positions to minimize to the total potential energy of the system. The resulting box dimensions and stress components are recorded as initial state for subsequent calculations.

### *Strain and Stress Computation:*

In the following step the simulation box is perturbed in different directions to induce strains. The deformation is applied in a controlled manner by changing the box dimensions. Specifically, negative and positive deformations are applied along the x, y, and z axes, as well as the xy, xz, and yz planes. Then the relaxation procedure was repeated for the deformed system. The relaxation ensures that the system reaches a stable state and allows for accurate stress computations.

### *Elastic Constants Calculation:*

Using the stress tensors obtained from positive and negative deformations, the derivatives of strain components with respect to stress components are calculated. These derivatives quantify the material's response to stress and are essential for determining the elastic constants. The computed derivatives are then used to compute the elastic constants ( $C_{ij}$ ) via appropriate formulas. The specific formulas used for finding elastic constants, bulk and shear modulus, and poisson ratio are discussed in article 3.18.

Thus, the presented MD simulation provides a comprehensive framework for investigating the mechanical properties of materials through molecular dynamics simulations. Generated bulk

modulus value from our computation is 23.92 GPa at room temperature, which is about 9.2% larger than the experimental bulk modulus of TKX-50 21.9 GPa [76]. On the other hand, Bulk modulus value of previous AMBER forcefield of TKX-50 is 32.719 GPa, much higher (49%) than the experimental result. No experimental shear modulus value of TKX-50 has been reported yet. However, Quin et. Al reported the shear modulus value from QM, which is 9.06 GPa. In our study we have found the shear modulus value at room temperature is 11.2 GPa, showing good agreement (22% higher) to the QM value. In contrast, shear modulus reported from AMBER forcefield is 12.385, 36.6% higher than the QM value of shear modulus. The experimental poisson ratio is 0.33 [72], whereas our forcefield predicts it to be 0.329, which is in excellent agreement with the experimental value. The 13 Elastic coefficient values for this monoclinic crystal structure are provided in the Table 4.9. These values obey the criteria for mechanical stability of the crystal structure provided in equations (3.22) to (3.26).

Table 4.10 has provided the elastic constant value for monoclinic crystal of energetic material, TKX-50.

**Table 4.10** *Elastic Constants*

<b>Elastic Constants</b>	<b>(GPa)</b>
<b>C<sub>11</sub></b>	72.11
<b>C<sub>22</sub></b>	70.33
<b>C<sub>33</sub></b>	73.54
<b>C<sub>44</sub></b>	10.98
<b>C<sub>55</sub></b>	25.31
<b>C<sub>66</sub></b>	39.64
<b>C<sub>12</sub></b>	56.98
<b>C<sub>13</sub></b>	28.998
<b>C<sub>23</sub></b>	20.172
<b>C<sub>15</sub></b>	2.47
<b>C<sub>25</sub></b>	-2.69
<b>C<sub>35</sub></b>	-2.98
<b>C<sub>46</sub></b>	0.583

#### **4.1.8.4 Constant volume Heat Capacity ( $C_v$ )**

To calculate the constant volume heat capacity of the TKX-50 material using MD simulation, a series of steps are followed. Initially, a 6x6x6 simulation cell is prepared from the experimental unit cell to represent the material. The simulation cell is then thermalized using the canonical ensemble at a temperature of 100K for a duration of 20 picoseconds. This allows the system to reach a stable temperature.

Following the thermalization, the system is heated from 100K to 400K using the microcanonical ensemble over a period of 20 picoseconds. This heating process facilitates the exploration of a range of temperatures and allows the material to undergo thermal expansion.

After reaching 400K, the system was slowly cooled down to a target temperature of 298.15K (room temperature) over a period of 400 picoseconds. This cooling phase ensured that the material reached a relaxed state at the desired temperature.

Once the system is at 298.15K, it is kept at this temperature while maintaining a constant volume for an additional 50 picoseconds using the canonical ensemble. During this period, the energy fluctuations of the system are recorded. This is represented by Figure 4.10. From this energy fluctuation data mean square energy fluctuation value is acquired.

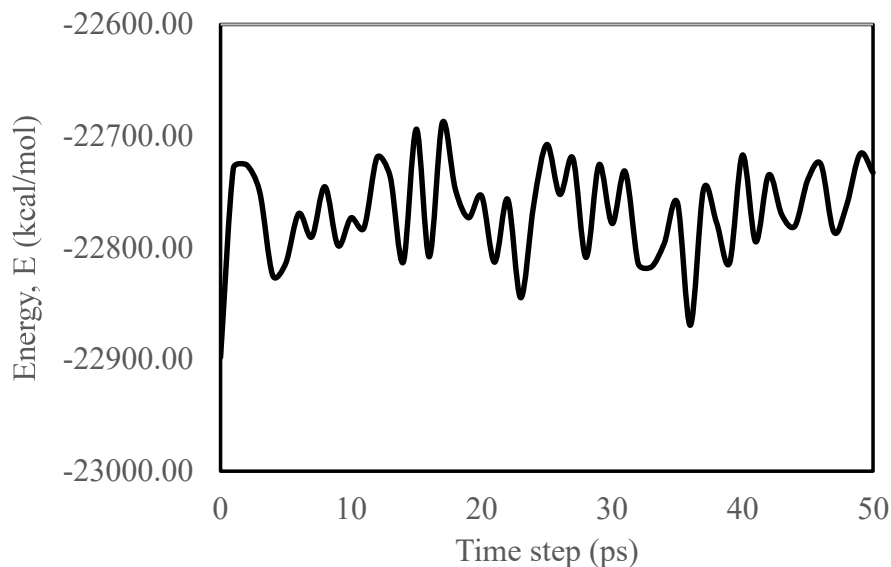


**Figure 4.10** Energy fluctuation for the last 50 picoseconds

To derive the constant volume heat capacity, the volume fluctuation formula is applied, which has been discussed in the article 3.19 (equation 3.25). This formula utilizes the recorded energy fluctuations to calculate the heat capacity at constant volume, which is a measure of the amount

of heat required to raise the temperature of the material without allowing it to expand. We recorded the constant volume heat capacity value of 246.03 J/mol-K, while the experimental value is 265.2 J/mol-K. The AMBER forcefield reported it to be 292 J/mol-K.

## 4.2 Uniaxial Hugoniosat Shock Simulation Study on TKX-50

Plastic deformation due to shock is often considered as the dominant mechanism for hot spot formation in energetic materials. We have performed uniaxial Hugoniosat shock simulation on TKX-50 to observe its behavior. A constant compression is applied to the system for a particular direction to simulate the shock. In order to run the simulation fruitfully, two additional degrees of freedom are utilized in the regulation of the system when utilizing the constant stress Hugoniosat method [65]. The first is a dimensionless heat-flow variable denoted by,  $\zeta$ , which is the factor that reduces the instantaneous internal energy  $E$  of the system to the Hugoniosat energy ( $E_H$ ), which is denoted by the equation (3.33).

The other is the dimensionless strain rate tensor, which equilibrates the component of the stress tensor in the direction of shock propagation to the value that is desired ( $P_{xx}$ ). From a simulation of constant stress uniaxial Hugoniosat equilibrium simulation using molecular dynamics, we were able to determine the Hugoniosat state, the Hugoniot Elastic Limit (HEL), information regarding plasticity, and other relevant data like temperature profile, as well as strain rate.

In this study two different structures have been used to examine the shock response along [100] direction. One structure is long and slender along the shock direction with 4800 molecules, similar to the structure used by a previous work done by An et. al [10]. The other system is more uniform along x-y plane with 6480 TKX-50 molecules, keeping it consistent with a similar study for energetic material RDX by Bedrov et. Al [21].

### 4.2.1 Simulation protocol

The finite difference integration scheme, which was provided by Holian and Ravelo [65] is utilized in order to carry out the Hugoniosat simulations that uses equation (3.33). At an initial

temperature of 300 K and at atmospheric pressure, periodic primary simulation cells with dimensions of  $276.8 \times 70.654 \times 52.49 \text{ \AA}^3$  and  $165.543 \times 105.563 \times 78.571 \text{ \AA}^3$  are investigated for the purpose of this study. These dimensions correspond to 4800 and 6480 TKX-50 molecules, respectively. These beginning conditions lead to a molecular volume of  $V_0=420 \text{ \AA}^3$ , and a total energy per molecule, including contributions from within the molecule, that is equal to  $E_0=-400.1 \text{ kcal/mol}$ . In every instance, a timestep of 1 femtosecond is applied so that precise handling of the quickly fluctuating intramolecular degrees of freedom (bonds and bends) can be achieved. For the nonbonded interactions and the actual fraction of the electrostatic interactions, a cutoff radius of 9.5 angstrom is utilized. The reciprocal component of electrostatic interactions was calculated using the particle particle particle mesh (PPPM) method for systems having either 4800 or 6480 molecules, depending on the case. For van der Waals interaction Buckingham potentials are employed. For both electrostatic interaction and van der Waals interaction 1-2, 1-3 atoms are factorized to 0, and 1-4 atoms are factorized by 0.5. Potential parameters are derived from the data presented earlier in this work and applied to bonded terms such as bonding stretch, angle bending, torsional, and inappropriate torsional moment interactions. The system is initially thermalized at 300 degrees Celsius by canonical ensemble for a period of one hundred picoseconds.

Afterwards the constant stress uniaxial Hugoniot simulation is done to these relaxed structured separately. 1 femtosecond time step is chosen for time integration. As described earlier for first degree of freedom, by default instantaneous internal energy  $e_0$  is chosen in our case, which is -55627.759 kcal/mol for system with 4800 molecules -109060.64 kcal/mol for system with 6480 molecules. In both cases we can see that there is no significant difference of the internal energy,  $E$  from the Hugoniot energy condition  $E_H$  (equation 3.33). This is going to represent short simulation trajectory time for ensuring complete sampling of Hugoniot condition.



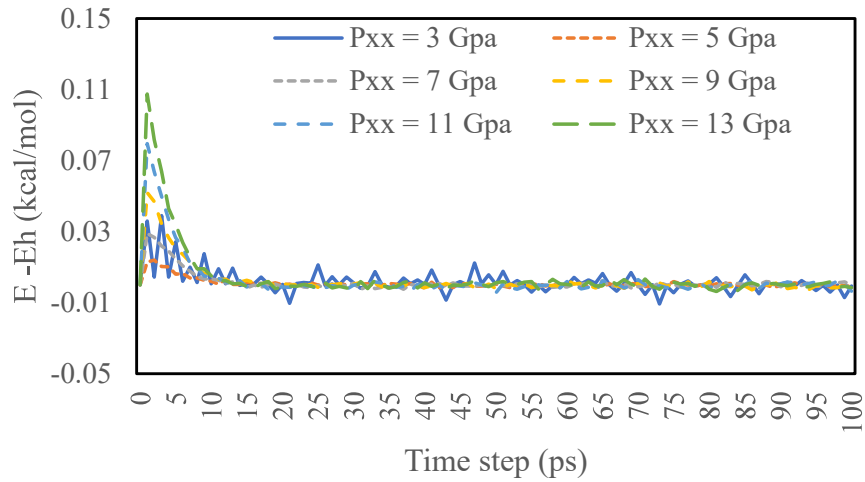


**Figure 4.11** Time Evolution of Hugoniot energy difference per molecule  $E-E_h$  obtained from Hugoniotstat simulations of shock compression along  $[100]$  using  $e_0 = -55627.759$  kcal/mol for the case of  $P_{xx} = 3$  to 13 GPa for simulation cell of 4800 molecules

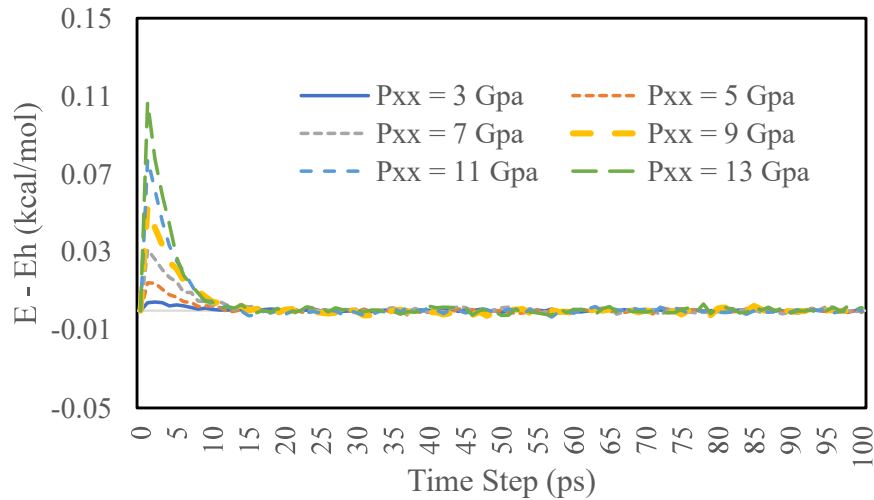


**Figure 4.12** Time Evolution of Hugoniot energy difference per molecule  $E-E_h$  obtained from Hugoniotstat simulations of shock compression along  $[100]$  using  $e_0 = -109060.64$  kcal/mol for the case of  $P_{xx} = 3$  to 13 GPa for simulation cell of 6480 molecules

This is clearly represented by Figures 4.10 and 4.11, where  $E-E_h$  evolution with respect to time is represented for both the systems with 4800 molecules and 6480 molecules for shock pressures of 3 GPa, 5 GPa, 7 GPa, 9 GPa, 11 GPa, and 13 GPa along  $x/[100]$  direction.

The drag value (damping parameter,  $\beta_p$ ) for controlling and smoothing the shock pressure along [100] direction was selected 20 picoseconds.

We can see from Figure 4.12 and Figure 4.13 that shock pressure reaches the assigned value smoothly and stays uniform without fluctuating. This approves the choice of parameter selection.

#### 4.2.2 Time evolution

In Figure 4.12-4.19, we show the time evolution of the stress component  $\sigma_{xx}$  parallel to [100] in the crystal, the temperature,  $T$  in Kelvin, the volume compression ratio,  $(V/V_0)$ , and the Von Mises shear stress,  $\tau = 0.5(\sigma_{xx} - 0.5(\sigma_{yy} + \sigma_{zz}))$  obtained from uniaxial Hugoniot simulation for shock pressures of  $P_{xx} = 3.0, 5.0, 7.0, 9.0, 11.0,$  and  $13.0$  GPa. Time evolution for both the systems with 4800 molecules and 6480 molecules are illustrated here.

Figure 4.12 and 4.13 depict that for all systems the desired stress along the shock direction is reached within 1 picoseconds of simulation time after which the instantaneous value fluctuates very little around the target value  $P_{xx}$ . One thing to be noted here is the absence of overshoot in  $\sigma_{xx}$  at early stages and also that at no point in the simulation is  $\sigma_{xx}$  significantly larger or smaller than the imposed shock pressure  $P_{xx}$ . This feature indicates that the value of damping parameter  $\beta_p$  is appropriate with the consequence that the probability of spurious structural deformations in the material arising due to artificial, large-amplitude overshoot or subsequent excursions of the stress is minimized. We have seen the similar trend for both the systems with 4800 molecules and 6480 molecules respectively.

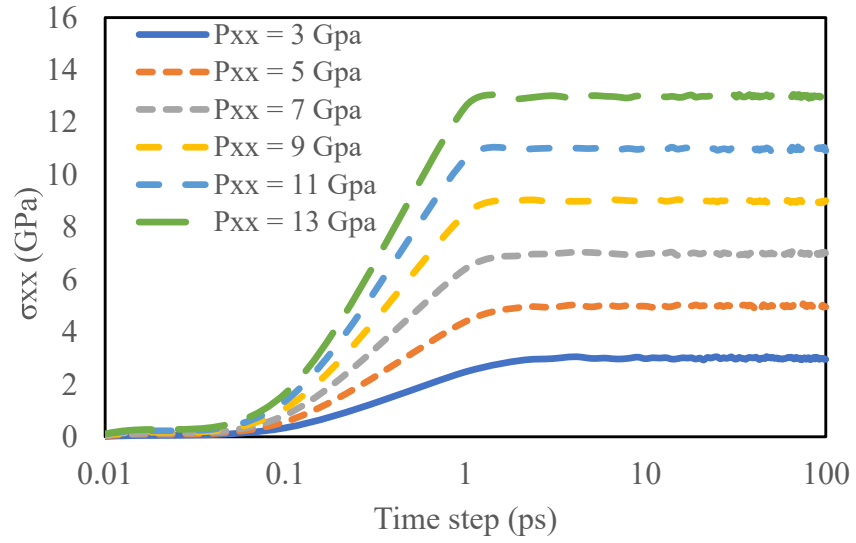


**Figure 4.13** Stress along [100] direction against time step for system with 4800 molecules

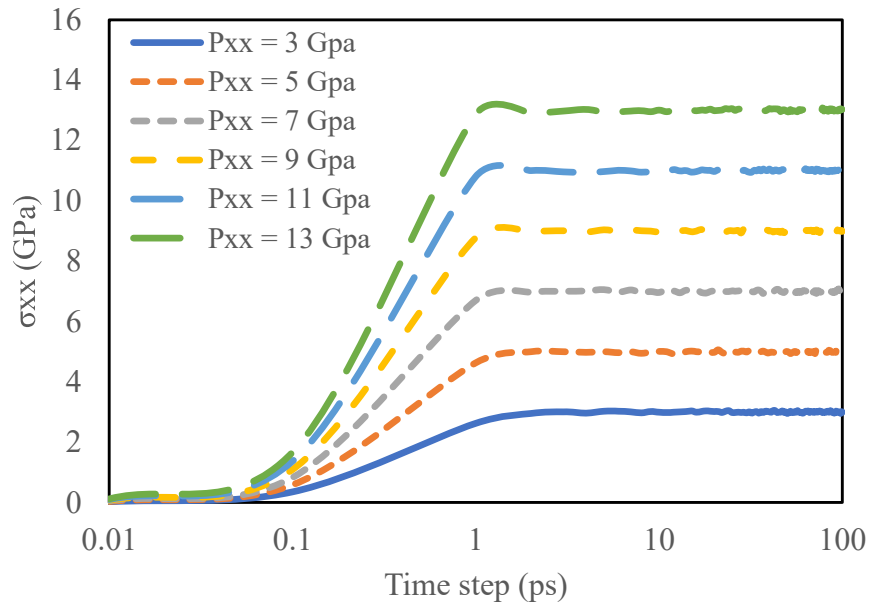


**Figure 4.14** Stress along [100] direction against time step for system with 6480 molecules

The time dependence of the average temperature (determined based on the total kinetic energy) in the system is depicted in Figures 4.15 and 4.16 for the identical set of shock pressures which are described in the previous paragraph. During the first 1-3 picoseconds of the simulation, the temperature rises for  $P_{xx} = 3$  GPa and 5 GPa, but it thereafter begins to fluctuate around a constant value. On the contrary for  $P_{xx} = 7$  GPa, 9 GPa, 11 GPa, and 13 GPa the temperature increased to a value in the first 1-3 picoseconds, afterwards dropped a little, and then kept fluctuation for the rest of the simulation around a constant value. This similar trend is observed for both systems with 4800 molecules and 6480 molecules. This difference in temperature profile suggests the presence of plastic deformation beyond shock pressure of 5 GPa. The second increase is due to the formation of shear bands in the material. This suggests a possible HEL of around 6 GPa for shock along [100] direction.

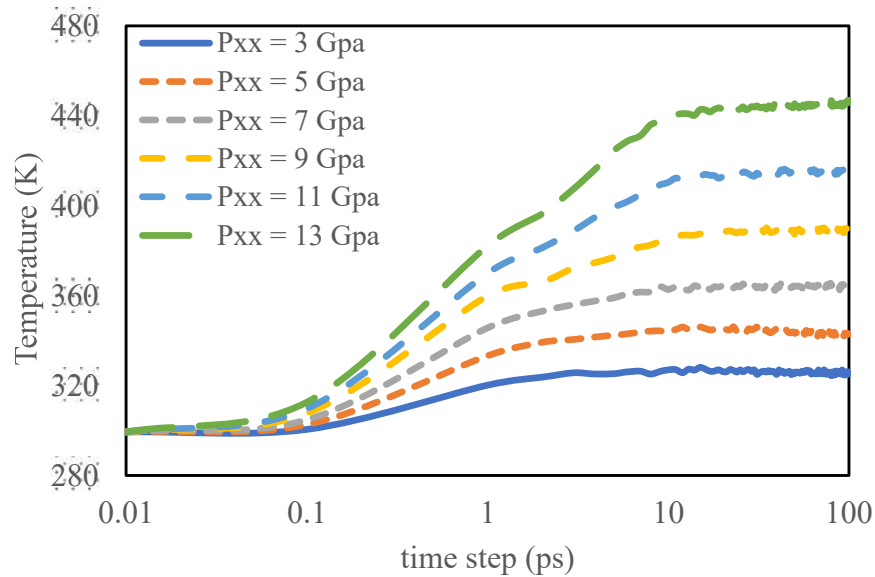


**Figure 4.15** Rise of temperature as a function of time step for shock pressure  $P_{xx} = 3$  GPa, 5 GPa, 7 GPa, 9 GPa, 11 GPa, and 13 GPa along [100] direction for system with 4800 molecules

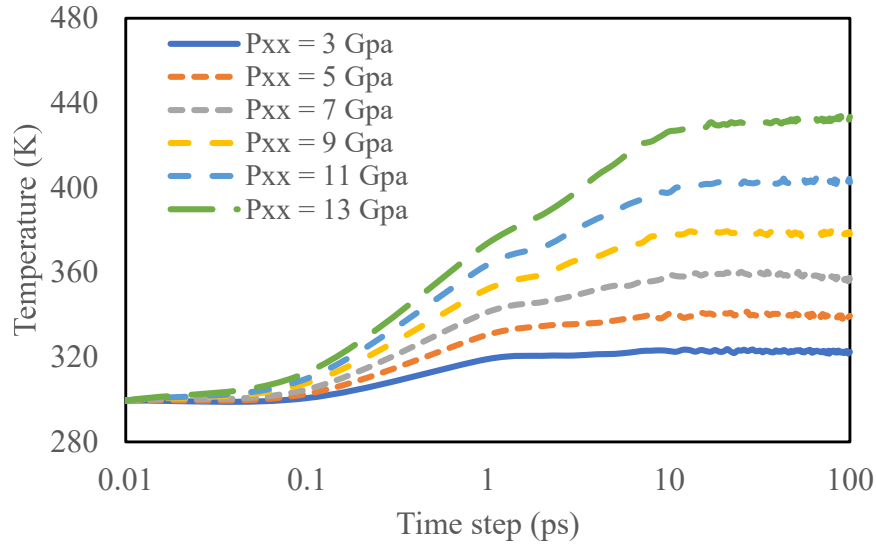


**Figure 4.16** Rise of temperature as a function of time step for shock pressure  $P_{xx} = 3$  GPa, 5 GPa, 7 GPa, 9 GPa, 11 GPa, and 13 GPa along [100] direction for system with 6480 molecules

In Figures 4.17 and 4.18 the evolution of volumetric compression,  $V/V_0$  (which in this study is equivalent to uniaxial compression ratio  $x/x_0$ ) is shown for the same set of shock pressures discussed earlier. For all the shock pressures studied here, the strain increases up to a certain value within first few picoseconds and kept constant for the remainder of the simulation. This is because formation of shear does not necessarily change the volume of the material. The volume changes only during the initial elastic compression of the material.

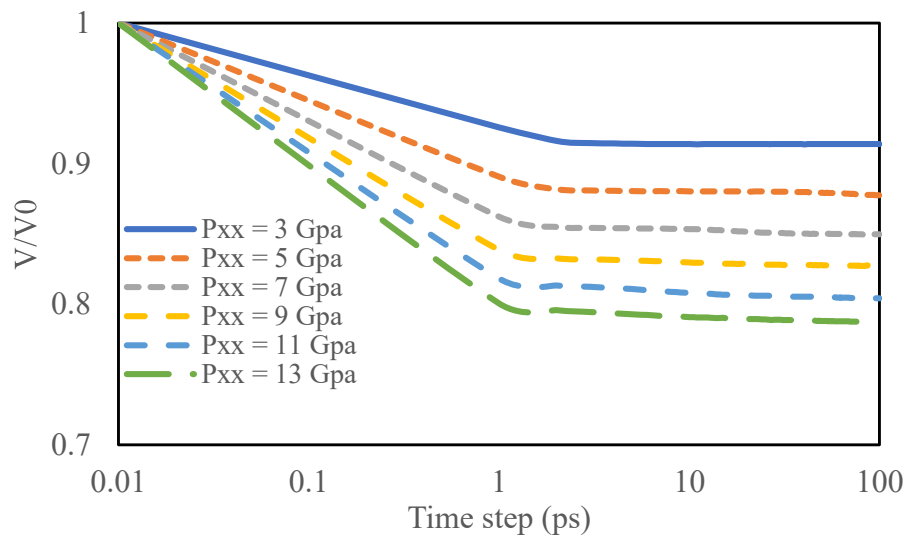


**Figure 4.17** Time evolution of Volume compression ratio ( $V/V_0$ ) for shock pressure  $P_{xx} = 3$  GPa, 5 GPa, 7 GPa, 9 GPa, 11 GPa, and 13 GPa along [100] direction for system with 4800 molecules

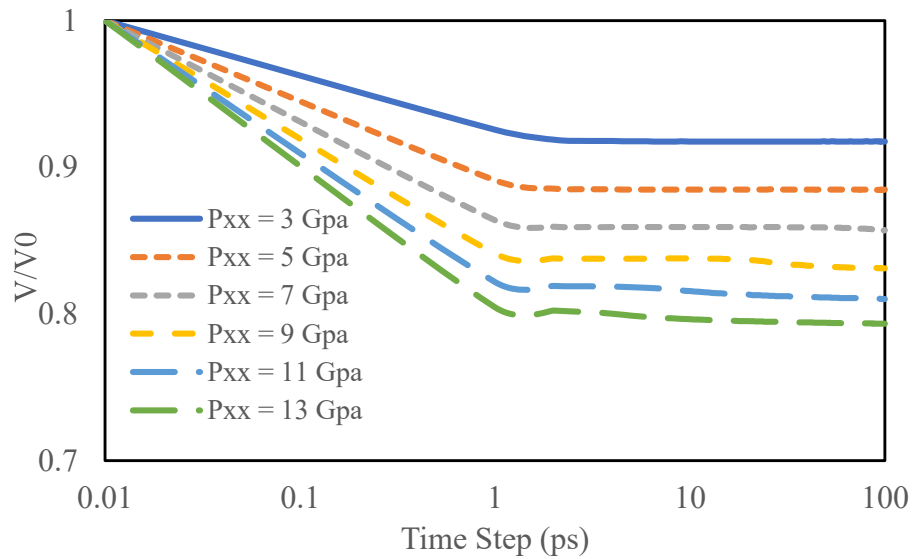


**Figure 4.18** Time evolution of Volume compression ratio ( $V/V_0$ ) for shock pressure  $P_{xx} = 3$  GPa, 5 GPa, 7 GPa, 9 GPa, 11 GPa, and 13 GPa along [100] direction for system with 6480 molecules

Now let us discuss about the time evolution of shear stress derived from the formula of von Mises shear stress  $\tau = 0.5(\sigma_{xx} - 0.5(\sigma_{yy} + \sigma_{zz}))$ , for the set of shock pressures studied here.. From Figures 4.19 and 4.20 we can see that for shock pressure  $P_{xx} = 3.0$ , and 5.0 GPa the shear stress ( $\tau$ ) reaches a certain value within first 5-6 picoseconds, and then keeps fluctuating around that value for the rest of the simulation. For example, for shock pressure  $P_{xx} = 5$  GPa, the shear stress reaches 0.648 GPa at 5 picosecond, and then keeps fluctuating around that value for the rest of the simulation. For  $P_{xx} = 3$  GPa shear stress value was 0.443 GPa at 5 picosecond, and followed the similar trend as that of 5 GPa shock pressure.

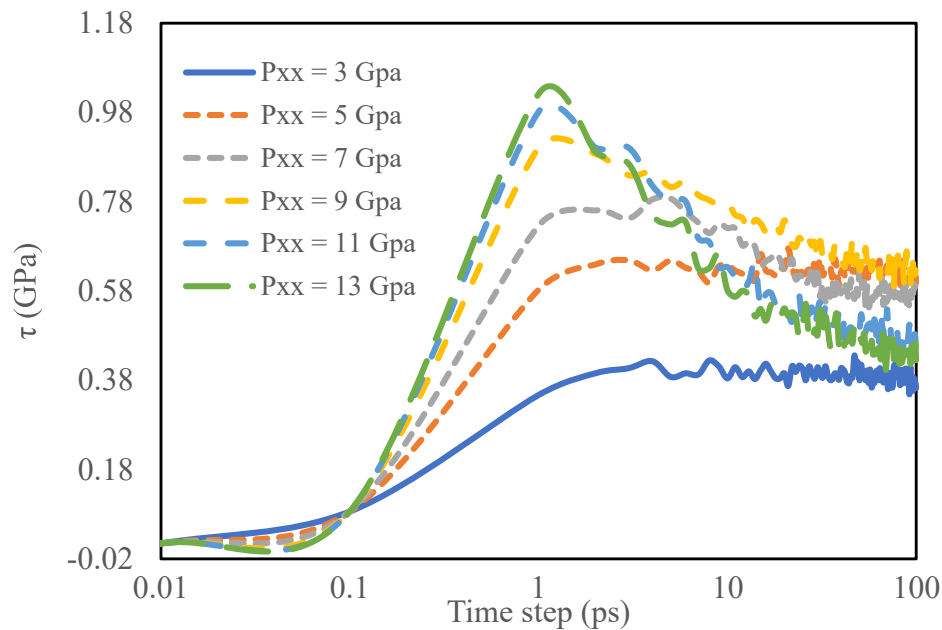


**Figure 4.19** Time evolution of von Mises Shear stress ( $\tau$ ) for shock pressure  $P_{xx} = 3$  GPa, 5 GPa, 7 GPa, 9 GPa, 11 GPa, and 13 GPa along [100] direction for system with 4800 molecules

For shock pressure of  $P_{xx} = 7, 9, 11,$  and 13 GPa, the shear stress value reaches a peak value at about 1 picosecond and starts dropping. The drop in shear stress happens as plastic deformation mechanisms (shear band) starts to activate and it drops until it reaches a steady flow stress. The

shear stress at which shear band starts to form varies with the shock pressure. This is due to the fact that shock pressure increases very fast and the formation of shear band is not fast enough in comparison to that. The final uniform flow stress results in decrease of the systems cohesive energy and as such the kinetic energy, i.e. temperature of the system increases during this stage as can be seen from Figure 4.15 and 4.16. The shear stress for the larger system is slightly higher than the smaller system as can be evident from Figure 4.21. This is rather a boundary issue and not related to the material plasticity value.

The lowest shear stress at which shear band forms is about 0.65 GPa for shock along [100] direction. We have not observed any dislocation activity in the shocked system which indicates nucleation of dislocation requires a higher shear stress for TKX-50. However, it is expected that the system with localized stress will have dislocation activity and the plastic deformation will start at a relatively lower shear stress.

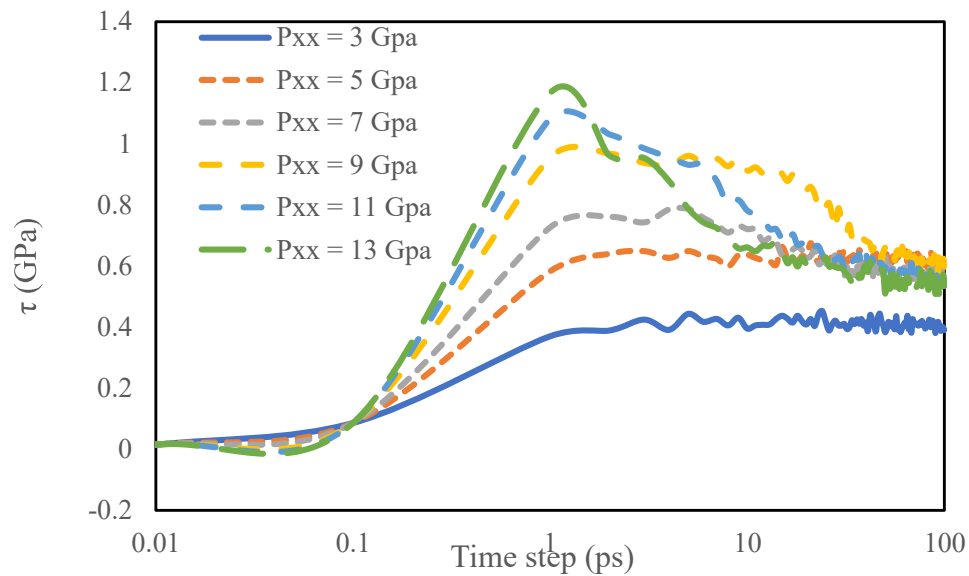




**Figure 4.20** Time evolution of von Mises Shear stress ( $\tau$ ) for shock pressure  $P_{xx} = 3$  GPa, 5 GPa, 7 GPa, 9 GPa, 11 GPa, and 13 GPa along [100] direction for system with 6480 molecules

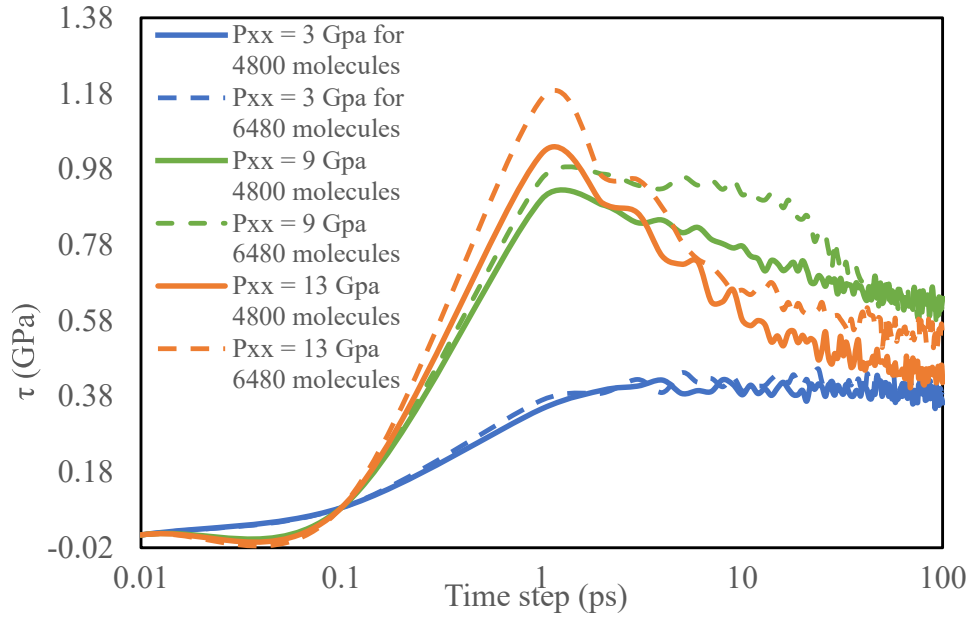


**Figure 4.21** Comparative analysis of von Mises shear stress for both systems with 4800 molecules and 6480 molecules for shock pressure  $P_{xx} = 3$  GPa, 9 GPa, 13 GPa.

When the Hugoniot equation of state (EOS) in LAMMPS is used to simulate shocks, this phenomenon, in which the shear stress rises quickly and then drops sharply for the rest of the simulation, is often seen [61]. This can be explained by the way the Hugoniot EOS is made and how the material reacts when it is hit.

The Hugoniot EOS, described in article 3.20 by equation (3.33) is an empirical equation that shows how the characteristics of a material and its thermodynamic state change when it is shocked. It shows the link between pressure and volume for a given material under conditions of high pressure and high strain rate. Most of the time, the Hugoniot EOS is used to describe what happens to materials when they are hit hard.

In a MD simulation, when a shock wave goes through a material, it gives the system a lot of energy and makes the pressure rise quickly. When the pressure goes up all of a sudden, the shear stress in the material also rises up. As the shock wave moves through the material, different mechanisms start to activate to dissipate the high shear stress.

The ability of the material to dissipate and shift the shock wave's energy is what causes the shear stress to go down after the first peak. As the material goes through plastic deformation and a change in its atomic structure, the shear force slowly goes down. This loosening up happens when the high pressure caused by the shock wave causes the material to reach a new state of equilibrium.

In Figure 4.19 and Figure 4.20 we have seen that the shear stress profile generated due to shock pressure  $P_{xx} = 7$  GPa is quite different than the shock pressure of  $P_{xx} = 9$  GPa, 11 GPa, and 13 GPa. The later conditions show kind of similar trend. While the shock pressure of 7 GPa, shows the slow relaxation of shear stress also the peak shear stress staying for quite longer simulation time as well. Also, in terms of temperature rise, it rises at greater value for shock pressure of  $P_{xx} = 9$  GPa, 11 GPa, and 13 GPa, compared to the shock pressure  $P_{xx} = 7$  GPa. We know that beyond the overdriven point the material undergoes tremendous compression and distortion, which typically results in substantial damage or failure. This is something that we are aware of. The excess energy may cause an increase in the material's internal pressure, temperature, and stress, which may cause it to be stretched beyond its mechanical limitations. Within the context of shock simulations, the overdriven point is of special relevance because it represents a crucial situation that has the potential to have major effects on the way the material behaves and reacts to the shock. Usually overdriven point is the point where wave velocity equals shock velocity

at HEL. From the above discussion, our study suggests that the shock pressure for overdriven point for TKX-50 is possibly about 8 GPa. An et. al [10] reported the possible overdriven point for shock along [100] direction for TKX-50 is 7.2 GPa. Which is also in good agreement with our prediction for overdriven point for shock pressure along [100] direction for TKX-50.

### 4.2.3 Pressure-Volume-Temperature dependence

Thermodynamic properties on the Hugoniot locus for TKX-50 crystal shock loaded along [100] as gathered from Hugoniotat simulations are shown in Figure 4.20 and 4.21. In Figure 4.22 the final volume compression ratio  $V / V_0$  of the system obtained from averaging over the last 50 picoseconds of the trajectory is shown as a function of applied shock pressure  $P_{xx}$ . A clear change in the P- $V/V_0$  dependence that corresponds to the HEL can be seen in between shock pressure of 5 GPa and 7 GPa. Therefore, we can predict that the HEL stays in around shock pressure of 6 GPa along [100] direction.

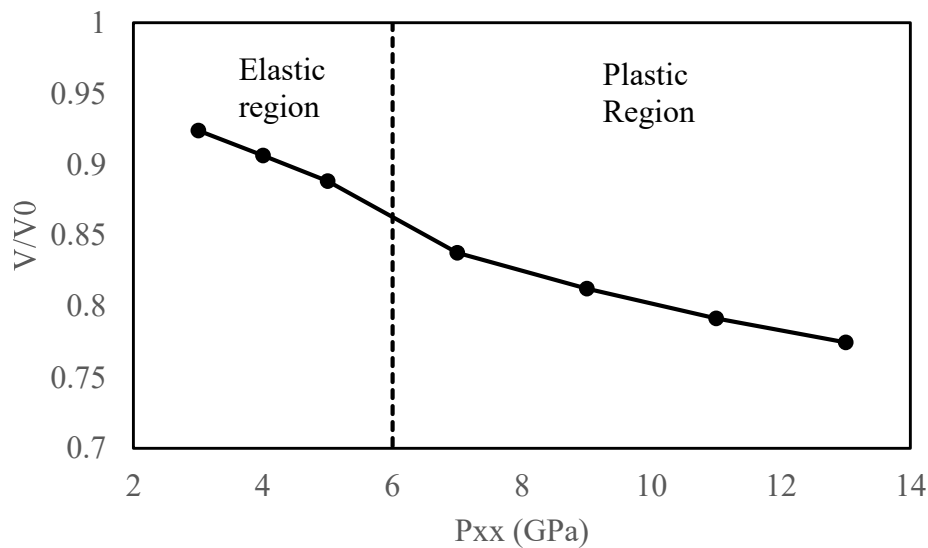


**Figure 4.22** Volumetric strain of TKX-50 shocked along [100] as a function of shock pressure  $P_{xx}$  obtained from Hugoniot simulation for systems with 4800 molecules. The dotted line here representing the approximated HEL while distinguishing the plot into elastic and plastic region

The temperature difference as a function of shock pressure  $P_{xx}$  also shows similar trend (Figure 4.23) as the volumetric strain vs shock pressure graph of Figure 4.22 showed. For shock pressure of 3 GPa the temperature increases about 13.8 K, and for the shock pressure of 13 GPa the temperature increases by 142.55 K for the system with 4800 molecules. This high increase of temperature beyond the HEL or in the plastic region refers to existence of possible overdriven point.

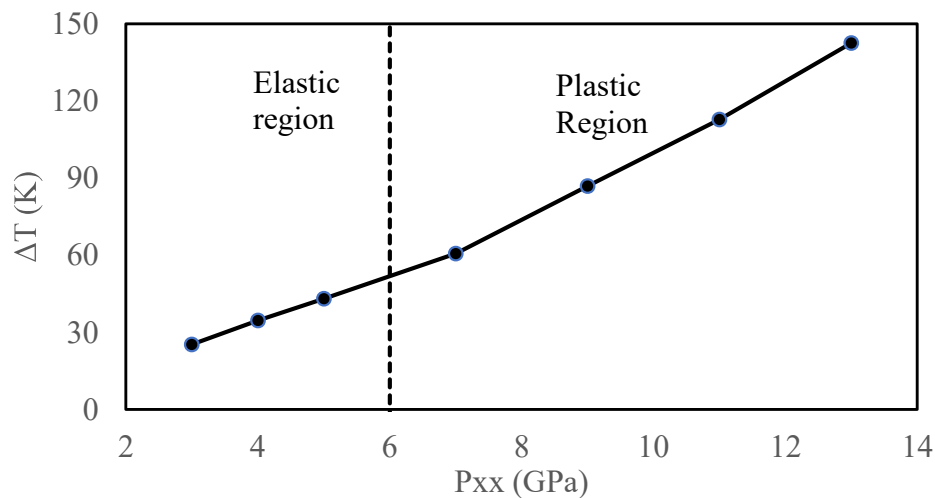


**Figure 4.23** Final temperature difference of TKX-50 shocked along [100] as a function of shock pressure  $P_{xx}$  obtained from Hugoniot simulation for systems with 4800 molecules. The dotted line here representing the approximated HEL while distinguishing the plot into elastic and plastic region

Therefore, from the pressure-volume-temperature dependence we can firmly decide that HEL exists approximately at 6 GPa. For 5 GPa shock pressure strain was 0.112. For 7 GPa shock pressure strain was 0.152. So, we can assume the strain at HEL is in the vicinity of 0.132.

#### **4.2.4 Study of Shear band formation**

In this work we have studied the plastic deformation mechanism for stress relaxation for the shock along [100]. To examine the atomic level shear, we use maximum relative displacement (MRD) [78], which is defined by  $s_i = (x_{ij} - X_{ij}) / |x_{ij} - X_{ij}|$ . Here the  $x_{ij}$  and  $X_{ij}$  vectors correspond to the difference between the current and reference configurations for atoms  $i$  and  $j$  (slipped neighbors of atom  $i$ ), respectively. In our case, the reference configurations are taken to be pre-shock structures and proper color coding in MRD is selected in the visualization tool Ovito.

In the following Figures we can see the shear band formation for shock pressure of 13 GPa along [100] direction viewed along two different directions (001) and (010).

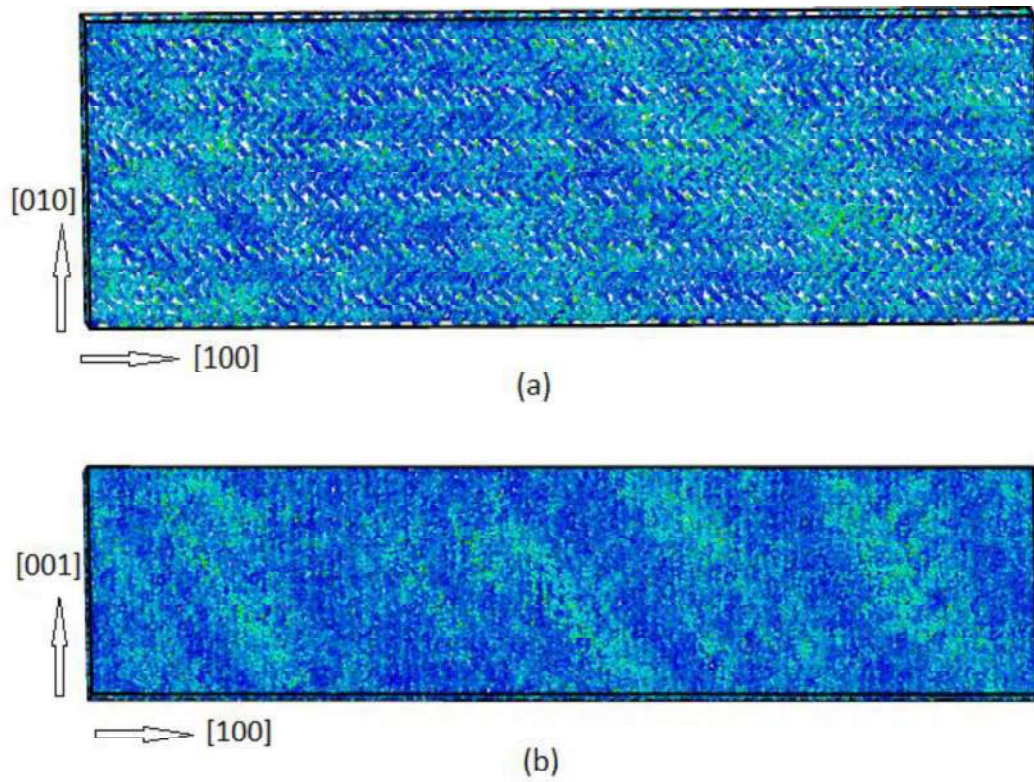


**Figure 4.24** Snapshots showing shear band in single crystal TKX-50 with 4800 molecules shock loaded along  $[100]$  direction for the shock pressure of 13GPa viewed along (a)  $(001)$  direction, and (b)  $(010)$  direction

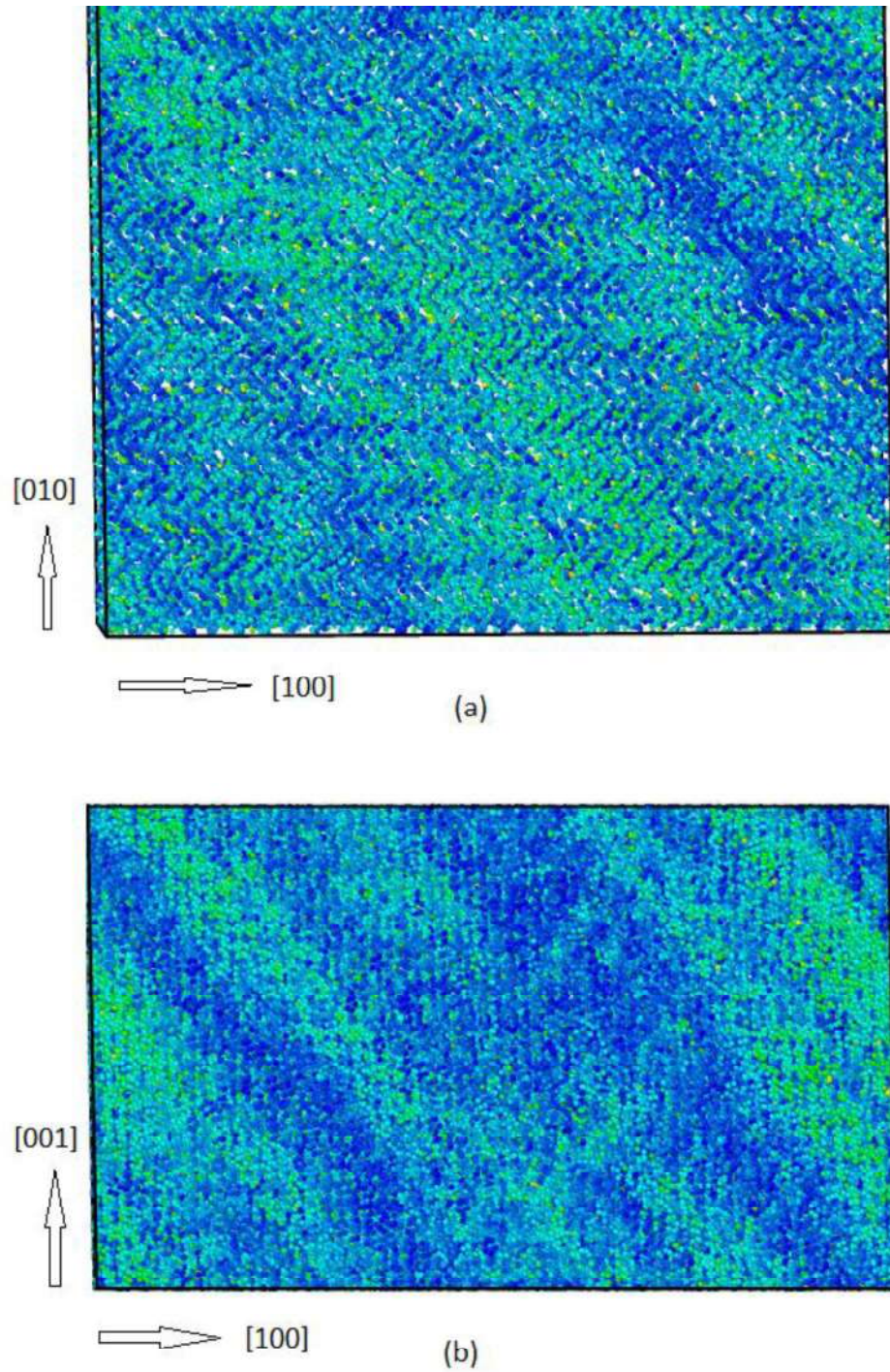


**Figure 4.25** Snapshots showing shear band in single crystal TKX-50 with 6480 molecules shock loaded along [100] direction for the shock pressure of 13GPa viewed along (a) (001) direction, and (b) (010) direction

Figure 4.24 and Figure 4.25 depict that for the shock pressure along [100] direction obvious shear bands are formed. For both the cases with 4800 molecules and 6480 molecules systems shear bands are formed with width  $\sim 3.5$  nm. The shear bands are formed along the  $\{101\}$  slip planes for the [100] shock.

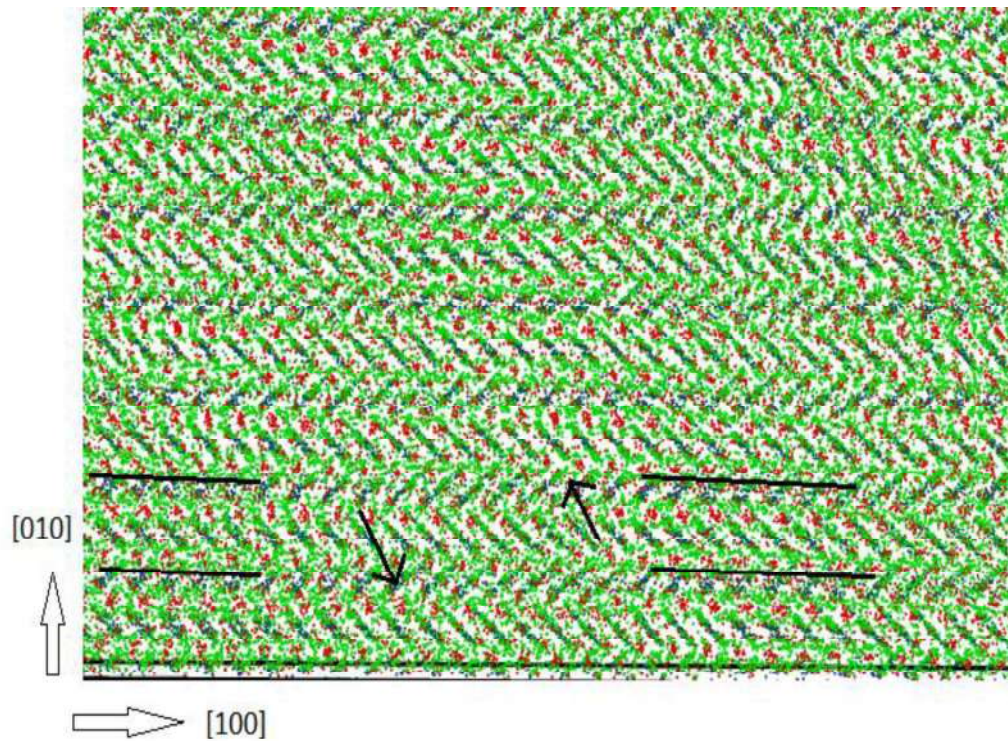


**Figure 4.26** Atomic configuration of TKX-50 for [100] shock compression with  $P_{xx} = 13$  GPa. The black arrows indicate the slip direction. The black line is to help distinguish the unit cell. The C, N, O atoms are represented by black, green, and red.

To illustrate the atomic mechanism of slip through shear band formation of single crystal TKX-50 under shock compression, we examine the atomic configuration for the [100] shock as shown in Figure 4.26. For [100] shock the maximum shear is at  $\sim 45^\circ$  to the [100] direction. Figure 4.26 clearly shows the shear band between two crystalline regions being shifted about  $\frac{1}{2}$  unit along



[010] direction relative to each other. The shear band is about 7 unit cells along the [100] shock direction with the width of ~3.5 nm.

Usually, the HELs from MD simulations are higher than the experimental values because we simulate defect free crystals with small system size (~nm scale). Furthermore, it is well-known that Lj 12-6 vdW repulsion interactions are too repulsive at short distances. So, there is a possibility that our FF might overestimate the pressure under shock compression, leading to predicted HEL higher than the experimental value. However, as no experimental shock study has been done for TKX-50 as of now, it can serve as a good reference point for now and for future when experimental studies take place.

The formation of shear bands in a molecular system with 6480 molecules when subjected to uniaxial shock pressure along the [100] axis at 9 GPa, 11 GPa, and 13 GPa, respectively, is presented in Figure 4.27. The shear band that formed as a result of the shock pressure  $P_{xx} = 13$  GPa is the sharpest when compared to the other two shock pressures that occurred in the plastic region, as can be seen clearly.

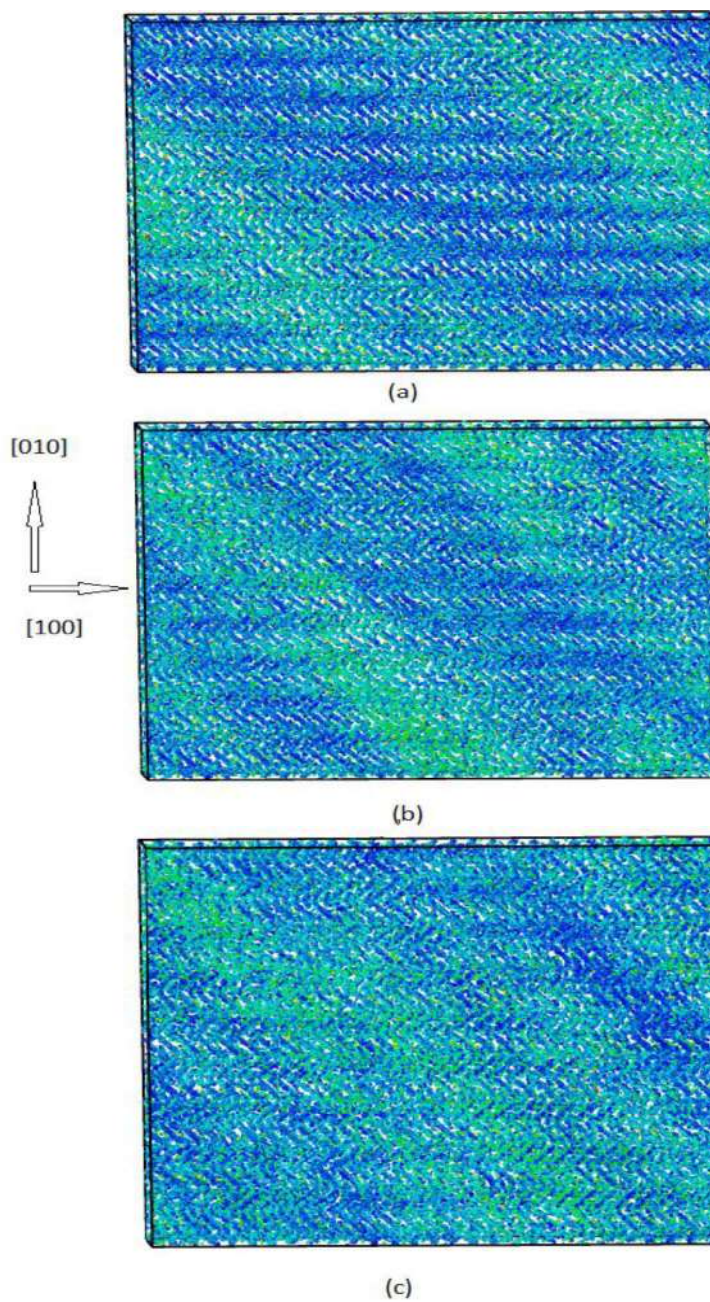


**Figure 4.27** Snapshots showing shear bands in single crystal TKX-50 shock-loaded along [100] direction viewed along (010) direction for shock pressure, (a)  $P_{xx} = 9$  GPa, (b)  $P_{xx} = 11$  GPa, (c)  $P_{xx} = 13$  GPa for systems with 4800 molecules viewed along (001) direction

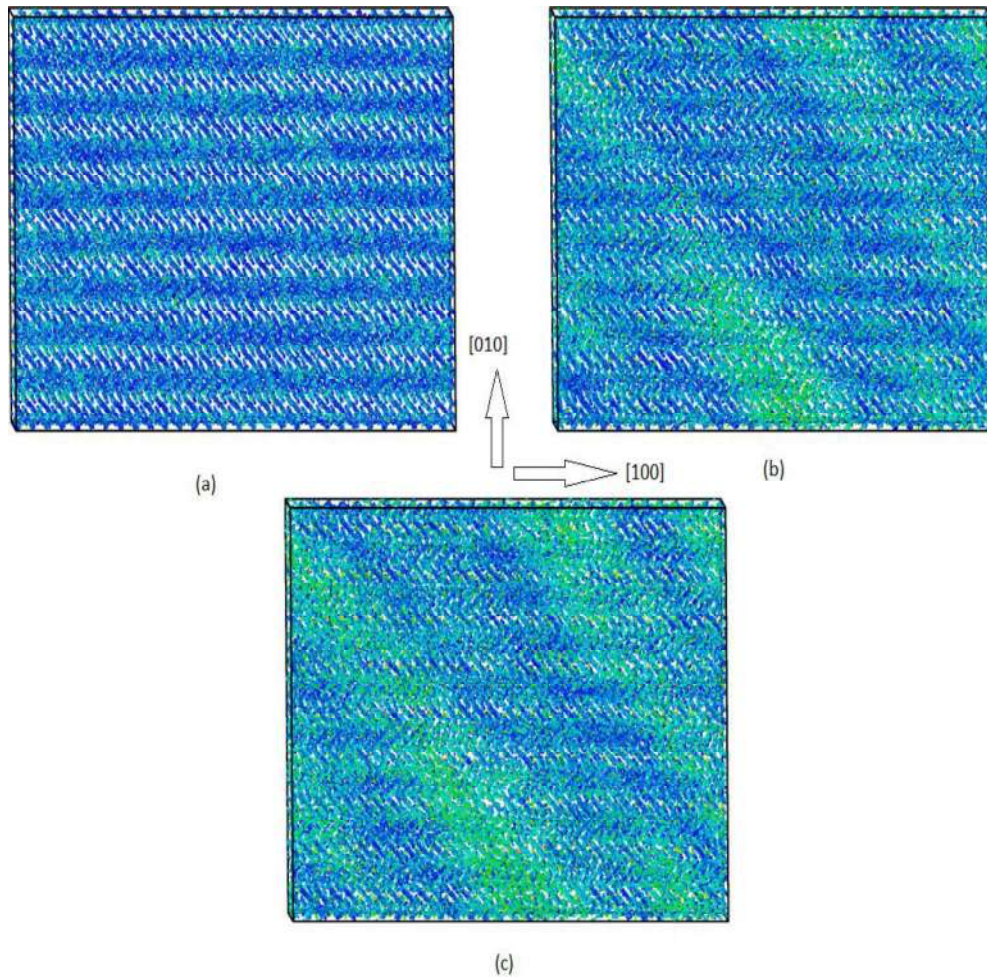


**Figure 4.28** Snapshots obtained from uniaxial Hugoniot simulation for TKX-50 along  $[100]$  direction from shock pressure  $P_{xx} = 11$  GPa after (a) 5ps (b) 40 ps and (c) 93 ps.

Figure 4.28 and Figure 4.29 depict the time evolution of shear band formation for the molecular system with 6480 molecules for shock pressure  $P_{xx} = 11$  GPa and 13 GPa, respectively. As the simulation time increases, the shear band becomes more visible and clear with a higher width. The shear bands are denser for shock pressure of 13 GPa than the shear bands for 11 GPa.

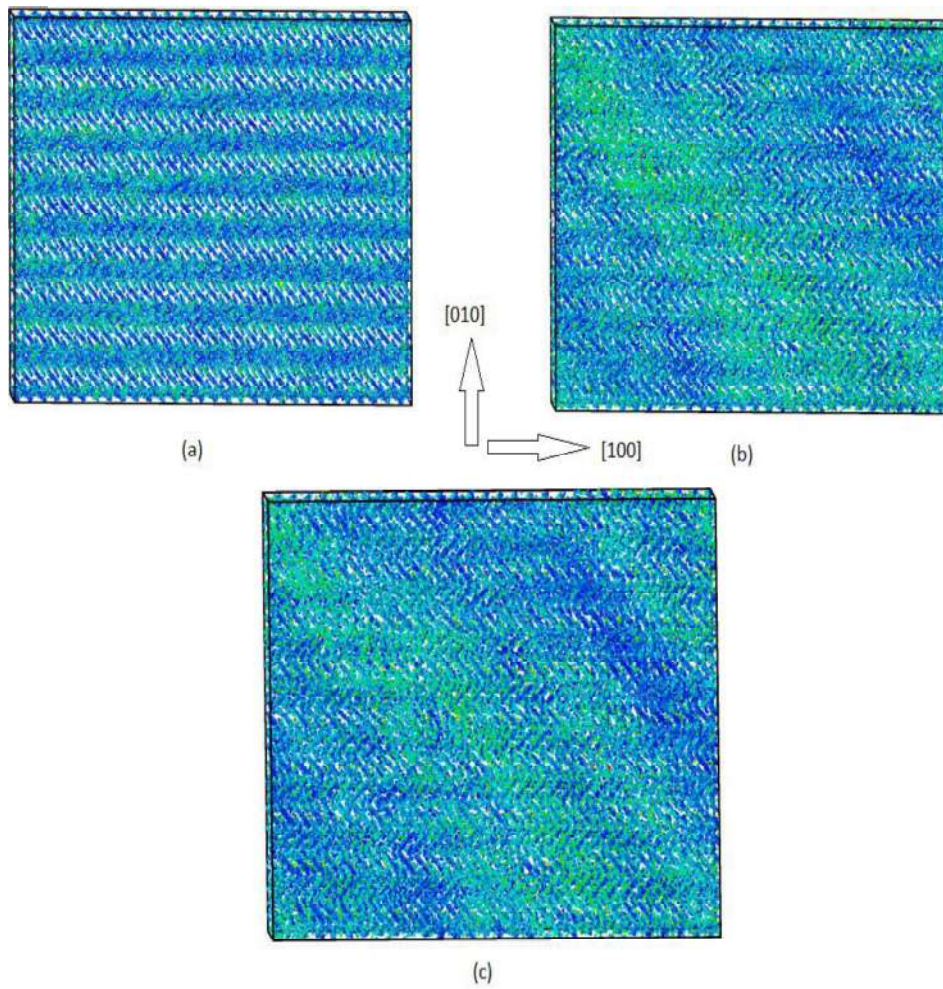


**Figure 4.29** Snapshots obtained from uniaxial Hugoniot simulation for TKX-50 along [100] direction from shock pressure  $P_{xx} = 13$  GPa after (a) 5 ps (b) 40 ps and (c) 93 ps viewed along (001)

## CHAPTER 5

### CONCLUSION AND FUTURE RECOMMENDATIONS

This thesis is concerned with developing a quantum chemistry based classical molecular dynamics forcefield, as well as studying various thermo-mechanical properties and mechanical behavior under shock. The findings of this study are discussed in the later section. Finally, some recommendations for future work are proposed in this chapter.

#### 5.1 Conclusion

In this study, an in-depth evaluation of the atomistic properties of TKX-50, a recently synthesized energetic and explosive material, is carried out. The development of a classical molecular dynamics forcefield for TKX-50 utilizing typical quantum chemistry approach is the major purpose of this investigation. Subsequently, the forcefield is verified and used to evaluate a variety of thermodynamic and mechanical properties. In addition, a shock sensitivity analysis is carried out in order to obtain significant information regarding the material's flexibility. The most important outcomes from this investigation are summed up as follows:

1. A novel classical forcefield that is more accurate than the available forcefield is developed here for TKX-50. An iterative post-SCF method is used here which takes into account the impacts of electron correlation, which results in an increase in accuracy.
2. The Electrostatic Potential (ESP) method is utilized in order to make an estimate of the nonbonded electrostatic potential. This allows for the partial atomic charges for the system to be calculated. This study was able to make the system charge neutral, which got rid of instability issues that are present with the currently available forcefields.
3. The crystal structure, cohesive energy, and material density of TKX-50 have been validated, and the results show a good agreement with quantum mechanical predictions

and experimental evidence. The value of  $\beta$  has found to be within 0.2% agreement to the original value. Constant volume heat capacity of the material is also evaluated for validation purpose. The heat capacity value matches well with the experimental results and shows 3% improvement compared to the existing forcefield's estimation.

4. The developed forcefield is utilized in the computation of mechanical parameters such as bulk modulus, shear modulus, Poisson's ratio, and elastic constants. The results show excellent agreement with experimental data for the bulk modulus and the QM-predicted shear modulus. The bulk modulus and shear modulus are improved by 40% and 15% respectively compared to the existing forcefield's estimation.
5. Uniaxial hugoniot shock compression simulations have been performed for TKX-50 along the [100] direction. Plastic deformation starts by forming shear band for a shock pressure of about 6 GPa. This pressure is equivalent to shear stress of  $\sim 0.65$  GPa which is responsible for the [100] shock, shear band forms along the {101} plane.
6. The Rankine-Hugoniot jump condition is applied to explore the time evolution of temperature, volume fluctuation, and shear stress. This temporal analysis reveals that the Hugoniot Elastic Limit (HEL) is about 6 GPa and the potential shock pressure for the overdriven point is about 8 GPa.

Overall, the findings of this study add to fundamental knowledge of TKX-50 at the atomic level by providing important new insights into the material's thermodynamic, and mechanical properties, and shock response. The newly constructed forcefield, in conjunction with the findings that were provided in this article, lays a solid platform for future research and applications employing TKX-50.

## 5.2 Future Recommendations

This research work has several potential extensions that could be investigated further in the future. With the help of these recommendations, we hope to better comprehend TKX-50 and its properties as well as investigate cutting-edge computational methods for investigating energetic materials. The following recommendations are made:

1. Machine Learning based Forcefield: Development of the TKX-50 forcefield using machine learning techniques is one possible approach to enhancing the forcefield's precision and effectiveness. A machine learning-based forcefield can be created by combining the training datasets from the produced forcefield and the prior AMBER forcefield. While drastically lowering computing costs, this method has the potential to capture complicated interactions and correctly forecast the behavior of TKX-50. Incorporating cutting-edge data-driven techniques can also make it easier to explore higher-dimensional chemical regions and create new energetic materials with the needed attributes.
2. Non-equilibrium Molecular Dynamics Shock Simulations: In this thesis, equilibrium Hugoniot shock simulations were run along the [100] direction to look at how the TKX-50 will react to shock circumstances. However, it is essential to investigate non-equilibrium molecular dynamics (NEMD) shock simulations as well in order to fully comprehend the material's behavior. This study can be a good reference point for the future NEMD simulations to take place for TKX-50 at extreme condition.
3. Investigation of Sensitivity and Stability: For practical applications, it is crucial to comprehend the TKX-50's sensitivity and stability. Future research should concentrate on determining how sensitive the TKX-50 is to environmental stimuli including impact, friction, and heat. Sensitivity analysis can be used to do this utilizing sophisticated computational methods, such as reactive forcefields and molecular dynamics simulations. Additionally, stability study can offer important

insights into the TKX-50's long-term behavior under diverse environmental circumstances, assisting in the creation of reliable formulations and guaranteeing security in handling and storage.

4. Exploration of Multiscale Modeling: Detonation in an energetic material involves different phenomena happening on a wide variety of length and time scales, and as such multiscale modeling techniques must be used to understand detonation in TKX-50. To bridge various scales, future research should investigate the combination of atomistic simulations with coarse-grained models and continuum techniques. This will allow for the exploration of mesoscale processes while balancing computational efficiency and accuracy, such as crack propagation, shock wave interactions, and energy dissipation.
5. Collaboration between computational researchers and experimentalists is essential for the validation and improvement of computational models. Future work should involve close interaction with experimentalists to verify the forcefield's established predictions and look into characteristics that are difficult to fully understand using only computational methods. The design of future experiments can be influenced by experimental validation, which can also improve the accuracy of computational models and offer fresh insights into the behavior of the TKX-50.

The recommendations for the future studies made above are intended to increase knowledge about TKX-50 and advance the study of energetic materials. The implementation of multiscale modeling, cooperation with experimentalists, development of machine learning-based forcefields, investigation of sensitivity and stability, exploration of non-equilibrium molecular dynamics simulations, and application to other energetic materials all contribute to the ongoing development and optimization of computational tools and techniques for studying the hot spot formation in energetic materials.



## REFERENCES

1. Olah, G. A., & Squire, D. R. (Eds.). (2012, December 2). *Chemistry of Energetic Materials*. Academic Press.
2. Son, S. F., Yetter, R. A., & Yang, V. (2007, July). Introduction: Nanoscale Composite Energetic Materials. *Journal of Propulsion and Power*, 23(4), 643–644. <https://doi.org/10.2514/1.31508>
3. Badgajar, D., Talawar, M., Asthana, S., & Mahulikar, P. (2008, March). Advances in science and technology of modern energetic materials: An overview. *Journal of Hazardous Materials*, 151(2–3), 289–305. <https://doi.org/10.1016/j.jhazmat.2007.10.039>
4. Singh, H., & Tiwari, S. P. (2008). New Energetic Materials for the Propulsion of Space Vehicles and Rockets. *International Journal of Energetic Materials and Chemical Propulsion*, 7(3), 253–262. <https://doi.org/10.1615/intjenergeticmaterialschemprop.v7.i3.60>
5. Bhattacharya, S., Agarwal, A. K., Rajagopalan, T., & Patel, V. K. (Eds.). (2018, November 19). *Nano-Energetic Materials*. <https://doi.org/10.1007/978-981-13-3269-2>
6. Zlotin, S. G., Churakov, A. M., Egorov, M. P., Fershtat, L. L., Klenov, M. S., Kuchurov, I. V., Makhova, N. N., Smirnov, G. A., Tomilov, Y. V., & Tartakovskiy, V. A. (2021, November). Advanced energetic materials: novel strategies and versatile applications. *Mendeleev Communications*, 31(6), 731–749. <https://doi.org/10.1016/j.mencom.2021.11.001>
7. Wen, L., Yu, T., Lai, W., Liu, M., Wang, B., Shi, J., & Liu, Y. (2022, September). Transferring the available fused cyclic scaffolds for high—throughput combinatorial design of highly energetic materials via database mining. *Fuel*, 324, 124591. <https://doi.org/10.1016/j.fuel.2022.124591>
8. Parate, B. A. (2020, September 1). Propellant Actuated Device for Parachute Deployment during Seat Ejection for an Aircraft Application. *HighTech and Innovation Journal*, 1(3), 112–120. <https://doi.org/10.28991/hij-2020-01-03-03>
9. Tian, X. L., Song, S. W., Chen, F., Qi, X. J., Wang, Y., & Zhang, Q. H. (2022, September). Machine learning-guided property prediction of energetic materials: Recent advances,

- challenges, and perspectives. *Energetic Materials Frontiers*, 3(3), 177–186. <https://doi.org/10.1016/j.enmf.2022.07.005>
10. An, Q., Cheng, T., Goddard, W. A., & Zybin, S. V. (2015, January 17). Anisotropic Impact Sensitivity and Shock Induced Plasticity of TKX-50 (Dihydroxylammonium 5,5'-bis(tetrazole)-1,1'-diolate) Single Crystals: From Large-Scale Molecular Dynamics Simulations. *The Journal of Physical Chemistry C*, 119(4), 2196–2207. <https://doi.org/10.1021/jp510951s>
  11. Fischer, N., Fischer, D., Klapötke, T. M., Piercey, D. G., & Stierstorfer, J. (2012). Pushing the limits of energetic materials – the synthesis and characterization of dihydroxylammonium 5,5'-bistetrazole-1,1'-diolate. *Journal of Materials Chemistry*, 22(38), 20418. <https://doi.org/10.1039/c2jm33646d>
  12. Song, H. J., Zhang, Y. G., Li, H., Zhou, T., & Huang, F. L. (2014, August 14). All-atom, non-empirical, and tailor-made force field for  $\alpha$ -RDX from first principles. *RSC Adv.*, 4(76), 40518–40533. <https://doi.org/10.1039/c4ra07195f>
  13. Mayo, S. L., Olafson, B. D., & Goddard, W. A. (1990, December). DREIDING: a generic force field for molecular simulations. *The Journal of Physical Chemistry*, 94(26), 8897–8909. <https://doi.org/10.1021/j100389a010>
  14. Jorgensen, W. L., Maxwell, D. S., & Tirado-Rives, J. (1996, November 13). Development and Testing of the OPLS All-Atom Force Field on Conformational Energetics and Properties of Organic Liquids. *Journal of the American Chemical Society*, 118(45), 11225–11236. <https://doi.org/10.1021/ja9621760>
  15. Bedrov, D., Borodin, O., Smith, G. D., Sewell, T. D., Dattelbaum, D. M., & Stevens, L. L. (2009, December 14). A molecular dynamics simulation study of crystalline 1,3,5-triamino-2,4,6-trinitrobenzene as a function of pressure and temperature. *The Journal of Chemical Physics*, 131(22), 224703. <https://doi.org/10.1063/1.3264972>
  16. Kroonblawd, M. P., & Sewell, T. D. (2013, August 19). Theoretical determination of anisotropic thermal conductivity for crystalline 1,3,5-triamino-2,4,6-trinitrobenzene (TATB). *The Journal of Chemical Physics*, 139(7). <https://doi.org/10.1063/1.4816667>
  17. Sorescu, D. C., Boatz, J. A., & Thompson, D. L. (2001, April 24). Classical and Quantum-Mechanical Studies of Crystalline FOX-7 (1,1-Diamino-2,2-dinitroethylene). *The Journal of Physical Chemistry A*, 105(20), 5010–5021. <https://doi.org/10.1021/jp010289m>

18. Smith, G. D., & Bharadwaj, R. K. (1999, April 21). Quantum Chemistry Based Force Field for Simulations of HMX. *The Journal of Physical Chemistry B*, 103(18), 3570–3575. <https://doi.org/10.1021/jp984599p>
19. Smith, G. D., Bharadwaj, R. K., Bedrov, D., & Ayyagari, C. (1999, January 13). Quantum-Chemistry-Based Force Field for Simulations of Dimethylnitramine. *The Journal of Physical Chemistry B*, 103(4), 705–713. <https://doi.org/10.1021/jp9834006>
20. Pang, Y. (2016, July 21). FF12MC: A revised AMBER forcefield and new protein simulation protocol. *Proteins: Structure, Function, and Bioinformatics*, 84(10), 1490–1516. <https://doi.org/10.1002/prot.25094>
21. Mirijanian, D. T., Mannige, R. V., Zuckermann, R. N., & Whitelam, S. (2013, November 29). Development and use of an atomistic CHARMM-based forcefield for peptoid simulation. *Journal of Computational Chemistry*, 35(5), 360–370. <https://doi.org/10.1002/jcc.23478>
22. Qian, W., Xue, X., Liu, J., & Zhang, C. (2022, February 28). Molecular Forcefield Methods for Describing Energetic Molecular Crystals: A Review. *Molecules*, 27(5), 1611. <https://doi.org/10.3390/molecules27051611>
23. Badgular, D., & Talawar, M. (2017, May 19). Thermal and Sensitivity Study of Dihydroxyl Ammonium 5,5'-Bistetrazole-1,1'-diolate (TKX-50)-based Melt Cast Explosive Formulations. *Propellants, Explosives, Pyrotechnics*, 42(8), 883–888. <https://doi.org/10.1002/prop.201600168>
24. Cao, X., Shang, Y., Meng, K., Yue, G., Yang, L., Liu, Y., Deng, P., & Hu, L. (2019, April 23). Fabrication of three-dimensional TKX-50 network-like nanostructures by liquid nitrogen-assisted spray freeze-drying method. *Journal of Energetic Materials*, 37(3), 356–364. <https://doi.org/10.1080/07370652.2019.1585491>
25. Dong, W., Chen, S., Jin, S., & Chen, Y. (2019, January 7). Effects of carboxymethylcellulose sodium on the morphology and properties of TKX-50, an insensitive high-energy explosive. *Journal of Energetic Materials*, 37(2), 199–211. <https://doi.org/10.1080/07370652.2018.1559260>
26. Gottfried, J. L., Klapötke, T. M., & Witkowski, T. G. (2017, February 21). Estimated Detonation Velocities for TKX-50, MAD-X1, BDNAPM, BTNPM, TKX-55, and DAAF

- using the Laser-induced Air Shock from Energetic Materials Technique. *Propellants, Explosives, Pyrotechnics*, 42(4), 353–359. <https://doi.org/10.1002/prop.201600257>
27. Huang, H., Shi, Y., Yang, J., & Li, B. (2014, September 10). Compatibility Study of Dihydroxylammonium 5,5'-Bistetrazole-1,1'-diolate (TKX-50) with Some Energetic Materials and Inert Materials. *Journal of Energetic Materials*, 33(1), 66–72. <https://doi.org/10.1080/07370652.2014.889781>
28. Jia, J., Liu, Y., Huang, S., Xu, J., Li, S., Zhang, H., & Cao, X. (2017). Crystal structure transformation and step-by-step thermal decomposition behavior of dihydroxylammonium 5,5'-bistetrazole-1,1'-diolate. *RSC Adv.*, 7(77), 49105–49113. <https://doi.org/10.1039/c7ra08816g>
29. Bedrov, D., Hooper, J. B., Smith, G. D., & Sewell, T. D. (2009, July 21). Shock-induced transformations in crystalline RDX: A uniaxial constant-stress Hugoniotat molecular dynamics simulation study. *The Journal of Chemical Physics*, 131(3). <https://doi.org/10.1063/1.3177350>
30. Cawkwell, M. J., Sewell, T. D., Zheng, L., & Thompson, D. L. (2008, July 17). Shock-induced shear bands in an energetic molecular crystal: Application of shock-front absorbing boundary conditions to molecular dynamics simulations. *Physical Review B*, 78(1). <https://doi.org/10.1103/physrevb.78.014107>
31. Zhou, T., Lou, J., Zhang, Y., Song, H., & Huang, F. (2016). Hot spot formation and chemical reaction initiation in shocked HMX crystals with nanovoids: a large-scale reactive molecular dynamics study. *Phys. Chem. Chem. Phys.*, 18(26), 17627–17645. <https://doi.org/10.1039/c6cp02015a>
32. Computer simulation in materials science. (1992, January). *Materials & Design*, 13(2), 123. [https://doi.org/10.1016/0261-3069\(92\)90146-9](https://doi.org/10.1016/0261-3069(92)90146-9)
33. Kawazoe, Y. (2010, October). Paradigm shift of materials design by computer simulation – From explanation to prediction. *Computational Materials Science*, 49(4), S158–S160. <https://doi.org/10.1016/j.commatsci.2010.02.007>
34. Ziesche, P. (1994, December). Pair density functional theory — a generalized density functional theory. *Physics Letters A*, 195(3–4), 213–220. [https://doi.org/10.1016/0375-9601\(94\)90155-4](https://doi.org/10.1016/0375-9601(94)90155-4)

35. Su, N. Q. (2021, November 16). Unity of Kohn-Sham density-functional theory and reduced-density-matrix-functional theory. *Physical Review A*, *104*(5). <https://doi.org/10.1103/physreva.104.052809>
36. Ludeña, E. V. (2004, November). Is the Hohenberg–Kohn–Sham version of DFT a semi-empirical theory? *Journal of Molecular Structure: THEOCHEM*, *709*(1–3), 25–29. <https://doi.org/10.1016/j.theochem.2004.03.047>
37. Parr, R. G. (1983, October). Density Functional Theory. *Annual Review of Physical Chemistry*, *34*(1), 631–656. <https://doi.org/10.1146/annurev.pc.34.100183.003215>
38. Pokluda, J., Černý, M., Šob, M., & Umeno, Y. (2015, August). Ab initio calculations of mechanical properties: Methods and applications. *Progress in Materials Science*, *73*, 127–158. <https://doi.org/10.1016/j.pmatsci.2015.04.001>
39. Kutzelnigg, W. (1989, December). Ab initio calculation of molecular properties. *Journal of Molecular Structure: THEOCHEM*, *202*, 11–61. [https://doi.org/10.1016/0166-1280\(89\)87003-4](https://doi.org/10.1016/0166-1280(89)87003-4)
40. Pople, J. A., Krishnan, R., Schlegel, H. B., & Binkley, J. S. (2009, June 18). Derivative studies in hartree-fock and møller-plesset theories. *International Journal of Quantum Chemistry*, *16*(S13), 225–241. <https://doi.org/10.1002/qua.560160825>
41. Lykos, P., & Pratt, G. W. (1963, July 1). Discussion on The Hartree-Fock Approximation. *Reviews of Modern Physics*, *35*(3), 496–501. <https://doi.org/10.1103/revmodphys.35.496>
42. Théry, V., Rinaldi, D., Rivail, J. L., Maigret, B., & Ferenczy, G. G. (1994, March). Quantum mechanical computations on very large molecular systems: The local self-consistent field method. *Journal of Computational Chemistry*, *15*(3), 269–282. <https://doi.org/10.1002/jcc.540150303>
43. Prigogine, I., & Rice, S. A. (Eds.). (1988, January 1). Advances in Chemical Physics. *Advances in Chemical Physics*. <https://doi.org/10.1002/9780470141199>
44. Häser, M., & Ahlrichs, R. (1989, January). Improvements on the direct SCF method. *Journal of Computational Chemistry*, *10*(1), 104–111. <https://doi.org/10.1002/jcc.540100111>
45. Simandiras, E. D., Rice, J. E., Lee, T. J., Amos, R. D., & Handy, N. C. (1988, March 1). On the necessity of f basis functions for bending frequencies. *The Journal of Chemical Physics*, *88*(5), 3187–3195. <https://doi.org/10.1063/1.453963>

46. Grimme, S. (2003, May 9). Improved second-order Møller–Plesset perturbation theory by separate scaling of parallel- and antiparallel-spin pair correlation energies. *The Journal of Chemical Physics*, *118*(20), 9095–9102. <https://doi.org/10.1063/1.1569242>
47. Fedorov, D. G., & Kitaura, K. (2004, July 23). Second order Møller-Plesset perturbation theory based upon the fragment molecular orbital method. *The Journal of Chemical Physics*, *121*(6), 2483–2490. <https://doi.org/10.1063/1.1769362>
48. Carbó-Dorca, R., & Bultinck, P. (2004, July). Quantum Mechanical Basis for Mulliken Population Analysis. *Journal of Mathematical Chemistry*, *36*(3), 231–239. <https://doi.org/10.1023/b:jomc.0000044221.23647.20>
49. LU, T., & CHEN, F. (2012, February). ATOMIC DIPOLE MOMENT CORRECTED HIRSHFELD POPULATION METHOD. *Journal of Theoretical and Computational Chemistry*, *11*(01), 163–183. <https://doi.org/10.1142/s0219633612500113>
50. Reed, A. E., Weinstock, R. B., & Weinhold, F. (1985, July 15). Natural population analysis. *The Journal of Chemical Physics*, *83*(2), 735–746. <https://doi.org/10.1063/1.449486>
51. Nistor, R. A., Polihronov, J. G., Müser, M. H., & Mosey, N. J. (2006, September 7). A generalization of the charge equilibration method for nonmetallic materials. *The Journal of Chemical Physics*, *125*(9). <https://doi.org/10.1063/1.2346671>
52. Verstraelen, T., Van Speybroeck, V., & Waroquier, M. (2009, July 28). The electronegativity equalization method and the split charge equilibration applied to organic systems: Parametrization, validation, and comparison. *The Journal of Chemical Physics*, *131*(4), 044127. <https://doi.org/10.1063/1.3187034>
53. Zeng, J., Duan, L., Zhang, J. Z., & Mei, Y. (2012, December 28). A numerically stable restrained electrostatic potential charge fitting method. *Journal of Computational Chemistry*, *34*(10), 847–853. <https://doi.org/10.1002/jcc.23208>
54. Bultinck, P., Langenaeker, W., Lahorte, P., De Proft, F., Geerlings, P., Waroquier, M., & Tollenaere, J. P. (2002, July 27). The Electronegativity Equalization Method I: Parametrization and Validation for Atomic Charge Calculations. *The Journal of Physical Chemistry A*, *106*(34), 7887–7894. <https://doi.org/10.1021/jp0205463>
55. Snyder, H. D., & Kucukkal, T. G. (2021, February 18). Computational Chemistry Activities with Avogadro and ORCA. *Journal of Chemical Education*, *98*(4), 1335–1341. <https://doi.org/10.1021/acs.jchemed.0c00959>

56. Lu, T., & Chen, F. (2011, December 8). Multiwfn: A multifunctional wavefunction analyzer. *Journal of Computational Chemistry*, *33*(5), 580–592. <https://doi.org/10.1002/jcc.22885>
57. Hoover, W. G. (2007, January). Nosé–Hoover nonequilibrium dynamics and statistical mechanics. *Molecular Simulation*, *33*(1–2), 13–19. <https://doi.org/10.1080/08927020601059869>
58. Baranyai, A., & Tóth, G. (1995, June). Solvation Dynamics from Nonequilibrium Molecular Dynamics Simulation. *Molecular Simulation*, *14*(6), 403–407. <https://doi.org/10.1080/08927029508022033>
59. Hansson, T., Oostenbrink, C., & van Gunsteren, W. (2002, April). Molecular dynamics simulations. *Current Opinion in Structural Biology*, *12*(2), 190–196. [https://doi.org/10.1016/s0959-440x\(02\)00308-1](https://doi.org/10.1016/s0959-440x(02)00308-1)
60. Wang, X., Ramírez-Hinestrosa, S., Dobnikar, J., & Frenkel, D. (2020). The Lennard-Jones potential: when (not) to use it. *Physical Chemistry Chemical Physics*, *22*(19), 10624–10633. <https://doi.org/10.1039/c9cp05445f>
61. Brooks, C. L. (1989, January). Computer simulation of liquids. *Journal of Solution Chemistry*, *18*(1), 99–99. <https://doi.org/10.1007/bf00646086>
62. Plimpton, S. (1995, November). Computational limits of classical molecular dynamics simulations. *Computational Materials Science*, *4*(4), 361–364. [https://doi.org/10.1016/0927-0256\(95\)00037-1](https://doi.org/10.1016/0927-0256(95)00037-1)
63. Stukowski, A. (2009, December 15). Visualization and analysis of atomistic simulation data with OVITO—the Open Visualization Tool. *Modelling and Simulation in Materials Science and Engineering*, *18*(1), 015012. <https://doi.org/10.1088/0965-0393/18/1/015012>
64. Humphrey, W., Dalke, A., & Schulten, K. (1996, February). VMD: Visual molecular dynamics. *Journal of Molecular Graphics*, *14*(1), 33–38. [https://doi.org/10.1016/0263-7855\(96\)00018-5](https://doi.org/10.1016/0263-7855(96)00018-5)
65. Maillet, J. B., Mareschal, M., Soulard, L., Ravelo, R., Lomdahl, P. S., Germann, T. C., & Holian, B. L. (2000, December 27). Uniaxial Hugoniot: A method for atomistic simulations of shocked materials. *Physical Review E*, *63*(1). <https://doi.org/10.1103/physreve.63.016121>

66. Parrinello, M., & Rahman, A. (1981, December 1). Polymorphic transitions in single crystals: A new molecular dynamics method. *Journal of Applied Physics*, 52(12), 7182–7190. <https://doi.org/10.1063/1.328693>
67. Cornell, W. D., Cieplak, P., Bayly, C. I., Gould, I. R., Merz, K. M., Ferguson, D. M., Spellmeyer, D. C., Fox, T., Caldwell, J. W., & Kollman, P. A. (1995, May). A Second Generation Force Field for the Simulation of Proteins, Nucleic Acids, and Organic Molecules. *Journal of the American Chemical Society*, 117(19), 5179–5197. <https://doi.org/10.1021/ja00124a002>
68. Critical phenomena in gases - I. (1937, November 5). *Proceedings of the Royal Society of London. Series A - Mathematical and Physical Sciences*, 163(912), 53–70. <https://doi.org/10.1098/rspa.1937.0210>
69. Verlet, L. (1967, July 5). Computer “Experiments” on Classical Fluids. I. Thermodynamical Properties of Lennard-Jones Molecules. *Physical Review*, 159(1), 98–103. <https://doi.org/10.1103/physrev.159.98>
70. Tzou, D. Y. (2014, September 26). *Macro- to Microscale Heat Transfer: The Lagging Behavior*. Wiley-Blackwell. <https://doi.org/10.1002/9781118818275>
71. *File:TKX-50 structure.svg - Wikimedia Commons*. (2017, January 2). *File:TKX-50 structure.svg - Wikimedia Commons*. [https://commons.wikimedia.org/wiki/File:TKX-50\\_structure.svg](https://commons.wikimedia.org/wiki/File:TKX-50_structure.svg)
72. Herrmann, M., & Förter-Barth, U. (2021, February). Thermal Behavior and Micro Structure of TKX-50. *Propellants, Explosives, Pyrotechnics*, 46(2), 262–266. <https://doi.org/10.1002/prop.202000257>
73. Yu, Y., Chen, S., Li, X., Zhu, J., Liang, H., Zhang, X., & Shu, Q. (2016). Molecular dynamics simulations for 5,5'-bistetrazole-1,1'-diolate (TKX-50) and its PBXs. *RSC Advances*, 6(24), 20034–20041. <https://doi.org/10.1039/c5ra27912g>
74. Fu, J. (2018, May 16). Elastic Constants and Homogenized Moduli of Monoclinic Structures Based on Density Functional Theory. *Density Functional Calculations - Recent Progresses of Theory and Application*. <https://doi.org/10.5772/intechopen.72301>
75. Wu, Z. J., Zhao, E. J., Xiang, H. P., Hao, X. F., Liu, X. J., & Meng, J. (2007, August 14). Crystal structures and elastic properties of superhard IrN<sub>2</sub> and IrN<sub>3</sub> from first principles. *Physical Review B*, 76(5). <https://doi.org/10.1103/physrevb.76.054115>



76. Beale, P. D. (2011, April 6). *Statistical Mechanics*. Academic Press.
77. Chung, D. H., & Buessem, W. R. (1967, May 1). The Voigt-Reuss-Hill Approximation and Elastic Moduli of Polycrystalline MgO, CaF<sub>2</sub>,  $\beta$ -ZnS, ZnSe, and CdTe. *Journal of Applied Physics*, 38(6), 2535–2540. <https://doi.org/10.1063/1.1709944>
78. Zimmerman, J. A., Kelchner, C. L., Klein, P. A., Hamilton, J. C., & Foiles, S. M. (2001, October 1). Surface Step Effects on Nanoindentation. *Physical Review Letters*, 87(16). <https://doi.org/10.1103/physrevlett.87.165507>
79. Smith, G. D., Bharadwaj, R. K., Bedrov, D., & Ayyagari, C. (1999, January 13). Quantum-Chemistry-Based Force Field for Simulations of Dimethylnitramine. *The Journal of Physical Chemistry B*, 103(4), 705–713. <https://doi.org/10.1021/jp9834006>
80. Bedrov, D., Borodin, O., Smith, G. D., Sewell, T. D., Dattelbaum, D. M., & Stevens, L. L. (2009, December 8). A molecular dynamics simulation study of crystalline 1,3,5-triamino-2,4,6-trinitrobenzene as a function of pressure and temperature. *The Journal of Chemical Physics*, 131(22). <https://doi.org/10.1063/1.3264972>
81. F. Jensen, *Introduction to Computational Chemistry*, 2<sup>nd</sup> ed, Wiley, 2007.

## Nomenclature

TKX-50	Dihydroxylammonium-5,5'-bistetrazole-1,1'-diolate (Secondary explosive)
PES	Potential Energy Surface
HEL	Hugoniot Elastic Limit
GGA	gradient-corrected functionals (GGA)
LAMMPS	Large-scale Atomic/Molecular Massively Parallel Simulator
MD	Molecular Dynamics
L-J	Lennard-Jones
NVE	micro-canonical ensemble
NVT	canonical ensemble
NPT	Isothermal Isobaric Ensemble
PPPM	particle particle particle mesh method
PBC	periodic boundary condition
EMD	Equilibrium molecular dynamics

NEMD	Non-equilibrium molecular dynamics
$V_{XC}$	Exchange-correlation potential
$\psi$	wave function
$h$	plank's constant
$r$	bond length
$\theta$	angle in between three atoms
$\varphi$	Dihedral angle
$E$	total energy,
$E_{XC}$	Exchange correlation functional
$C_v$	Constant Volume Heat Capacity
$C_{ij}$	Elastic coefficient
$K$	Bulk modulus
$G$	Shear Modulus
$\kappa_b$	Boltzman constant, $1.38 \times 10^{-23}$ J/K

$\text{\AA}$	Angstrom
$\nu$	Poisson's ratio
$\rho$	Density
$\tau$	Shear Stress
$P_{xx}$	Shock Pressure along [100] direction
$\sigma_{ii}$	Normal stress
$\Phi$	Stands for the interatomic potential between the two particles
$\epsilon$	Interaction Strength
CHARMM	Chemistry at Harvard Molecular Mechanics
AMBER	Assisted Model Building with Energy Refinement
L-J	Lennard-Jones Potential
$\langle \Delta E^2 \rangle$	Mean squared Energy Fluctuation
MO	Molecular orbitals
EOS	Equation of State

$\zeta$	Dimensionless Heat Flow Variable
$\beta_p$	Damping parameter
a,b,c	Lattice parameters
$\alpha$	Angle between lattice parameter a and b
$\beta$	Angle between lattice parameter a and c
$\gamma$	Angle between lattice parameter b and c
CCDC	Cambridge Crystallographic Data Center
ps	picoseconds
vdW	van der Waals interaction

